Organic Matter Sulfurization in the Modern Ocean

Thesis by

Morgan Reed Raven

In Partial Fulfillment of the Requirements for the

Degree of

Doctor of Philosophy

CALIFORNIA INSTITUTE OF TECHNOLOGY

Pasadena, California

2016

(Defended May 6, 2016)

Morgan Reed Raven
ORCID: 0000-0003-4953-9966

ACKNOWLEDGEMENTS

I have been incredibly fortunate to have support and inspiration from some truly fantastic people throughout the process of creating this thesis. The first name that comes to mind is of course Brendan O.P.B. Raven. Brendan gave up his home and his friends in San Francisco to follow me to a very hot and very small apartment and watch me work, and he never tried to talk me out of it. Thanks for taking care of all those logistics, B., and thanks for getting us out of that awful apartment. And, you know, other stuff too.

At Caltech I got to be part of two fantastic lab groups with a perpetually rotating cast of characters that made long group meetings and purification protocols downright entertaining. Many thanks to Adam Subhas, Sophie Hines, Ted Present, Guillaume Paris, James Rae, Andrea Burke, Jena Johnson, David Case, and all of the other members of the Sessions and Adkins groups. A special mention is appropriate for the Queen Cat herself, Maggie Osburn, for demonstrating the power of the combination of fearlessness and high expectations. Thanks also go to Chris Williams, Westley Procino, Ross Hooper, and David M.F. Kane for being my music family and my sanity through a novel-worthy four years. No list of this sort could be complete without giving due credit to my parents, Stan Reed and Marlyce Reed, and my roommate, Sir Winston Fuzzbutt, for sticking with me through all of my crazy ideas. And of course thanks to you, crazy ideas.

On a more professional note, it is not an exaggeration to say that I am in awe of the geobiochemists in the GPS department at Caltech. In particular, I owe thanks to Woody Fisher for sharing his ideas and his enthusiasm, and to Victoria Orphan for sharing her ideas, enthusiasm, and endless supplies of syringes. I have learned an enormous amount from Jess Adkins, whose ideas and mass spectrometers significantly improved the quality of the science in this thesis. Finally, I am exceptionally grateful for having had the opportunity to work with my primary research advisor, Alex Sessions, who has taught me a great deal by example, both about how to do great science and about how to be a good collaborator and member of the science community. This thesis owes a great deal to all of these scientists.

ABSTRACT

Only a tiny fraction of the carbon fixed by primary producers in the surface ocean is preserved in sediments, but this organic matter (OM) burial is one of the main processes linking the short and long-term carbon cycles, giving it important roles in global biogeochemistry. OM-rich deposits often contain abundant organic S (OS), and sulfur incorporation is thought to make OM less available for heterotrophs and more likely to be preserved. Still, we have few constraints on the significance of sulfurization for OM burial in the modern ocean, and fewer on how that flux might have differed in the past. This thesis applies a new generation of analytical tools for S-isotope analysis to investigate the timescales and mechanisms of OM sulfurization in the modern ocean. By measuring the $\delta^{34}S$ values of minor S phases and individual S-bearing organic compounds as well as major sedimentary phases, we are able to make progress on long-standing questions about the distribution of S isotopes among organic and inorganic S phases in sediments.

Chapters 2 and 3 focus on Cariaco Basin, where a large proportion of the OS in sediments appears to derive from OM sulfurization in particles sinking through the water column. Rapid sulfurization likely involves polysulfides and is associated with high primary productivity and OM export. In the sediments, low-molecular-weight organosulfur compounds accumulate over longer timescales and have low and distinctive $\delta^{34}S$ values. Chapter 4 presents records from Santa Barbara Basin, where OS appears to be exchanging with less abundant porewater sulfide and controlling its $\delta^{34}S$ value. As in many environments, pyrite in these sediments is more ^{34}S-depleted than either OS or sulfide. We attribute this pattern to pyrite formation within sulfide-generating microenvironments prior to equilibration between OS and sulfide in porewater. Chapter 5 tests the feasibility of the proposed OS–sulfide exchange and confirms that sulfide $\delta^{34}S$ can reflect equilibrium with natural OM. We also find evidence that sulfurization of thiols may involve an interim polysulfide that includes the thiol S atom, providing a mechanism to mix biogenic S into proto-kerogen and potentially helping explain differences between the global pyrite and OS S-isotope records.

PUBLISHED CONTENT AND CONTRIBUTIONS

Raven, M.R., Adkins, J.F., Werne, J.P., Lyons, T.W. Sessions, A.L. (2015). "Sulfur-isotopic compositions of individual organic compounds from Cariaco Basin sediments." *Organic Geochemistry* vol. 80, p53-59. DOI: 10.1016/j.orggeochem.2015.01.002

MRR helped improve analytical methods, prepared samples and analyzed samples, interpreted the data, and was the primary author of the manuscript.

Raven M.R., Sessions A.L., Adkins J.F., Thunell R.C. "Rapid organic matter sulfurization in the water column of Cariaco Basin." *Geochimica et Cosmochimica Acta* (submitted Dec. 2015).

MRR designed the project, prepared and analyzed samples, interpreted the data, and was the primary author of the manuscript.

Raven M.R., Sessions A.L., Fischer W.F., Adkins J.F. (2016). "Sedimentary pyrite $\delta^{34}S$ differs from porewater sulfide in Santa Barbara Basin: Proposed role of organic sulfur." *Geochimica et Cosmochimica Acta* (in press).

MRR helped design the project, prepared and analyzed samples, interpreted the data, and was the primary author of the manuscript.

TABLE OF CONTENTS

C h a p t e r 1

INTRODUCTION AND SUMMARY

The global biogeochemical cycles of carbon, sulfur, and oxygen are all affected by how much organic matter (OM) is buried in marine sediments (Berner, 1987; Bottrell and Newton, 2006). However, we currently have only a very general understanding of how marine organic matter, which is predominantly remineralized before reaching the sediments, is converted into kerogen, which can survive in rocks for millions of years. Relatively high concentrations of OM can be buried in sediments underlying highly productive parts of the ocean, especially where O_2 is depleted in the water column (e.g., Hartnett et al., 1998). In the absence of available O_2, microbial communities turn to a web of sulfur- and nitrogen-based metabolisms (etc.) to oxidize OM and produce energy. These metabolic networks can generate substantial amounts of sulfide (HS^-), which in addition to being further metabolized can react abiotically with organic matter, forming abiogenic organic sulfur (OS) and making the OM more resistant to remineralization (Kohnen et al., 1989; Boussafir et al., 1995). Organic matter sulfurization is thought to have facilitated the deposition and burial of massive amounts of OM in the Kimmeridge Clay and other important petroleum source-rocks (van Dongen et al., 2006). It has received less attention, however, as a potential mechanism affecting the burial of sulfur and carbon in modern marine sediments.

We have a general understanding of mechanisms by which sulfide and specific organic structures, like aldehydes and alkenes, can react in the laboratory. Many studies have also identified individual organosulfur compounds in natural environments and have tracked the bulk increase of S in total OM. Still, it has been difficult to link these scales and understand the role of OM sulfurization in global and regional OM preservation. Other work has emphasized the potential role of OM, particularly humic acids, as an oxidant for sulfide (Heitmann and Blodau, 2006). Outside of these fields, however, OS is often disregarded or combined with inorganic sedimentary S (pyrite) in models of global biogeochemistry.

A primary impediment to the study of sedimentary OS was for a long time methodological. Throughout the thesis, we have made use of recently developed analytical techniques that permit the analysis of a wide variety of organic and inorganic sulfur species, including individual compounds, from small samples (Paris et al., 2014; Amrani et al., 2010). These methods have made it possible to make progress on several long-standing questions about the formation of OS and its S-isotope composition. Specifically, we use the distribution of the two main isotopes of sulfur, ^{32}S and ^{34}S, to track important transformations in the sulfur cycle. The enzymes driving microbial S metabolisms often exhibit strong isotopic effects and leave characteristic $\delta^{34}S$ signals in the residual reactant and product S pools. We can therefore use the relationships among the S-isotope compositions of different sedimentary phases to infer how sulfur is cycling in the environment. In rocks, solid phases like pyrite and OM may preserve this isotopic information and allow us to learn about sulfur- and carbon-cycling processes in the geologic past.

This thesis is motivated by two questions that are relevant to both geologic and modern timescales. First, how and where does sulfurization occur in O_2-depleted marine environments? And secondly, how are the S-isotopic compositions of OS and pyrite affected by processes and conditions in the sedimentary environment?

This thesis is divided into four main chapters. Chapters 2 and 3 investigate rates and mechanisms of OM sulfurization in Cariaco Basin, where the water column is sulfidic. Chapter 4 presents high-resolution records of OS, pyrite, and other important sedimentary phases from a less strongly O_2-depleted environment along with hypotheses to explain them. Finally, Chapter 5 describes experiments testing aspects of a hypothesis from the previous chapter.

GC-amenable, solvent–extractable organosulfur compounds from Cariaco Basin were the targets of the first part of this work. We measured the S-isotopic compositions of these compounds in one of the first applications of compound-specific S isotope analysis by GC–ICP–MS. All of the organosulfur compounds are more ^{34}S-depleted than bulk extractable OS pools and porewater sulfide. They are also generally unrepresentative of the S-isotope composition of total extractable OS, which is more similar to proto-kerogen. At least some of these low-molecular-weight compounds form over hundreds of years of sediment diagenesis. They may have a distinct S-isotope composition from other sedimentary OS because they form by intramolecular sulfurization, which could impart a large kinetic-type isotope effect. Alternatively, they could form from relatively ^{34}S-depleted sulfide within

biogenic microenvironments like those that we invoke to explain the S-isotope composition of pyrite in Santa Barbara Basin. If these compounds incorporate sulfur that is more ^{34}S-depleted than porewater, their synthesis could impart a smaller isotope effect while still being less reversible than most OM sulfurization reactions. Unlike individual organosulfur compounds, most of the OS in proto-kerogen appears to have formed within the upper centimeters of sediment. Although several studies have argued for very early sulfurization (Francois, 1987; Bruchert and Pratt, 1997), it has been difficult to estimate OM sulfurization rates given the temporal resolution of surface sediments. In Chapter 3, we take advantage of our ability to measure OS in particle trap samples to gain a more high-resolution view into OM sulfurization in Cariaco Basin.

The S:C ratios and δ^{34}S values of OM from particles from Cariaco Basin indicate that substantial OM sulfurization can occur in sinking particles on timescales of days or less, given the right environmental conditions. We find evidence for particularly extensive OM sulfurization in particles during periods of strong upwelling and high surface productivity. Depending on the frequency of these periods, the amount of abiogenic OS delivered to sediments from particles can account for most of the OS in proto-kerogen in shallow sediments. OM sulfurization in particles could be an important mechanism for enhancing the preservation of OM under O_2-limited conditions, and may have been particularly important during periods of Earth history characterized by enhanced OM burial like the Cretaceous ocean anoxic events.

Chapter 4 presents geochemical records for multi- and gravity cores from Santa Barbara Basin, a basin off the coast of California with a restricted circulation and generally 'sub-oxic' bottom water. We measure the concentrations and isotopic compositions of sedimentary S, C, and Fe phases in 2.5-cm resolution over multi- and gravity cores from the center of the basin. We find that pyrite is much more ^{34}S-depleted than porewater sulfide, which has an S-isotope composition closer to OM. The distribution of S isotopes in Santa Barbara Basin sediments is inconsistent with the hypothesis that strongly ^{34}S-depleted pyrite is derived from recycling and disproportionation of more ^{34}S-enriched sulfide. We propose that pyrite is forming in microenvironments near sulfide-generating microbial communities and takes on the initial δ^{34}S value of this sulfide. In environments like the upper 40 cm of Santa Barbara Basin sediments where sulfide generation rates are low (<0.01 mM/yr) and reducible Fe is available, relatively little sulfide escapes precipitation and diffuses into porewater, where it interacts with a much larger pool of organic S and apparently exchanges with it. In deeper sediments, the exchangeability of OS appears to decline while the concentration of sulfide increases due to upward diffusion of relatively ^{34}S-enriched sulfide from the sulfate-methane transition zone. Under these conditions, which may be common in OM-rich sediments, exchange between sulfide and OS pulls the δ^{34}S value of OS toward higher values, potentially increasing its δ^{34}S offset from concurrent pyrite.

The experiments in Chapter 5 test the hypothesis that OS can exchange S atoms with sulfide under environmentally relevant conditions. Using ^{34}S-labeled polysulfide solutions,

we find evidence for exchange between sulfide and several types of OS, including thiols and low-molecular-weight organic (di)sulfides as well as natural sedimentary OM. Natural OM and dissolved sulfide $\delta^{34}S$ values indicate extensive S-isotope exchange within 14 days, indicating that this process may have important effects on the distribution of ^{34}S in Santa Barbara Basin and other O_2-depleted environments. The details of OS–H_2S interaction in the cysteine incubations may also provide insights into mechanisms for incorporating biogenic OS into proto-kerogen.

Taken together, Chapters 1–5 yield some fresh answers to decades-old questions.

When and how does OM sulfurization occur in modern, O_2-depleted environments?

Sulfur-rich OM (S:C > 1%, mol/mol) is frequently observed near the sediment–water interface in O_2-depleted environments, and OM sulfurization is also frequently described as a kyr-scale process in sediments. Our results confirm and clarify that OM sulfurization processes operate on at least two distinct timescales. In one case, OM and S_x^{-2} react within days or less in sinking OM-rich particles or near a sedimentary redox interface. Given the right environmental conditions, rapid OM sulfurization can be a major source of relatively stable, S-rich OM to sediments. A second category of sulfurization reactions occur during early sediment diagenesis (hundreds to thousands of years) and can also contribute substantially to total proto-kerogen S. Extractable, S-bearing organic compounds generally accumulate on these timescales. In Cariaco Basin, we estimate that nearly half of proto-kerogen S at 6 m

depth is water column-derived while about one-third formed below 10 cm. The situation is similar in Santa Barbara Basin, where the majority of proto-kerogen S forms in sediments near the sediment-water interface, but slower sulfurization reactions also contribute significantly to total proto-kerogen S in deeper sediments.

Polysulfides appear to have a central role in rapid organic matter sulfurization. The $\delta^{34}S$ values of proto-kerogen, a sulfurized organic compound, and elemental S are correlated throughout a period of enhanced OM sulfurization in Cariaco particles, implicating polysulfides as key reactants. Additionally, we find evidence for organic polysulfides as intermediate structures during the formation and maturation of OS over days to weeks in the laboratory. When polysulfides are absent, OM and sulfide continue to interact via both gradual sulfurization and exchange, but both of these processes are more kinetically limited.

How are the S-isotopic compositions of OS and pyrite affected by processes and conditions in the sedimentary environment?

The canonical interpretation of the distribution of S isotopes in sediments is that pyrite records the $\delta^{34}S$ value of sulfide in porewater, which records the $\delta^{34}S$ value of the sulfide generated by microbial sulfate reduction. To explain pyrites that are more ^{34}S-depleted than sulfide, additional S-cycling metabolisms have been invoked to generate a separate sulfide source. The results of this thesis challenge that standard

model and propose an alternative that is capable of explaining several widespread, but often overlooked, observations in the literature.

We propose that pyrite precipitation is favored in sulfide–forming microenvironments, where it should sample the initial products of microbial sulfate reduction. The $\delta^{34}S$ value of this sulfide does not need to be the same as that of the equilibrated sulfide in porewater, especially in the presence of abundant OS. In shallow sediments, a substantial proportion of the OS in proto-kerogen can react and/or equilibrate with sulfide. Because sulfide tends to become more ^{34}S-enriched with depth, its ongoing equilibration with OS in deeper sediments may help explain why proto-kerogen is variably more ^{34}S–enriched than pyrite in rocks. Through this mechanism, OM $\delta^{34}S$ values may retain information about the relative abundances of sulfide and OS in the depositional environment, which should help constrain important environmental variables like rates of microbial sulfate reduction and the position of the chemocline in the geologic past.

Overall, we conclude that OS is a more active and important player in the sedimentary cycles of carbon and sulfur than generally assumed, and it is also a potentially useful archive of environmental information. Given the recent and ongoing expansion in our analytical capabilities, there is great potential for future investigations into OS to continue to yield valuable insights into aspects of global biogeochemistry.

REFERENCES

Amrani, A., Sessions, A., & Adkins, J. (2009). Compound-specific δ34S analysis of volatile organics by coupled GC/multicollector-ICPMS. *Anal. Chem.*, *81*, 9027–9034.

Berner, R. A. (1987). Models for carbon and sulfur cycles and atmospheric oxygen; application to Paleozoic geologic history. *American Journal of Science* (Vol. 287, pp. 177–196). American Journal of Science. http://doi.org/10.2475/ajs.287.3.177

Bottrell, S., & Newton, R. (2006). Reconstruction of changes in global sulfur cycling form marine sulfate isotopes. *Earth Science Reviews*, *75*, 59–83.

Boussafir, M., Gelin, F., Lallier-Verges, E., Derenne, S., Bertrand, P., & Largeau, C. (1995). Electron microscopy and pyrolysis of kerogens from the Kimmeridge Clay Formation, UK: Source organisms, preservation processes, and origin of microcycles, *59*(18), 3731–3747.

Brüchert, V., & Pratt, L. M. (1996). Contemporaneous early diagenetic formation of organic and inorganic sulfur in estuarine sediments from St. Andrew Bay, Florida, USA. *Geochimica Et Cosmochimica Acta*, *60*(13), 2325–2332.

Francois, R. (1987). A study of sulphur enrichment in the humic fraction of marine sediments during early diagenesis. *Geochimica Et Cosmochimica Acta*, *51*, 17–27.

Hartnett, H. E., Keil, R. G., Hedges, J. I., & Devol, A. (1998). Influence of oxygen exposure time on organic carbon preservation in continental margin sediments. *Nature*, *391*(6667), 572–575. http://doi.org/10.1038/35351

Heitmann, T., & Blodau, C. (2006). Oxidation and incorporation of hydrogen sulfide by dissolved organic matter. *Chemical Geology*, *235*, 12–20.

Kohnen, M., Damste, J. S., Haven, ten, H. L., & De Leeuw, J. W. (1989). Early incorporation of polysulfides in sedimentary organic matter. *Nature*, *341*, 640–641.

Paris, G., Adkins, J. F., Sessions, A. L., & Subhas, A. (2013). MC-ICP-MS measurement of δ34S and Δ33S in small amounts of dissolved sulfate. *Chemical Geology*, *345*, 50–61.

van Dongen, B. E., Schouten, S., & Sinninghe Damsté, J. S. (2006). Preservation of carbohydrates through sulfurization in a Jurassic euxinic shelf sea: Examination of the Blackstone Band TOC cycle in the Kimmeridge Clay Formation, UK. *Organic Geochemistry*, *37*(9), 1052–1073. http://doi.org/10.1016/j.orggeochem.2006.05.007

C h a p t e r 2

THE SULFUR ISOTOPIC COMPOSITIONS OF INDIVIDUAL ORGANIC COMPOUNDS FROM CARIACO BASIN

"Raven, M. R., Adkins, J. F., Werne, J. P., Lyons, T. W., & Sessions, A. L. (2015). Sulfur isotopic composition of individual organic compounds from Cariaco Basin sediments. *Organic Geochemistry*, *80*, 53–59. http://doi.org/10.1016/j.orggeochem.2015.01.002

ABSTRACT

Reactions between reduced inorganic sulfur and organic compounds are thought to be important for the preservation of organic matter in sediments, but the sulfurization process is poorly understood. Sulfur isotopes are potentially useful tracers of sulfurization reactions, which often occur in the presence of a strong porewater isotopic gradient driven by microbial sulfate reduction. Prior studies of bulk sedimentary organic matter indicate that sulfurized products are ^{34}S-enriched relative to coexisting sulfide, and experiments have produced ^{34}S-enriched organosulfur compounds. However, analytical limitations have prevented this relationship from being tested at the molecular level in natural environments. Here we apply a new method, coupled gas chromatography – inductively coupled plasma mass spectrometry, to measure the compound-specific sulfur isotopic compositions of volatile organosulfur compounds over a six-meter-long core of anoxic Cariaco Basin sediments. In contrast to current conceptual models, nearly all extractable organosulfur compounds are substantially depleted in ^{34}S relative to coexisting kerogen and porewater sulfide. We hypothesize that this ^{34}S depletion is due to a normal kinetic isotope effect during the initial formation of a carbon-sulfur bond and

that the source of sulfur to this relatively irreversible reaction is most likely the bisulfide anion in sedimentary pore water. The ^{34}S-depleted products of irreversible bisulfide addition alone cannot explain the isotopic composition of total extractable or residual organic matter. Therefore, at least two different sulfurization pathways must operate in Cariaco Basin, generating isotopically distinct products. Compound-specific sulfur isotope analysis thus provides new insights into the timescales and mechanisms of organic matter sulfurization.

1. INTRODUCTION

Organic matter is preserved in sediments as a complex macromolecular structure known as kerogen. However, many of the mechanisms for forming kerogen are still poorly understood. (Aizenshtat et al., 1995; Eglinton et al., 1994; Francois, 1987; Vandenbroucke and Largeau, 2007). Organic molecules are sometimes bound to the kerogen matrix by sulfur bridges, and organic sulfur in a variety of aromatic and aliphatic ring structures can also be extracted from immature sediments (Sinninghe Damsté et al., 2007; Vairavamurthy and Mopper, 1987; Vairavamurthy et al., 1994) and crude oils (e.g., Schmid et al., 1987; Sinninghe Damsté et al., 1987; Sinninghe Damsté and De Leeuw, 1990). Although some of the organic sulfur compounds (OSC) observed in marine sediments have been reproduced under laboratory conditions (Amrani and Aizenshtat, 2004a; 2004b; de Graaf et al., 1992; Kok et al., 2000; LaLonde et al., 1987; Rowland et al., 1993; Schouten et al., 1994), the relationship between sulfurization reactions in natural systems and the sulfur-isotopic composition of sedimentary organic matter has not yet been determined.

Organic sulfur (OS) in kerogen or proto-kerogen, which we refer to as 'residual' OS, is typically more enriched in ^{34}S than its likely sulfur sources, either bisulfide or polysulfide species in coexisting porewater (Anderson and Pratt, 1995; Bottrell and Raiswell, 2000). This phenomenon has been difficult to explain based on experimental (Amrani and Aizenshtat, 2004) and initial compound-specific $\delta^{34}S$ results (Werne et al., 2008).

Moreover, only a subset of available functionalized organic compounds are affected by sulfurization reactions, while others persist in sediments without experiencing sulfurization. In this study, we investigate whether sulfur isotopes can provide a tracer for mechanisms of organic sulfur formation at the molecular level. We use a newly developed method for compound-specific sulfur isotope analysis (Amrani et al., 2009) to obtain $\delta^{34}S$ values for individual, GC-amenable organosulfur compounds from Cariaco Basin sediments.

Sulfur isotopic compositions are a potentially powerful tool for exploring the timing and mechanisms of organic sulfurization reactions due to the large down-core porewater sulfur isotope gradients typically generated by microbial sulfate reduction in anoxic sediments. The sulfur isotopic compositions of bulk pools have previously been used to constrain the timing of kerogen and extractable OSC formation relative to pyrite and other sedimentary sulfur sinks. However, because OSC form at different rates and during various stages of early diagenesis (Sinninghe Damsté et al., 2007; Vairavamurthy et al., 1994; Vairavamurthy and Mopper, 1987; Werne et al., 2008), bulk organic sulfur potentially represents a mixture of OSC with diverse $\delta^{34}S$ values. Our results represent the first $\delta^{34}S$ measurements for individual organosulfur compounds in complex lipid extracts from marine sediments.

2. SITE BACKGROUND

Samples for this study were taken from Cariaco Basin, located north of Venezuela. The Cariaco Basin water column is anoxic and sulfidic below 300 m, which facilitates the delivery of moderately high concentrations of reduced inorganic sulfur species and organic carbon (up to 6 wt%) to the sediments, making this an excellent site to study organic sulfurization reactions. Sample material was obtained from Ocean Drilling Program (ODP) Core 1002B, which was collected from the western side of Cariaco Basin at Site 165 at approximately 900 m water depth (Shipboard Scientific Party, 1997). The core was frozen immediately following collection, with the exception of the shallowest material (40 cm sample), which was squeezed to extract porewater onboard and then frozen. The core has been stored frozen since that time. Eight subsamples of the core were obtained from the frozen archive in 2011, and three additional subsamples were collected in 2012. The subsamples represent approximately 2 cm of homogenized material each and are spaced at eight roughly equal depth intervals between 40 and 535 cm, all within the upper laminated section of the core that appears to have experienced continuous anoxic and sulfidic deposition (Lyons et al., 2003). Our deepest sample is near the contact with underlying massive sediments at approximately 650 cm and represents nearly 12.6 ^{14}C kyr (14.5 calendar kyr) of deposition. The age model for this core is based on correlation of magnetic susceptibility to a nearby core (PL07-39PC) that has been well-dated using radiocarbon (Lin et al., 1997; Werne et al., 2000).

The lithology and geochemistry of Core 1002B have been studied extensively, providing valuable context for our work. Werne and colleagues (2003) presented depth profiles of the concentrations and sulfur-isotopic compositions of pyrite, reactive iron, extractable OS ('bitumen'), residual OS ('kerogen'), total sulfur, and porewater sulfate and sulfide. Other available data for this core include concentrations of organic and inorganic carbon, molybdenum, iron, and aluminum (Lyons et al., 2003), and major biomarker distributions (Werne et al., 2000b).

Porewater sulfate concentrations in Cariaco Basin decline steadily from more than 27 mM at the sediment-water interface to 3.8 mM by 590 cm depth. Porewater sulfide concentrations increase from water column-like concentrations of less than 0.1 mM near the surface to 9.0 mM at 215 cm and then decrease below. Both sulfate and sulfide become progressively ^{34}S-enriched in deeper sediments, a common pattern associated with distillation of the porewater sulfate reservoir by dissimilatory microbial sulfate reduction (Amrani and Aizenshtat, 2004b; 2004a; de Graaf et al., 1992; Kok et al., 2000; LaLonde et al., 1987; Rowland et al., 1993; Schouten et al., 1994; Werne et al., 2003). Pyrite sulfur is present at approximately 1.3 wt% in surface sediments. Deeper diagenetic pyrite formation is relatively minor and likely iron-limited. Throughout the profile, pyrite is similar in its $\delta^{34}S$ values to water column HS^- and is ^{34}S-depleted relative to both coexisting sulfide and kerogen, which is consistent with early formation of pyrite, including formation in the water column (Aizenshtat et al., 1995; Anderson and Pratt, 1995; Lyons et al., 2003). Organic matter is abundant (up to 6 wt% TOC) and sulfur rich

(up to 0.6 wt% kerogen S) (Werne et al., 2003). Organosulfur compounds have also been observed in the extractable lipid fraction below 240 cm (Werne et al., 2000).

3. METHODS AND INSTRUMENTATION

The data presented here were collected iteratively, as separation and analytical methods were incrementally improved over the course of the study (described below). In all cases, two to five grams of frozen sediment were dried under vacuum, and free lipids were obtained by microwave extraction at 100°C for 15 minutes (Mars 5, CEM Corp.) in 9:1 v/v dichloromethane (DCM):methanol (MeOH). Compounds were separated by polarity on a silica gel column (4g) by sequential elution with 4:1 hexane:DCM (F1, 40 mL, all depths), DCM (F2, 40 mL, for 40, 70, 265, and 535 cm depths only), and 1:1 DCM:MeOH (F3, 40 mL, all depths). Initial analysis by gas chromatography (GC) was conducted on a Varian CP-3800 GC equipped with a HP DB5-MS (30 m x 320 μm ID x .25 μm film) capillary column and programmed temperature vaporizing (PTV) injector. GC effluent was split between a Varian Saturn 2200 ion trap mass spectrometer with electron impact (EI) ionization and a Sievers 355 sulfur chemiluminescence detector (SCD) for simultaneous identification and quantification of organosulfur compounds.

3.1 Compound-specific $\delta^{34}S$ analysis by GC-ICPMS

The sulfur-isotopic compositions of individual GC-amenable organic compounds from all fractions were measured with a multicollector inductively-coupled plasma mass spectrometer (MC-ICPMS, Thermo Neptune^{+}) using an Agilent 6890 GC for gas-phase sample introduction and separation following the approach described by Amrani (2009). This GC was operated with the same column type and operating conditions as the Varian instrument but differs in that it has a split/splitless injector. Accuracy was established by repeated analyses of external standard mixtures containing three to six OSC with known $\delta^{34}S$ values. Mean $\delta^{34}S$ values for the combined data for each standard are within 1.4‰ of published EA-IRMS values (Amrani et al., 2009) and have a root-mean-squared variance of 1.5‰. Due to improvements in chromatography and baseline standardization, the 2012 data are all accurate to within 1.0‰ and have a root-mean-squared variance of 0.9‰. Many of the polar fractions (F3, see below) of Cariaco extracts were analyzed in triplicate to assess any additional uncertainty due to the complexity of sample chromatograms. Triplicate analyses for most of the major peaks in this fraction achieved $\delta^{34}S$ standard deviations of 1.3 to 1.8‰, although several peaks with less well-resolved baselines returned a larger range of values. F2 chromatograms were much less crowded, and $\delta^{34}S$ values for duplicate F2 runs varied by a maximum of 0.8‰. This performance is comparable to that reported by Amrani and colleagues for complex environmental samples (Amrani et al., 2012; 2009).

A gas-phase standard (SF_6) with known $\delta^{34}S$ value was used for tuning and calibration of isotope ratios. In our earliest analyses, the argon 'sample gas' for the plasma was preheated by flowing through the GC oven before entering the custom-built heated transfer line. With this arrangement, both sensitivity and $\delta^{34}S$ values drifted systematically (by nearly 10‰ in the latter case) as the GC oven ramped from 80° to 300°C. We now understand that this effect arises from an imperfect response of the Neptune mass flow controllers to changing flow resistance with GC temperature. To account for such effects, sample $\delta^{34}S$ values were standardized to a linear interpolation of frequent SF_6 reference gas peaks (Supplemental Figure 1). In later analyses, we eliminated this drift by isolating the sample gas heating system from the GC oven. In this system, the argon flow was preheated to a constant 320° outside the GC before entering the upstream end of the transfer line to the plasma torch. An additional heating tape was also added at the ground-glass connection between the transfer line and the injector torch to improve the transfer of higher-boiling-point analytes into the plasma. With these modifications, good peak shapes were obtained for compounds eluting at oven temperatures of up to 300°C, permitting sulfur-isotopic analysis of a wider range of GC-amenable compounds. Because $\delta^{34}S$ values for SF_6 drift by less than 1‰ across the GC temperature program under these conditions, drift correction is no longer necessary and standard peaks are not required in the midst of the GC oven temperature program, thus avoiding potential interferences between standard and analyte peaks.

GC-ICPMS data were exported from the Neptune Evaluation software into Isodat v. 3.1 (Thermo) for processing. Results are reported in the conventional $\delta^{34}S$ notation as permil (‰) deviations from the VCDT standard. Accurate and precise $\delta^{34}S$ values were obtained for analytes producing peak areas of at least ~1 Vs, representing approximately 50 pmol of analyte on-column. Unlike for other light isotopes (H, C, N), we have not observed chromatographic separation of sulfur isotopologues, meaning that $^{34}S/^{32}S$ ratios are invariant across even large chromatographic peaks. This is consistent with previous observations (Amrani et al., 2012; 2009). Poor chromatographic peak shapes and/or coelutions were the dominant source of measurement uncertainty, particularly during early analyses. Results were sometimes moderately sensitive to the manually selected background interval due to the contribution of unresolved OSC to the *m/z* 34/32 ratio of background signals, and peaks for which $\delta^{34}S$ values varied by more than 1.5‰ for alternative baseline definitions were discarded. In sum, we conservatively estimate that the data presented here have (1σ) uncertainties of 1.0‰ for F1 and F2 fractions and 1.5‰ for F3. Uncertainties are larger for F3 because the abundant OSC and other compounds in this fraction generate complex chromatograms with poorer baseline resolution. Although these analytical uncertainties are large compared to those typically achieved by conventional sulfur isotope analyses, they are nevertheless much smaller than the scale of isotopic variability observed in the Cariaco sulfur record and therefore still permit meaningful interpretations.

3.2 Analysis of bulk organic fractions by ICPMS

Aliquots of each fraction (F1, F2, F3) of the solvent extract were dried and then oxidized in 30% H_2O_2 at 90° C for 24 hrs to convert organic sulfur to sulfate. Resulting sulfate was then purified on AG1-X8 anionic exchange resin according to the method described in Paris et al. (2013). Resin was washed with ten column volumes (CV) 10% HNO_3^-, conditioned with 10 CV 10% HCl and 10 CV 0.5% HCl, loaded in trace HCl, and washed three times with 5 CV Milli-Q H_2O before sulfate was eluted in 0.5N HNO_3. Sulfate samples were quantified by ion chromatography (IC, Dionex ICS-2000) with an AS-19 anion column and AERS 500 ion regeneration. Concentrations were used to intensity-match samples and the required Na^+ supplement for ICP-MS analysis (Paris et al., 2013). Samples were injected into the plasma torch with a desolvating nebulizer (Aridus) and bracketed with known $\delta^{34}S$ $NaSO_4$ standards. The Neptune was operated in high resolution ($M/\Delta M \sim 10{,}000$) to fully resolve oxygen interferences on masses 33 and 34. Accuracy was assessed by repeated analyses of a seawater sulfate standard. Both accuracy and precision for $\delta^{34}S$ values in this mode of analysis were typically better than ±0.2‰.

4. RESULTS AND DISCUSSION

4.1 Abundance and $\delta^{34}S$ of bulk organic sulfur

Concentrations of extractable OS polarity fractions and total residual OS ('kerogen' from Werne et al. 2003) are shown in Figure 1. In sediments, extractable OS increases with

depth from 17 to 77 nmol S/g_{OC} and represents about 0.1‰ of residual OS. The $\delta^{34}S$ of extractable and residual OS are similar, especially below 40 cm, and range from -18.0‰ to -25.9‰. Polar (F3) material represents 92 to 98% of total extractable OS.

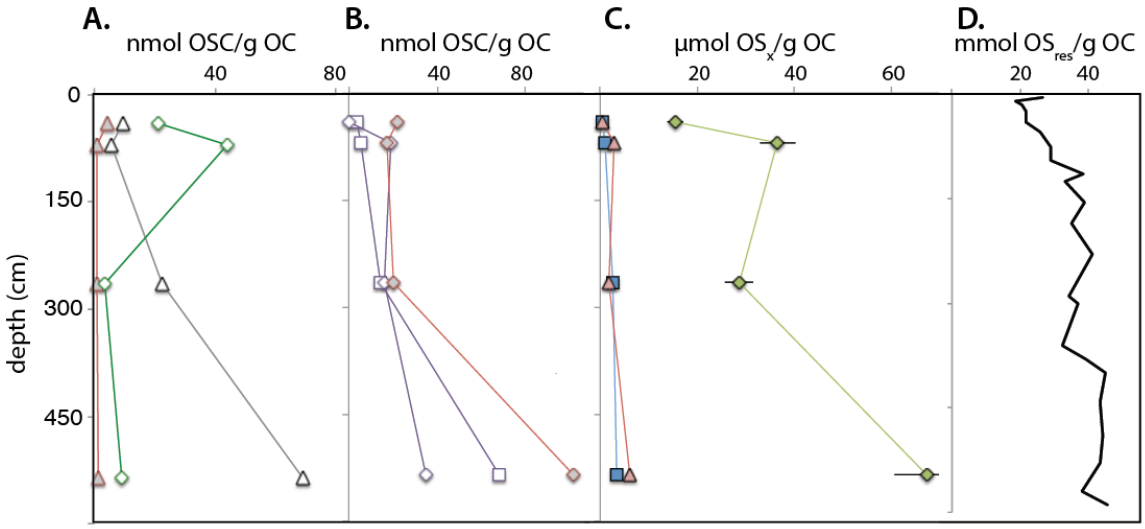

Figure 1: Concentrations of individual OSC and OS pools with depth in Cariaco sediments. *Triangles, squares, and diamonds represent data associated with fractions F1, F2, and F3, respectively. Panels A and B: concentrations of individual OSC. Panel A shows C_{20} isoprenoid thiophene (F1, shaded triangles), triterpenoid thiane (open triangles), and HBI thiolane (diamonds); these compounds are also highlighted in Figure 2. Panel B shows C_{20} isoprenoid thiophene (F3, shaded diamonds) and two unidentified compounds, U-14 (squares) and U-1 (diamonds). Panel C shows total extractable OS in F1 (triangles), F2 (squares), and F3 (diamonds); note scale change. Panel D shows concentration of residual OS. Note that this concentration is expressed relative to organic carbon (OC) rather than sediment mass. OC concentrations average 4.7% wt% throughout the core (data from* Werne et al. 2003*).*

4.2 OSC identification and abundance

A consistent suite of organosulfur compounds was observed by GC-MS-SCD and GC-ICP-MS at all sample depths. Two OSC with well-constrained EI mass spectra are identified as isomers of a C_{20} isoprenoid thiophene. They are inferred derive from the sulfurization of phytol and/or phytadiene based on comparison to published mass spectra (Brassell et al., 1986; Putschew et al., 1996). C_{20} isoprenoid thiophenes have been widely observed in non-polar fractions of extracts from sediments (e.g., Sinninghe Damsté et al., 1987; Wakeham et al., 1995) and experimental studies (de Graaf et al., 1992; Rowland et al., 1993; Krein and Aizenshtat, 1994; Gelin et al., 1998) . In the current work, two identical C_{20} isoprenoid thiophenes were observed in multiple polarity fractions and could not be isolated in a single fraction by column chromatography. The sulfur-isotopic compositions of C_{20} isoprenoids in F1 and F3 fractions from the same sample are similar but not identical, and their concentrations have different trends with depth (Figure 1, shaded compounds in panels A and B), consistent with the C_{20} isoprenoid thiophenes in F1 and F3 representing distinct precursor compounds. Those in the non-polar fraction (F1), which are comparable to previous observations in the literature (e.g., Brassell et al., 1986, Fukushima et al., 1992), are interpreted to represent C_{20} isoprenoid thiophenes present in the original sample. Because thiophenes can form at elevated temperatures, we interpret the more abundant C_{20} isoprenoid thiophenes observed in F3 as forming in the GC injector, for example by ring closure or aromatization of a more polar precursor with a similar phytol-derived skeleton. We find no evidence for either disulfide bonding or thiol groups in the precursors to the C_{20} isoprenoid thiophenes in F3, and the original functional form of these molecules remains the subject of ongoing investigation.

Peaks eluting at 28 min are identified as isomers of highly branched isoprenoid (HBI) thiolanes, presumably derived from the sulfurization of diatom HBI lipids. Mass spectra do not decisively establish whether the sulfur functionality is a thiolane or thiane, although the spectra share all major fragment ions with previously published HBI thiolane spectra (Kohnen, 1991; Kohnen et al., 1990). A single double bond in the molecule is indicated by the molecular ion at *m/z* = 380. HBI thiolanes have previously been observed in Cariaco Basin (Werne et al., 2000), and they were also physically isolated for conventional sulfur-isotopic analysis (Werne et al., 2008). Similar to the C_{20} isoprenoid thiophenes, identical HBI thiolanes are observed in both the apolar (F1) and polar (F3) fractions, with higher abundance in F3 (5 to 63 nmol/g OC) than in F1 (2 to 18 nmol/g OC).

We also observe the monounsaturated triterpenoid thiane that was previously described from Cariaco Basin sediments based on published EI mass spectra (Wakeham et al., 1990; Werne et al., 2000) The abundance of this triterpenoid thiane in our study (6 to 69 nmol/g OC) is in the same range as observed previously (16 to 115 nmol/g OC) (Werne et al., 2000).

One of the only volatile OSC in F2 with a clear EI fragmentation spectrum (designated U-14) is tentatively identified as a thiolane with a twelve-carbon skeleton ($C_{12}H_{20}S$). The fragment with a *m/z* ratio of 127 may represent $C_7H_{11}S$, which contains two double bond equivalents and appears to describe a thiane or thiolane aliphatic sulfide. Aliphatic

sulfides are likely to fragment at the α-β carbon bond, leading us to infer the existence of a five-carbon alkyl chain β to the sulfide sulfur.

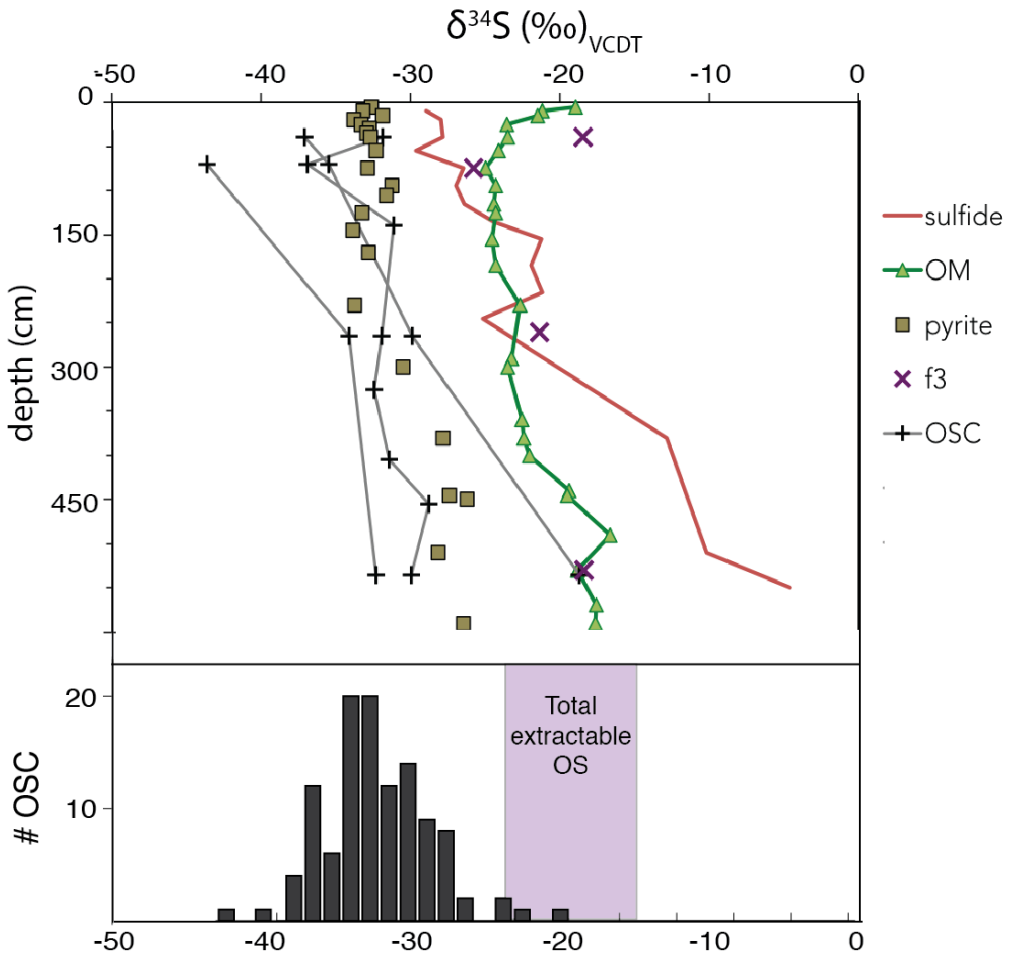

Figure 2: Sulfur-isotopic compositions of OSC and extractable OS fractions. *Porewater sulfide (red line) and residual OS (green triangles) data are from (Lyons et al., 2003; Werne et al., 2003). Panel A: $\delta^{34}S$ values for total polar (F3) OS shown as purple Xs. Crosses indicate $\delta^{34}S$ values of individual GC-amenable compounds in those fractions – triterpenoid thiane in F1, C_{20} isoprenoid in F1, and HBI thiolane in F3. Panel B: Histogram of all compound-specific measurements from Cariaco Basin*

sediment extracts, including both identified and unidentified compounds. The shaded area represents the range of $\delta^{34}S$ measured for total extractable OS.

We were also able to measure $\delta^{34}S$ values for nineteen other OSC in the Cariaco. These OSC are observable by S-specific detectors like the ICPMS and GC-SCD but coelute with much more abundant, non-S-bearing compounds in GC-MS analyses. We were thus unable to obtain useful mass spectra despite attempting a variety of cleanup and fractionation schemes and different ionization methods (EI, CI, MS/MS). Nevertheless, as shown in Figure 2, these unidentified compounds have generally similar sulfur-isotopic compositions and suggest that our identified compounds are representative of the larger population of volatile OSC.

The total amount of OSC observed by GC-ICP-MS was higher in F3 (83 to 306 nmol/g OC) than in F1 (34 to 117 nmol/g OC) or F2 (31 to 178 nmol/g OC). Individual compounds were present at concentrations of 1 to 100 nmol/g OC (Figure 1). The triterpenoid thiane, unidentified compound U-14, and the C_{20} isoprenoid thiophene in F3 were particularly abundant at 535 cm, with concentrations of 68 to 102 nmol/g OC. Their concentrations were consistently lower in the shallower samples (4 to 20 nmol/g OC, Figure 1B). In contrast, the concentrations of HBI thiolanes and C_{20} isoprenoid thiophenes in F1 drop to relatively low values below maxima at 40 cm.

Several compounds have consistently lower $\delta^{34}S$ values than pyrite and represent the most highly ^{34}S-depleted species observed in Cariaco Basin to date. In the shallowest sample, the triterpenoid thiane and HBI thiolane from F3 have $\delta^{34}S$ values of -43.6‰ and -40.9‰, respectively, and less negative $\delta^{34}S$ values in deeper samples (between -32.3‰ and -28.2‰). C_{20} isoprenoid thiophenes from both F1 and F3 are more ^{34}S-enriched than the triterpenoid thiane and HBI thiolanes, with $\delta^{34}S$ values between -37.1‰ and -18.7‰. Depth trends for these compounds are shown in Figure 2A. Figure 2B summarizes $\delta^{34}S$ values for all measured OSC at all depths, including unidentified compounds. OSC $\delta^{34}S$ values have a unimodal distribution around approximately -32 ± 10‰.

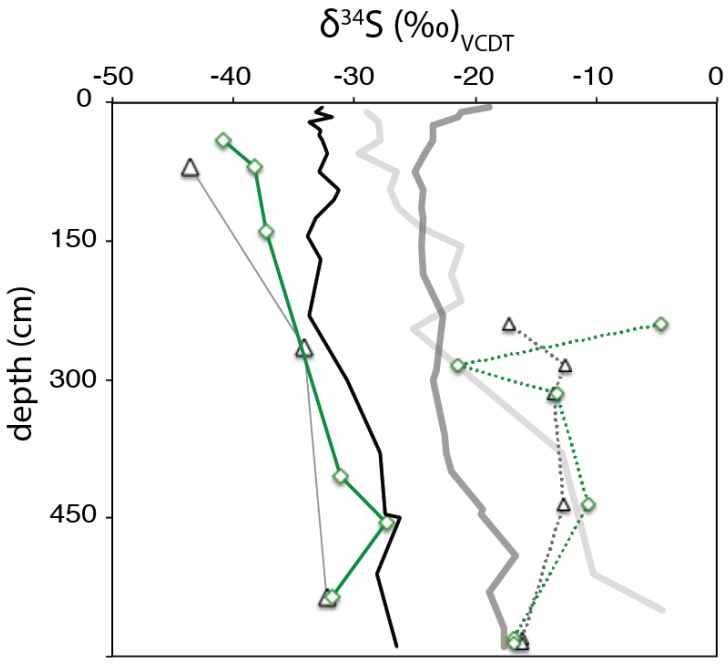

Figure 3: Comparison of compound-specific $\delta^{34}S$ results by different analytical techniques. *Sulfur-isotopic compositions of triterpenoid thiane (triangles) and HBI*

thiolane (diamonds) measured by two different analytical techniques. Symbols represent data obtained by GC-ICP-MS (this study, smooth lines) and prep-LC and EA-IRMS (Werne et al., 2008, dashed lines). Lines without symbols represent residual OS (dark grey), porewater sulfide (light grey), and pyrite (black) $\delta^{34}S$ values (from Lyons et al., 2003; Werne et al., 2003).

The sulfur-isotopic compositions of HBI thiolanes in F1 and the triterpenoid thiane were measured in a previous study of Cariaco Basin sediment extracts by Werne and colleagues (2008). Using preparative liquid chromatography (LC) followed by EA-IRMS, they obtained $\delta^{34}S$ values between -21‰ and -5‰ for depths between 240 and 580 cm, an enrichment of approximately 30‰ relative to our GC-ICP-MS results (Figure 3). As these results apply to the same compounds, both cannot be correct. Given the improved specificity of our GC-ICPMS technique, the LC-EA-IRMS results probably described a mixture of the target OSC and some other coeluting (by LC) or background sulfur species, though there was no indication of additional compounds in the fraction when analyzed by GC-FPD (Werne et al., 2008). Nevertheless, the presence of a sulfur blank in the isolated fractions could potentially explain the high $\delta^{34}S$ values for OSC in Werne et al. (2008), as these sulfur isotope compositions were determined via EA-IRMS.

4.4 Multiple timescales of OSC formation

Volatile OSC in Cariaco Basin sediments have sulfur-isotopic compositions and depth profiles that are similar to coexisting pyrite (Figure 3). A relatively large but variable

proportion of sedimentary pyrite forms in the water column (Lyons et al., 2003); this "syngenetic" pyrite forms in an effectively open system with respect to sulfide, and its $\delta^{34}S$ value is affected by processes at the oxygen-sulfide interface. A smaller component of pyrite in Cariaco Basin sediments is diagenetic, forming in a diffusion-controlled regime within sediments in which sulfide $\delta^{34}S$ values increase with depth (Werne et al., 2003). Like pyrite, Cariaco OSC are likely produced by both syngenetic and diagenetic processes. Different individual compounds, however, may preferentially form in one environment or the other. For example, Werne et al. (2000) conclusively demonstrated diagenetic production of the triterpenoid thiane based on the extent of precursor molecule conversion. Consistent with the conclusions of that study, we find that the triterpenoid thiane increases in concentration from 5.7 to 69 nmol/g OC as its $\delta^{34}S$ value increases from -43.6‰ to -32.3‰. Both concentration and sulfur-isotope data thus support predominantly diagenetic formation of this compound. C_{20} isoprenoid thiophenes in F3 and compound U-14 also have similar concentration profiles with only slightly smaller shifts in their $\delta^{34}S$ values between 70 and 535 cm (Figure 1). Thus they are also probably products of sedimentary diagenesis, forming on timescales of thousands of years.

In contrast, other OSC exhibit no concentration change with depth, thereby providing no conclusive evidence for accumulation during diagenesis. Nevertheless, the $\delta^{34}S$ values of HBI thiolanes from F3, C_{20} isoprenoid thiophene from F1, and compound U-1 also increase by 7‰ to 10‰ over the six-meter core, comparable to the pattern observed for diagenetic OSC and implying ongoing formation. Concentration and $\delta^{34}S$ profiles for

these compounds can be reconciled in one of two ways. First, these OSC may have a significant syngenetic source, with their concentration profiles reflecting variable production in the water column over time. Isotopic variability on the scale of a few permil would then reflect dynamic sulfur cycling near the chemocline, where sulfide $\delta^{34}S$ can vary due to changes in local redox state (Li et al., 2010; 2011). Alternatively, changes in the $\delta^{34}S$ values of non-accumulating OSC with depth could result from slow equilibration between the OSC and (poly)sulfides. Given the scale of depositional variability evident in this core, either scenario seems viable.

4.5 Isotope effects during organic matter sulfurization

The $\delta^{34}S$ profiles for individual OSC in Cariaco Basin reflect a combination of the $\delta^{34}S$ values of the reactant sulfur species, the mechanism of sulfurization, and any associated fractionation during incorporation. Our results help constrain the possible mechanisms of organic matter sulfurization in Cariaco sediments.

Both bisulfide and polysulfide species have been considered probable reactants for organic sulfurization (Anderson and Pratt, 1995). Under typical sedimentary conditions, the dominant species available to react with organic matter are the bisulfide anion (HS^-) and dianionic polysulfide (S_x^{-2}, Schwarzenbach and Fischer, 1960). These same species are involved in pyrite formation (Rickard and Luther, 2007), which occurs at low rates in Cariaco sediments (Lyons et al., 2003; Werne et al., 2003). In Cariaco sediment porewater, the $\delta^{34}S$ value of dissolved HS^- increases from -29‰ near the sediment-water interface to greater than -5‰ at 550 cm depth. Thus, all of the volatile OSC we observe

are more ^{34}S-depleted than coexisting dissolved sulfide, their likely sulfur source. The δ^{34}S difference between porewater sulfide and coexisting OSC is as much as 17‰ (triterpenoid thiane, 70 cm). Polysulfide δ^{34}S has not been measured directly in Cariaco Basin, but experimental work has documented a small ^{34}S enrichment in polysulfides relative to total sulfur at equilibrium (Amrani et al., 2006). We thus predict that polysulfides are slightly more ^{34}S-enriched than bisulfide in Cariaco Basin, and therefore the apparent kinetic isotope effect associated with OSC formation from polysulfides would be even larger than for bisulfide. We also note that oxidants are limiting in Cariaco sediments (Lyons et al., 2003), which should maintain very low polysulfide concentrations and potentially favor organic matter sulfurization reactions involving plentiful bisulfide.

If we assume that porewater (poly)sulfide is the source of sulfur to these ^{34}S-depleted OSC, their formation would appear to involve a normal kinetic isotope effect, i.e., the reaction between (poly)sulfide and an organic molecule proceeds more rapidly for the lighter S isotope. A normal kinetic isotope effect has been previously predicted for initial C-S bond formation (Brüchert and Pratt, 1996) during sedimentary organic matter sulfurization. In contrast, an equilibrium isotope effect will result in ^{34}S-enrichment in the compound with the stronger bond and would be expected to produce OSC that are enriched in ^{34}S relative to (poly)sulfides (Amrani et al., 2004). Reversible reactions should lead to isotopic compositions that are governed by equilibrium isotope effects, whereas irreversible reactions typically record kinetic isotope effects (Hayes, 1993).

Therefore, the sulfurization reactions leading to extractable OSC monomers in Cariaco sediments may be largely irreversible.

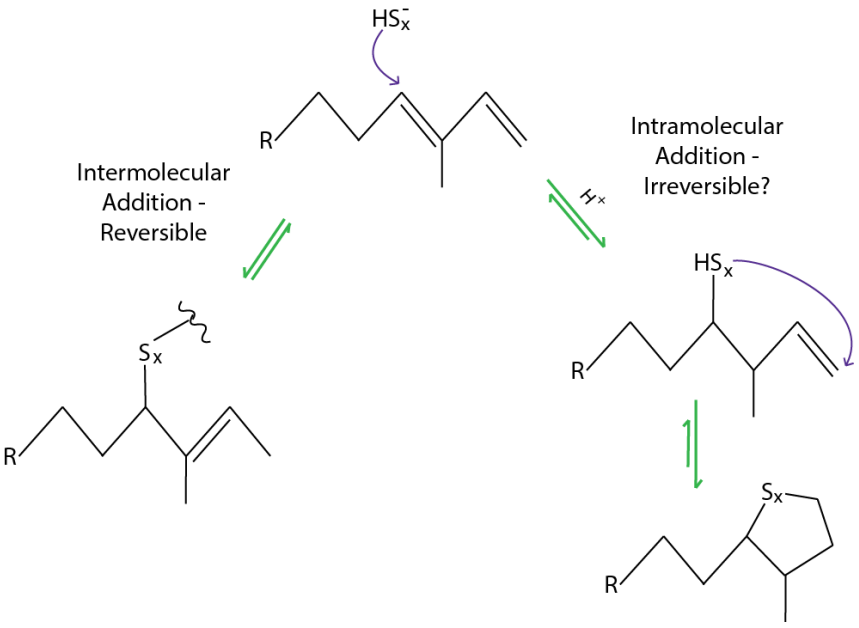

Figure 4: *Examples of intermolecular and intramolecular sulfurization pathways following initial (poly)sulfide attack on a diene. Based on* Kohnen et al. (1990).

Sulfur addition by the bisulfide anion is more likely to be rapid and irreversible than sulfur addition by polysulfide. Initial nucleophilic attack by a bisulfide anion on an organic functional group produces a thiol. In contrast, the initial product of nucleophilic attack by a polysulfide dianion has a chain of two sulfur atoms that retain a negative charge. These products may subsequently undergo reaction with another functional group, either on the same molecule, forming a ring, or on a different molecule, forming a (poly)sulfide bridge (Figure 4). Rapid intramolecular addition would be more energetically favorable for a bisulfide-derived thiol group than for a polysulfide chain due

to the relative strength of the S-S bond compared to the S-H bond. It is likely – although not certain for compounds appearing in multiple fractions – that all of the volatile compounds we identified in Cariaco lipid extracts experienced intramolecular addition for that second step. Therefore, if we assume that volatile OSC monomers in Cariaco Basin derive from either porewater polysulfides or bisulfide, their highly ^{34}S-depleted isotopic compositions appear to derive from the bisulfide anion and a strong kinetic isotope effect.

A large kinetic isotope effect has not been previously reported for organic matter sulfurization. Total residual OS is typically more ^{34}S-enriched than its sulfur source, broadly indicating an equilibrium isotope effect in its formation. This relationship holds both in a global compilation of rocks, where pyrite $\delta^{34}S$ is taken to represent sulfide (Bottrell and Raiswell, 2000) and in modern marine sediments (Dale et al., 2009). However, individual OSC need not conform to models based on total OS. In Cariaco Basin, both extractable and residual OS, which are similar below 70 cm, are significantly more ^{34}S-enriched than the GC-amenable OSC separated from the extractable OS pool. Thus, extractable OS in Cariaco Basin must represent a mixture of OS with distinct S-isotopic compositions.

Based on the preceding evidence, we propose that organic matter sulfurization may be associated with equilibrium or kinetic isotope effects under different conditions (Figure

4). Although all of the volatile OSC measured here by GC-ICP-MS fall in the second category, there is evidence for both types of isotope effect in Cariaco Basin. The formation of GC-amenable OSC in Cariaco Basin also appears to precede sulfur incorporation into residual OS, because all of the major species of volatile OSC are abundant by 40 cm depth, whereas lipid sulfur cross-linking remains minimal at 27 cm (Aycard et al., 2003). Different timescales for the onset of bitumen OSC and sulfurized polymer formation are also consistent with a mechanistic distinction between reversible and irreversible sulfurization pathways.

Alternatively, volatile OSC could potentially form with an equilibrium isotope effect if they derive from a (poly)sulfide pool that has a different isotopic composition than porewater sulfide. Such an isolated pool would need to be substantially more ^{34}S-depleted than porewater sulfide and might be present within cells or in microenvironments in the sediment. Without corroborating evidence for the existence of such an isolated reservoir, this explanation remains highly speculative. Still, if their existence is supported by future work, non-porewater (poly)sulfide reactants could explain OSC with δ^{34}S values that differ from porewater sulfide δ^{34}S without invoking a large kinetic isotope effect during OSC formation.

The hypothesized distinction between the δ^{34}S values of the products of inter- and intramolecular sulfurization reactions may provide a useful constraint on the processes

controlling kerogen formation and a path toward a better understanding of the preservation of organic carbon within the kerogen matrix. Previous attempts at interpreting the sulfur isotopic composition of bulk sedimentary organic matter have suffered from analytical limitations (Wakeham et al., 1995; Werne et al., 2008), presenting a serious impediment to paleoenvironmental studies that rely on sulfur isotopic signals or preserved biomarkers in kerogen to reconstruct paleoenvironmental conditions. Different sulfurization mechanisms may yield distinct isotopic fractionations that will have different effects on sulfur isotope mass balance and on the isotopic signals preserved in sedimentary records. This study is, in part, a proof of concept that should guide future efforts.

5. CONCLUSIONS

The sulfur-isotopic compositions of GC-amenable organosulfur compounds in Cariaco Basin sediments range from -43.6‰ to -18.7‰, similar to coexisting pyrite but more ^{34}S-depleted than total extractable and residual organic sulfur. Organic matter sulfurization in Cariaco Basin appears to occur on multiple timescales. Concentration increases and $\delta^{34}S$ enrichments with depth reflect primarily diagenetic production on kyr-timescales for a triterpenoid thiane, C_{20} isoprenoid thiophene in polar extracts (F3), and unidentified compound U-14, while either variable syngenetic sources or diagenetic sinks exist for HBI thiolanes in both polar and non-polar extracts (F1 and F3), C_{20} isoprenoid thiophene in non-polar extracts (F1), and compound U-1. Regardless of their concentration patterns, all of the observed compounds exhibit a normal kinetic isotope effect relative to their reactant sulfur source, which is most likely porewater bisulfide. This hypothesis contrasts with the equilibrium isotope effects observed for the formation of sulfur-cross-linked OSC polymers from polysulfide (Amrani et al., 2004) and with the incorporation of (apparently) similar sulfur species into kerogen in Cariaco Basin (Aycard et al., 2003). We hypothesize that at least two distinct pathways are at work in generating sedimentary organosulfur molecules and that they may be distinguished by their sulfur isotopic compositions. If correct, compound-specific $\delta^{34}S$ analysis of OSC should provide a powerful tool for unraveling the complex pathways of kerogen formation.

ACKNOWLEDGMENTS

We thank Nathan Dalleska and Guillaume Paris at Caltech for significant analytical assistance, and James Rae, Alon Amrani, Chris Marotta, and Adam Subhas for helpful advice. We also thank two anonymous reviewers, whose comments significantly improved the manuscript. Financial support was provided by the National Science Foundation through award EAR-1024919 to ALS and JFA.

REFERENCES

Aizenshtat, Z., Krein, E., Vairavamurthy, M.A., Goldstein, T., 1995. Role of sulfur in the transformations of sedimentary organic matter: a mechanistic overview, in: Geochemical Transformations of Sedimentary Suflur, Geochemical Transformations of Sedimentary Suflur. ACS Symposium Series 612, Washington, D.C., pp. 16–37.

Amrani, A., Aizenshtat, Z., 2004a. Mechanisms of sulfur introduction chemically controlled: δ34S imprint. Organic Geochemistry 35, 1319–1336. doi:10.1016/j.orggeochem.2004.06.019

Amrani, A., Aizenshtat, Z., 2004b. Reaction of polysulfide anions with α, β unsaturated isoprenoid aldehydes in aquatic media: simulation of oceanic conditions. Organic Geochemistry 35, 909–921.

Amrani, A., Deev, A., Sessions, A., Tang, Y., Adkins, J., Hill, R., Moldowan, M., Wei, Z., 2012. The sulfur-isotopic compositions of benzothiophenes and dibenzothiophenes as a proxy for thermochemical sulfate reduction. Geochimica et Cosmochimica Acta 84, 152–164.

Amrani, A., Kamyshny, A., Jr, Lev, O., Aizenshtat, Z., 2006. Sulfur Stable Isotope Distribution of Polysulfide Anions in an (NH4) 2S n Aqueous Solution. Inorganic chemistry 45, 1427–1429.

Amrani, A., Sessions, A., Adkins, J., 2009. Compound-specific δ34S analysis of volatile organics by coupled GC/multicollector-ICPMS. Anal. Chem. 81, 9027–9034.

Anderson, T.F., Pratt, L.M., 1995. Isotopic evidence for the origin of organic sulfur and elemental sulfur in marine sediments 612, 378–396.

Aycard, M., Derenne, S., Largeau, C., Mongenot, T., Tribovillard, N., Baudin, F., 2003. Formation pathways of proto-kerogens in Holocene sediments of the upwelling influenced Cariaco Trench, Venezuela. Organic Geochemistry 34, 701–718.

Bottrell, S., Newton, R., 2006. Reconstruction of changes in global sulfur cycling form marine sulfate isotopes. Earth Science Reviews 75, 59–83.

Bottrell, S.H., Raiswell, R., 2000. Sulphur isotopes and microbial sulphur cycling in sediments, in: Microbial Sediments, Microbial Sediments. pp. 96–104.

Brassell, S.C., Lewis, C.A., De Leeuw, J.W., de Lange, F., Damste, J.S., 1986. Isoprenoid thiophenes: novel products of sediment diagenesis? Nature 320, 160–162.

Brüchert, V., Pratt, L.M., 1996. Contemporaneous early diagenetic formation of organic and inorganic sulfur in estuarine sediments from St. Andrew Bay, Florida, USA. Geochimica et Cosmochimica Acta 60, 2325–2332.

Dale, A.W., Bruchert, V., Alperin, M., Regnier, P., 2009. An integrated sulfur isotope model for Namibian shelf sediments. Geochimica et Cosmochimica Acta 73, 1924–1944. doi:10.1016/j.gca.2008.12.015

Damste, J., Rijpstra, I., Coolen, M., Schouten, S., Volkman, J., 2007. Rapid sulfurisation of highly branched isoprenoid (HBI) alkenes in sulfidic Holocene sediments from Ellis Fjord, Antarctica. Organic Geochemistry 38, 128–139.

Damsté, J.S.S., De Leeuw, J.W., 1990. Analysis, structure and geochemical significance of organically-bound sulphur in the geosphere: state of the art and future research. Organic Geochemistry 16, 1077–1101.

Damsté, J.S.S., De Leeuw, J.W., Dalen, A.K.-V., de Zeeuw, M.A., de Lange, F., Rijpstra, W., Schenck, P.A., 1987. The occurrence and identification of series of organic sulphur compounds in oils and sediment extracts. I. A study of Rozel Point Oil (U.S.A.). Geochimica et Cosmochimica Acta 51, 2369–2391.

de Graaf, W., Damste, J.S., De Leeuw, J.W., 1992. Laboratory simulation of natural sulphurization: I. Formation of monomeric and oligomeric isoprenoid polysulphides by low-temperature reactions of inorganic polysulhides with phytol and phytadienes. Geochimica et Cosmochimica Acta 56, 4321–4328.

Do Dinur, Spiro, B., Aizenshtat, Z., 1980. The distribution and isotopic composition of sulfur in organic-rich sedimentary rocks. Chemical Geology 31, 37–51.

Eglinton, T.I., Irvine, J.E., Vairavamurth, Zhou, W., Manowitz, B., 1994. Formation and diagenesis of macromolecular organic sulfur in Peru margin sediments. Organic Geochemistry 22, 781–799.

Francois, R., 1987. A study of sulphur enrichment in the humic fraction of marine sediments during early diagenesis. Geochimica et Cosmochimica Acta 51, 17–27.

Fukushima, K., Yasukawa, M., Muto, N., Uemura, H., Ishiwatari, R., 1992. Formation of C20 isoprenoid thiophenes in modern sediments. Organic Geochemistry 18, 83–91.

Gelin, F., Kok, M.D., De Leeuw, J.W., Damsté, J.S.S., 1998. Laboratory sulfurisation of the marine microalga Nannochloropsis salina. Organic Geochemistry 29, 1837–1848.

Hayes, J., 1993. Factors controlling 13C contents of sedimentary organic compounds: principles and evidence. Marine Geology 113, 111–125.

Isotopic evidence for the origin of organic sulfur and elemental sulfur in marine sediments, 1995. Isotopic evidence for the origin of organic sulfur and elemental sulfur in marine sediments, in: Geochemical Transformations of Sedimentary Sulfur. ACS Symposium Series 612, Washington, D.C., pp. 378–396.

Kohnen, M., 1991. Origin and diagenetic transformations of C25 and C30 highly branched isoprenoid sulfur-compounds—further evidence for the formation of organically bound sulfur during early diagenesis. Geochimica et Cosmochimica Acta.

Kohnen, M.E.L., Damsté, J.S., Dalen, A.C.K.-V., Haven, H.L.T., Rullkötter, J., De Leeuw, J.W., 1990. Origin and diagenetic transformations of C 25 and C 30 highly branched isoprenoid sulphur compounds: Further evidence for the formation of organically bound sulphur during early diagenesis. Geochimica et Cosmochimica Acta 54, 3053–3063.

Kok, M., Schouten, S., Damste, J.S., 2000. Formation of insoluble, nonhydrolyzable, sulfur-rich macromolecules via incorporation of inorganic sulfur species into algal carbohydrates. Geochimica et Cosmochimica Acta 64, 2689–2699.

Krein, E.B., Aizenshtat, Z., 1994. The formation of isoprenoid sulfur compounds during diagenesis: simulated sulfur incorporation and thermal transformation. Organic Geochemistry 21, 1015–1025.

LaLonde, R., Ferrara, L., Hayes, M., 1987. Low-temperature, polysulfide reactions of conjugated ene carbonyls: A reaction model for the geologic origin of S-heterocycles. Organic Geochemistry 11, 563–571.

Lyons, T.W., Werne, J.P., Hollander, D.J., Murray, R.W., 2003. Contrasting sulfur geochemistry and Fe/Al and Mo/Al ratios across the last oxic-to-anoxic transition in the Cariaco Basin, Venezuela. Chemical Geology 195, 131–157. doi:10.1016/S0009-2541(02)00392-3

Putschew, A., Scholz-Böttcher, B.M., Rullkötter, J., 1996. Early diagenesis of organic matter and related sulphur incorporation in surface sediments of meromictic Lake Cadagno in the Swiss Alps. Organic Geochemistry 25, 379–390.

Rickard, D., Luther, G.I., 2007. Chemistry of Iron Sulfides. Chemical Reviews 107, 514–562.

Rowland, S., Rockey, C., Al-Lihaibi, S.S., Wolff, G.A., 1993. Incorporation of sulphur into phytol derivatives during simulated early diagenesis. Organic Geochemistry 20, 1–5.

Schimmelmann, A., Kastner, M., 1993. Evolutionary changes over the last 1000 years of

reduced sulfur phases and organic carbon in varved sediments of the Santa Barbara Basin, California. Geochimica et Cosmochimica Acta 57, 67–78.

Schmid, J.C., Connan, J., Albrecht, P., 1987. Occurrence and geochemical significance of long-chain dialkylthiacyclopentanes. Nature 329, 54–56.

Schouten, S., de Graaf, W., Damste, J.S., van Driel, G., De Leeuw, J.W., 1994. Laboratory simulation of natural sulphurization: II. Reaction of multi-functionalized lipids with inorganic polysulphides at low temperatures. Organic Geochemistry 22, 825–834.

Site 1002, 1997. Site 1002, in: Proceedings of the Ocean Drilling Program, Initial Reports. College Station, TX.

Vairavamurthy, A., Mopper, K., 1987. Geochemical formation of organosulphur compounds (thiols) by addition of H2S to sedimentary organic matter. Nature 329, 623–625.

Vairavamurthy, A., Zhou, W., Eglinton, T., Manowitz, B., 1994. Sulfonates: a novel class of organic sulfur compounds in marine sediments. Geochimica et Cosmochimica Acta 58, 4681–4687.

Vandenbroucke, M., Largeau, C., 2007. Kerogen origin, evolution and structure. Organic Geochemistry 38, 719–833.

Wakeham, S., Damste, J.S., Kohnen, M., De Leeuw, J.W., 1995. Organic sulfur compounds formed during early diagenesis in Black Sea sediments. Geochimica et Cosmochimica Acta 59, 521–533.

Werne, J., Hollander, D., Behrens, A., Schaeffer, P., Albrecht, P., Damste, J., 2000. Timing of early diagenetic sulfurization of organic matter: A precursor-product relationship in early Holocene sediments of the anoxic Cariaco Basin, Venezuela. Geochimica et Cosmochimica Acta 65, 1741–1751.

Werne, J., Lyons, T., Hollander, D., Formolo, M., Damste, J., 2003. Reduced sulfur in euxinic sediments of the Cariaco Basin: sulfur isotope constrains on organic sulfur formation. Chemical Geology 195, 159–179.

Werne, J., Lyons, T., Hollander, D., Schouten, S., Hopmans, E., Damste, J., 2008. Investigating pathways of diagenetic organic matter sulfurization using compound-specific sulfur isotope analysis. Geochimica et Cosmochimica Acta 72, 3489–3502.

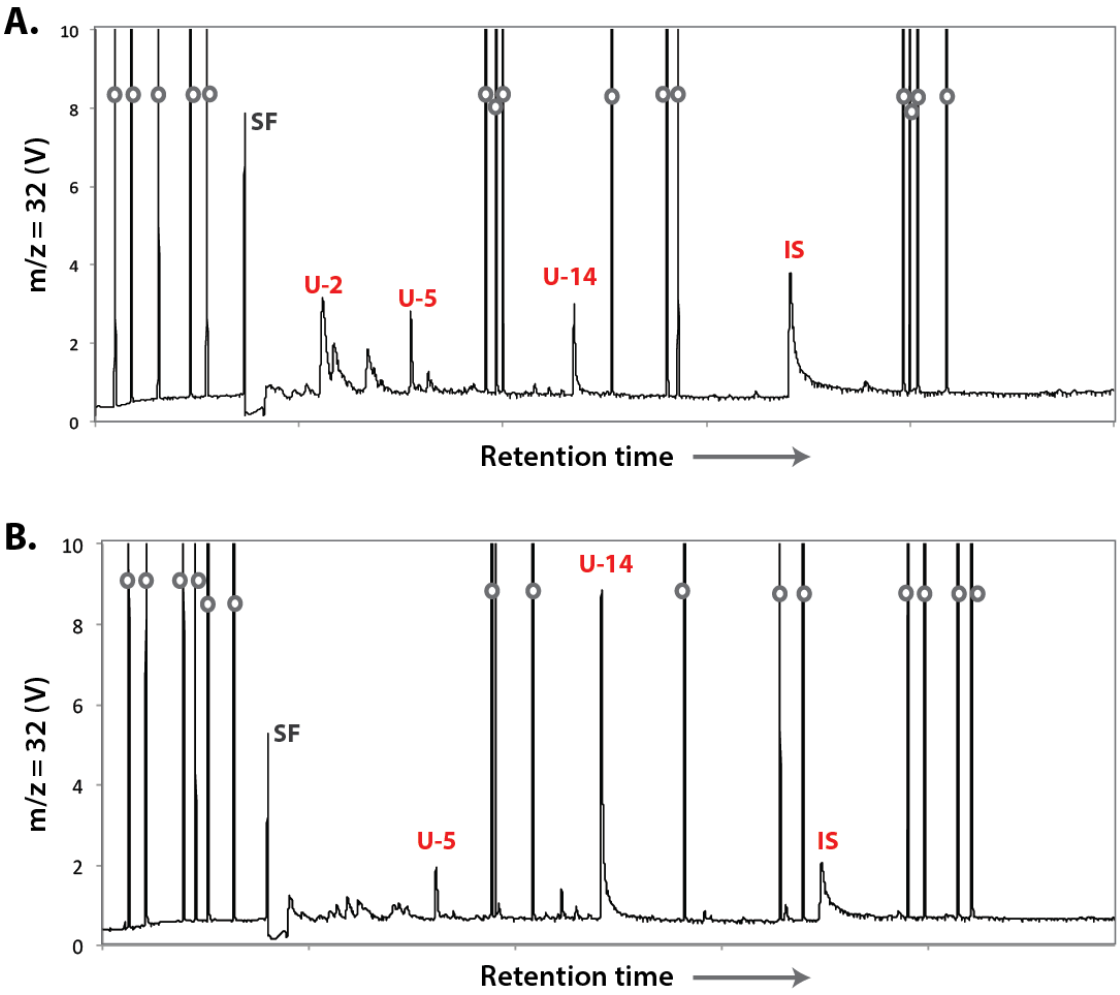

Supplemental Figure 1: Examples of chromatography by GC-ICPMS. *A: 70 cm, F2. B: 535 cm, F2. Grey circles mark SF_6 reference gas peaks; SF = solvent front; IS = internal standard. Both examples include a large number of SF_6 peaks because they were run prior to modification of the sample gas heating system (Section 3.1).*

Chapter 3

RAPID ORGANIC MATTER SULFURIZATION IN THE WATER COLUMN OF CARIACO BASIN

Raven M.R., Sessions A.L., Adkins J.F., Thunell R.C. "Rapid organic matter sulfurization in the water column of Cariaco Basin." *Geochimica et Cosmochimica Acta* (submitted Dec. 2015).

ABSTRACT

Organic matter (OM) burial in marine sediments is a potentially important control on global climate and the long-term redox state of the earth's surface. Still, we have only a limited understanding of the processes that stabilize OM and facilitate its preservation in the geologic record. Abiotic reactions with (poly)sulfides can enhance the preservation potential of OM, but for this process to be significant it needs to compete with OM remineralization, the majority of which occurs before sinking particles reach the sea floor. Here we investigate whether OM sulfurization occurs within sinking particles in the Cariaco Basin, a modern sulfidic marine environment with high rates of OM burial. Proto-kerogen in sinking particles is frequently more sulfur-rich and ^{34}S-depleted than expectations for biomass, with a composition that is difficult to explain by mixing with resuspended or terrigenous material. Instead, it appears that sulfur is being incorporated into OM on a timescale of days in sinking particles. The flux of this abiogenic organic S from particles is equivalent to approximately two-thirds of the total amount of proto-kerogen S at 10 cm depth in underlying sediments (ODP Core 1002B); after 6000 years of more gradual sulfurization reactions, potential water column sources are still

equivalent to nearly half of the total proto-kerogen S in Cariaco sediments. Water column sulfurization is most extensive during periods of upwelling and high primary productivity and appears to involve elemental S, possibly via polysulfides. This process has the potential to deliver large amounts of OM to the sediments by making it less available for remineralization, generating OM-rich deposits. It represents a potentially dynamic sink in the global carbon cycle that can respond to changes in environmental conditions, including the size and intensity of O_2-depleted environments. Water column OM sulfurization could also have played a more significant role in the carbon cycle during ocean anoxic events, for example during the Cretaceous.

1. INTRODUCTION

Only a small fraction of organic matter (OM) produced in the surface ocean escapes remineralization and is buried in marine sediments. Under certain conditions, however, large amounts of OM can be preserved in sediments and enter the long-term carbon cycle, potentially driving major changes in global climate and forming important petroleum source-rocks. OM-rich sediments are commonly associated with sub-oxic or anoxic conditions (Canfield, 1989; Emerson and Hedges, 1988; Hartnett et al., 1998), but the details of the relationship between O_2 availability and OM preservation have been contentious for decades. As the OM produced in the photic zone of the ocean sinks, it is both degraded and transformed (Fig. 1). Especially following plankton blooms, OM can agglomerate and combine with other biogenic material into macro-aggregates that sink to the seafloor within hours to days while some proportion of the OM they contain is remineralized by heterotrophic microorganisms. The sinking flux of OM is less attenuated with depth when O_2 concentrations in the water column are low (Devol and Hartnett, 2001; Keil et al., 2015), and OM is generally more resistant to microbial degradation under anoxic conditions (Harvey et al., 1995; Hulthe et al., 1998). This effect, however, is apparently not due to slower rates of heterotrophic metabolism under anoxic conditions. Previous work suggested that it may instead reflect differences in the accessibility of certain classes of OM to anaerobic microorganisms or their metabolic demands (Lee, 1992; Van Mooy et al., 2002).

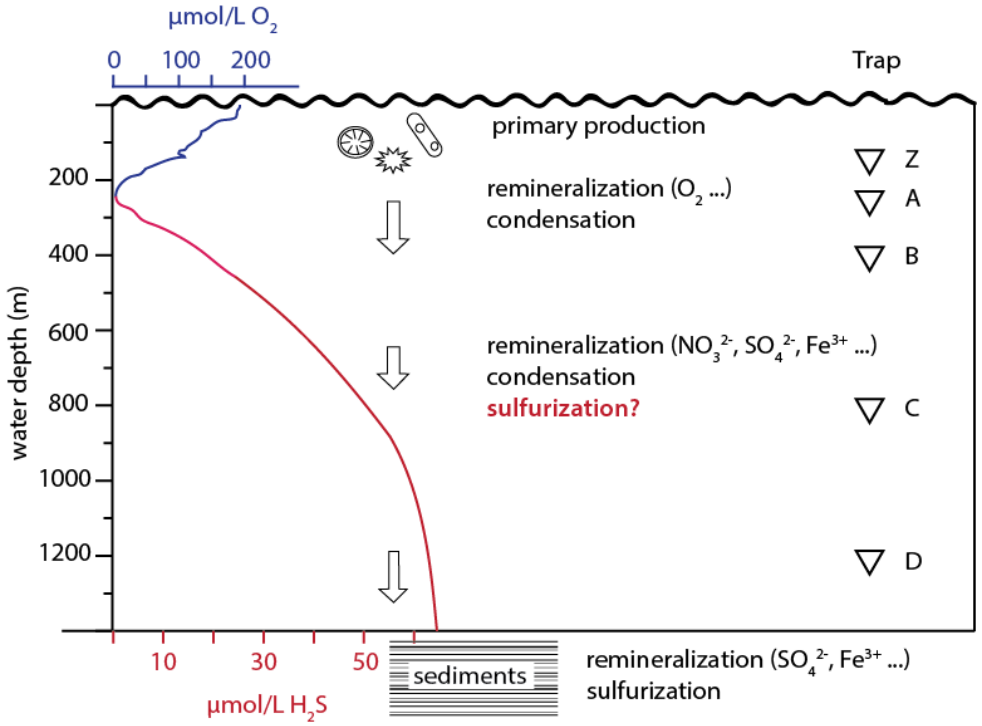

Figure 1. Cartoon of processes affecting sinking organic matter in the oxic and sulfidic parts of the Cariaco water column and underlying sediments. *Dissolved O_2 and sulfide concentration profiles (left) are redrawn from Li et al. (2010). The species listed after 'remineralization' are the canonical electron acceptors for microbial heterotrophy in each zone. Sediment trap depths are shown at right.*

Organic matter sinking through the water column is consumed by microorganisms using a variety of electron acceptors (Fig. 1), generating both dissolved inorganic carbon and small organic molecules. This reactive organic material can subsequently undergo abiotic condensation and polymerization reactions to generate stable, macromolecular, amorphous material called kerogen (Vandenbrouke and Largeau, 2007). Special condensation reactions can occur in the presence of sulfide (e.g., Sinninghe Damsté et al.,

1988; Kohnen et al., 1991) in which sulfur is added to OM by reaction with functionalized organic compounds, generating 'abiogenic organic S.' The resulting sulfur-rich OM is relatively resistant to biodegradation (Boussafir et al., 1995; Sinninghe Damsté and De Leeuw, 1990), making OM sulfurization a potential mechanism for enhancing OM preservation. Still, the timescale of this process – i.e., whether it occurs within sinking particles, versus solely in sediments – remains unclear.

The literature includes examples of sulfurization occurring over thousands of years of sediment diagenesis (e.g., Eglinton et al., 1994) as well as immediately near the sediment surface (e.g., Francois, 1987). Sulfurized OM is commonly observed in very shallow sediments, suggesting rapid formation in the uppermost parts of euxinic environments (Bruchert and Pratt, 1996; Putschew et al., 1996; Werne et al., 2003; Wakeham et al., 1995) or even within anoxic microzones above the H_2S–O_2 interface (Francois, 1987). Li et al. (2011) found elevated concentrations of organic sulfur in suspended particles near the chemocline in the Cariaco Basin water column and proposed that this indicated early OM sulfurization. Rapid OM sulfurization in particles sinking through the water column was also proposed to explain the high S:C ratios in certain OM-rich rocks (van Dongen et al., 2006; Tribovillard et al., 2004). Support for the feasibility of more rapid OM sulfurization is also provided by laboratory experiments. In the presence of phase transfer catalysts and at moderate temperature, kerogen-like polymers and organic sulfur (OS) compounds have been generated from reactions with dissolved polysulfides within weeks (Rowland et al., 1993; Krein and Aizenshtat, 1994; Gelin et al., 1998; Kok et al., 2000; van Dongen et al., 2003). Similar products can form with similar mechanisms and rates

under environmental temperatures and without catalysis (Amrani and Aizenshtat, 2004a). Rapid OM sulfurization could thus substantially enhance the stabilization and burial of OM in anoxic environments. Nevertheless, there is little direct evidence for this process in the modern ocean.

Complicating matters, OM sulfurization in modern, early diagenetic sediments is often described as a process occurring on timescales of hundreds to thousands of years rather than days. The sulfur content of OM increases steadily with depth below the sediment-water interface in Cariaco Basin (Werne et al., 2003, Aycard et al., 2003) as well as Jervis Inlet (Francois, 1987) and the Peru margin (Eglinton et al., 1994), which is thought to reflect gradual, kyr-scale sulfurization. Some lipid-derived organosulfur compounds (OSC) also appear to form on this timescale (Werne et al., 2000; Sinninghe Damsté et al., 2007; Raven et al., 2015). Currently, we have few constraints on the quantitative importance of gradual versus rapid sulfurization reactions or their significance for proto-kerogen formation in marine sediments.

In this study, we approach these questions by interrogating the distribution of sulfur and its isotopic composition in sediment trap material from Cariaco Basin in the context of hydrographic profiles and particle composition time-series data (Thunell et al., 2000; http://imars.marine.usf.edu/CAR/). These μg-scale analyses are made possible via the novel use of use of multicollector inductively coupled plasma mass spectrometry (ICP–MS) to analyze bulk organic fractions (Raven et al., 2016). Sulfide is present in the

Cariaco Basin water column below approximately 250 m depth, and underlying sediments are rich in organic C (~4 wt%) and organic S (~0.3 wt%). We present concentrations and $\delta^{34}S$ values for various pools of organic and elemental sulfur in particles, including individual organosulfur compounds. The results indicate that OM sulfurization does occur in the Cariaco water column following phytoplankton blooms and permit us to make the first quantitative estimates of the significance of water column sulfurization for OM burial in sediments.

2. METHODS

2.1 Study site

Cariaco Basin, located off the north coast of Venezuela, has restricted circulation and becomes sulfidic below its chemocline at approximately 250 m depth (Li et al., 2010, Fig. 1). Seasonal, wind-driven upwelling events fuel strong phytoplankton blooms in the photic zone. As the organic products of these blooms sink, they are remineralized at rates comparable to those from the oxic open ocean and even higher near the chemocline (Muller-Karger et al., 2001). Nevertheless, about 10 $g/m^2/yr$ organic carbon escapes remineralization in the water column and is delivered to underlying sediments. A time-series study was initiated in Cariaco Basin in 1995 (Muller-Karger et al., 2001) and utilizes a set of automated sediment traps positioned at various depths in the water

column (Fig. 1). Trap Z (150 m) is located in water with ~100 μM O_2; Trap A (at 225 m) is typically just above the chemocline, where <10 μM O_2 was recently measured (Li et al., 2011); and Traps B, C, and D (at 400, 880, and 1200 m depth, respectively) are bathed in >20 μM sulfide. Each cone-shaped trap collects sinking particles within a 0.5 m^2 area during 13 sequential two-week-long periods and preserves them with a formalin solution. The sediment trap mooring is recovered and re-deployed every six months. Samples have been stored frozen since collection.

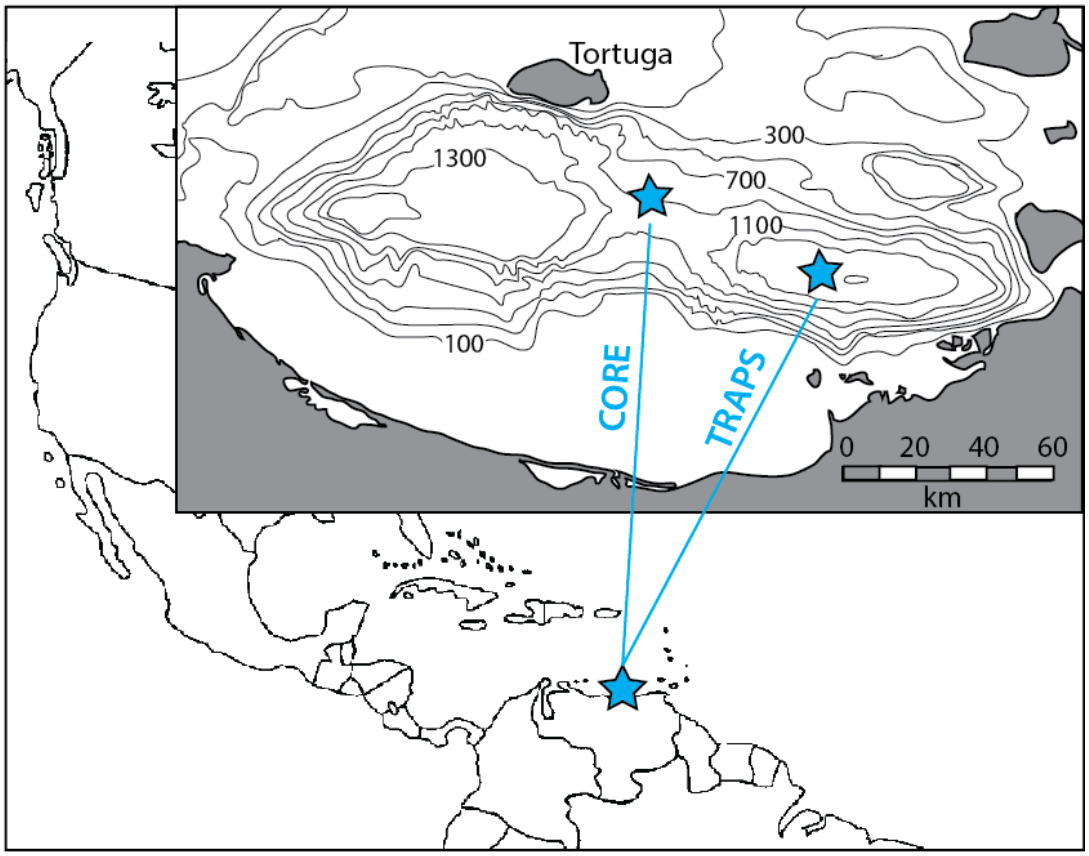

Figure 2: Site Map. *Bathymetry of Cariaco Basin, showing locations of traps and sediment core ODP 1002B.*

Our samples represent splits of the trap material collected during 12, two-week periods between May 1999 and February 2010. For each collection period, we use samples from three or more traps to document depth-related patterns. An initial round of investigation focused on individual sulfur-bearing compounds, and the scope of work was subsequently expanded to include bulk extractable organosulfur fractions and proto-kerogen. Sediment trap samples are compared with previously published data from ODP Core 1002B, primarily Raven et al. (2015), Lyons et al. (2003), and Werne et al. (2003). The core was collected in a shallower part of the basin (900 m water depth, Fig. 2) than the sediment trap mooring.

2.2 Sample Preparation and Analysis

Samples were freeze-dried and microwave-extracted twice into 9:1 dichloromethane (DCM):methanol (MeOH) at 100°C for 15 minutes (MARS 5, CEM Corp). Extracts were separated by silica gel chromatography into non-polar (f1, 4:1 hexane:DCM), intermediate polarity (f2, DCM), and polar (f3, 1:1 DCM:MeOH) fractions. Extractable material that was immiscible in 4:1 hexane:DCM – similar to an asphaltene fraction from a mature deposit – was termed 'strongly polar' (f4). Each fraction was split into aliquots for compound-specific and bulk analysis. Elemental sulfur was removed from the non-polar fraction by exposure to activated Cu (Blumer, 1957), after which an additional aliquot was taken for bulk analysis of non-polar S_{org} (below). Solvent-extracted sediments were washed with Milli-Q water and leached with 1M nitric acid at 20° C for ten days

(Schimmelmann and Kastner, 1993) to oxidize pyrite and hydrolysable organic matter. We refer to the remaining sulfur, which is not soluble in organic solvent, water, or nitric acid, as 'proto-kerogen' for consistency with Raven et al. (2015). Proto-kerogen abundance and $\delta^{34}S$ values were measured by combustion elemental analysis – isotope ratio mass spectrometry (EA-IRMS) with typical analytical uncertainties based on standard replicates of ± 2.5% and ± 0.5‰, respectively.

Aliquots for bulk analysis were dried and oxidized in 30% H_2O_2 (reagent grade) at 90° for 24 hours in glass vials with teflon-coated septa. Sulfate was separated from other ions on AG1-X8 anionic exchange resin (Paris et al., 2013). Resin was washed with ten column volumes (CV) 10% HNO_3^-, conditioned with 10 CV 10% HCl and 10 CV 0.5% HCl, loaded in .05% HCl, and washed with 3 x 5 CV H_2O before sulfate was eluted in 0.5N HNO_3. Sulfate samples were stored dry in Teflon vials until analysis. The sulfur content of each OS fraction was measured as sulfate by ion chromatography (IC, Dionex ICS-2000) with an AS-19 anion column and AERS 500 ion regeneration. Concentrations were used to intensity-match samples and the required Na^+ supplement for analysis using a Thermo Neptune$^+$ multicollector inductively coupled plasma mass spectrometer (ICP-MS) (Paris et al., 2013). Samples were injected into the plasma torch with a desolvating nebulizer (Aridus) and bracketed with known $\delta^{34}S$ $NaSO_4$ standards. The Neptune was operated in medium resolution ($M/\Delta M \sim 8000$) to resolve oxygen interferences on masses 32 and 34. Analytical precision for $\delta^{34}S$ was typically better than ±0.2‰.

Individual organic sulfur compounds within the non-polar and intermediate-polarity fractions were initially investigated with a Varian CP-3800 gas chromatograph (GC) coupled in parallel to a mass spectrometer (MS, Varian Saturn 2200 ion trap) and a sulfur chemiluminescence detector (SCD, Sievers 355). When possible, compounds were identified by their EI mass spectra. The abundance of individual compounds was calculated relative to an internal standard. Subsequently, compound-specific sulfur-isotopic measurements were made using the system originally described in Amrani et al. (2009) as modified by Raven et al. (2015). An Agilent 6890 GC was coupled via a custom-built heated transfer line to the plasma torch of the Neptune^{+} ICPMS operated in medium resolution. Isotope ratios were standardized to a gas-phase standard (SF_6) that can be injected as either discrete peaks or a continuous flow for machine tuning. The argon 'sample gas' constituting the core of the plasma was preheated to 320° prior to meeting the GC helium carrier gas effluent at the downstream end of the 320° transfer line. This system is capable of obtaining accurate and precise (typically better than ±1.0‰) $\delta^{34}S$ values for as little as 100 picomoles of sulfur in an individual, volatile compound. Uncertainties improved to approximately ±0.3‰ for larger, well-resolved chromatographic peaks. Data were exported from the Neptune software to Isodat 3.0 for integration and processing.

3.1 Carbon and sulfur in particulate proto-kerogen

Table 1. Carbon and sulfur data for sinking particles

Date	Trap	Depth	Mass Flux	Proto-kerogen C		Proto-kerogen S		S:C
cup opened		m	$g/m^2/d$	$mmol/m^2/d$	$\delta^{13}C$ (‰)	$\mu mol/m^2/d$	$\delta^{34}S$ (‰)	mol/mol
10/18/06	Z	150	0.33	1.9	--	13	16.8	0.7%
	B	400	1.68	9.0	--	92	12.2	1.0%
	C	880	0.52	2.5	--	--	--	--
	D	1200	0.18	1.0	--	11	10.3	1.1%
2/10/10	Z	150	0.67	4.0	--	58	17.4	1.4%
	A	225	0.66	7.3	-19.5	--	--	--
	B	400	1.91	16.1	-19.4	342	16.3	2.1%
	C	880	1.18	10.2	-19.4	259	14.3	2.5%
	D	1200	0.55	5.6	-19.3	114	14.6	2.1%
1/31/07	B	400	0.58	3.8	-20.0	24	10.6	0.6%
	C	880	0.35	2.5	-19.5	35	9.3	1.4%
	D	1200	0.14	1.4	--	20	8.7	1.5%
2/14/07	B	400	1.56	9.9	-19.5	284	11.8	2.9%
	C	880	1.12	8.5	-19.3	190	13.1	2.2%
	D	1200	0.72	5.5	-19.2	120	10.6	2.2%
2/28/07	Z	150	0.52	2.3	--	31	12.8	1.3%
	B	400	0.71	3.6	-19.8	56	9.8	1.5%
	C	880	0.48	3.0	-19.5	46	10.3	1.5%
	D	1200	0.50	3.2	--	55	8.2	1.7%
3/14/07	A	225	0.65	4.6	-18.5	173	15.4	3.7%
	B	400	0.36	2.6	-18.6	77	13.3	3.0%
	C	880	0.26	1.8	-18.9	68	8.8	3.8%
	D	1200	0.18	1.5	--	--	--	--
3/28/07	B	400	2.08	10.6	-20.4	145	11.1	1.4%
	C	880	2.30	11.8	-20.0	188	9.0	1.6%
	D	1200	0.26	1.6	-20.4	24	11.0	1.5%
averages	A,Z	150-225	0.57	4.0	-19.01	69	15.6	1.8%
	B	400	1.27	7.9	-19.61	146	12.2	1.8%
	C	880	0.89	5.8	-19.43	131	10.8	2.2%
	D	1200	0.36	2.8	-19.62	57	10.6	1.7%
	all		**0.79**	**5.2**	**-19.5**	**105**	**12.0**	**1.9%**

Table 2. Concentration and sulfur isotopic composition of extractable organic fractions and elemental sulfur in sinking particles

Date	Trap	Depth	Elemental S		Non-polar OS		Polar OS		Strongly polar OS	
cup opened		(m)	μmol/m^2/d	δ^{34}S (‰)	μmol/m^2/d	δ^{34}S (‰)	μmol/m^2/d	δ^{34}S (‰)	μmol/m^2/d	δ^{34}S (‰)
10/18/06	Z	400	0.03	-5.2	0.03	10.8	0.33	4.3	0.10	8.2
	B	880	0.21	-8.1	0.32	5.2	1.60	5.0	0.37	8.5
	D	1200	0.01	-1.6	0.05	7.8	0.31	3.1	0.64	0.6
2/10/10	Z	150	0.04	-5.2	0.02	8.9	0.62	14.8	0.18	13.7
	B	400	0.05	-8.1	0.03	10.4	1.99	12.1	0.71	12.4
	D	1200	0.16	-1.6	0.03	7.5	0.54	11.2	0.24	6.2
1/31/07	B	400	0.07	--	0.02	--	0.57	1.8	--	--
	C	880	0.00	--	0.01	--	0.24	-2.6	--	--
	D	1200	0.00	--	0.01	--	0.09	3.8	--	--
2/14/07	B	400	1.31	10.6	0.23	--	2.04	11.5	--	--
	C	880	1.70	10.8	0.13	--	1.83	16.8	--	--
	D	1200	1.51	4.6	0.06	--	1.21	10.4	--	--
2/28/07	Z	150	--	9.7	0.18	5.9	1.56	5.1	0.16	5.9
	B	400	0.00	-4.4	0.08	9.7	1.13	4.0	0.53	13.6
	C	880	0.41	6.9	0.05	--	0.93	10.6	--	--
	D	1200	0.10	-3.9	0.02	8.6	0.94	6.2	0.59	9.6
3/14/07	A	225	4.71	18.9	0.77	--	4.94	7.9	--	--
	B	400	--	--	0	--	--	--	--	--
	C	880	--	--	0	--	--	--	--	--
	D	1200	--	--	0	--	--	--	--	--
3/28/07	B	400	0.17	-5.9	0.07	--	4.14	1.7	--	--
	C	880	4.62	0.0	0.18	--	6.75	10.0	--	--
	D	1200	0.00	--	0.02	--	0.19	2.9	--	--
averages	A,Z	150-225	1.60	4.5	0.25	8.5	1.86	8.0	0.15	9.3
	B	400	0.30	-3.2	0.13	8.4	1.91	6.0	0.54	11.5
	C	880	1.68	5.91	0.09	--	2.44	8.7	--	--
	D	1200	0.30	-0.6	0.03	7.9	0.55	6.3	0.49	5.5
	all		**0.80**	**0.5**	**0.12**	**8.3**	**1.60**	**7.0**	**0.39**	**8.7**

Tables 1 and 2 present results for 26 sediment trap samples collected on seven dates between 2006 and 2010, including five consecutive periods in Winter 2007. Mass flux data in Table 1 are from http://imars.marine.usf.edu/CAR/. The fluxes of organic carbon and sulfur in proto-kerogen average 5.2 mmol C/m^2/d and 105 μmol S/m^2/d (Table 1),

and particles have an average molar S:C ratio of 1.9% (ranging from 0.6% to 3.8%). About fifty-fold less organic S is present in the extractable fractions (Table 2) than in proto-kerogen. The largest fluxes of extractable organic S are for material in the polar fraction (f3, averaging 1.6 μmol S/m^2/d), followed by the strongly polar (f4, 0.39 μmol S/m^2/d) and non-polar (f1, 0.12 μmol S/m^2/d) fractions. The intermediate polarity extractable OS fraction (0.24 μmol S/m^2/d) potentially includes the products of reactions between the trap preservative (formaldehyde) and dissolved sulfide, so we do not discuss it further here. Fluxes of elemental sulfur (S^0) average 0.8 μmol S/m^2/d and range from 0.0 to 4.7 μmol S/m^2/d.

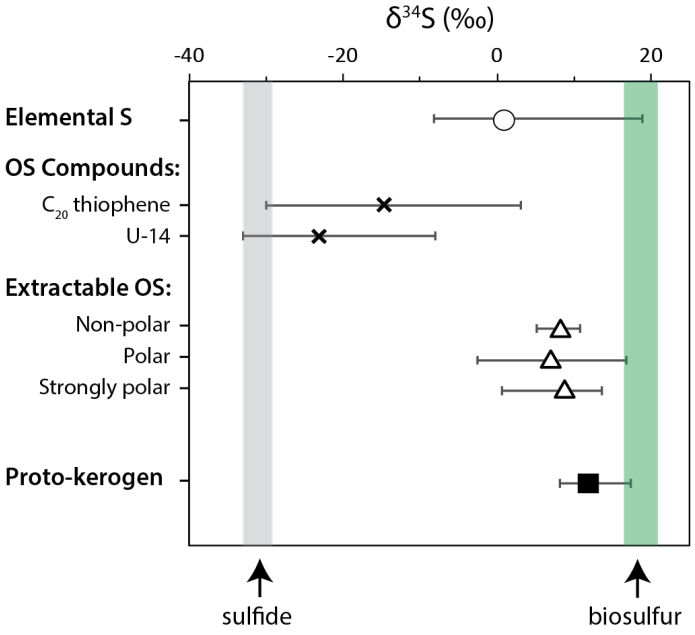

Figure 3. Isotopic compositions of distinct sulfur pools in Cariaco trap materials. *Symbols represent average $\delta^{34}S$ values(in ‰ relative to VCDT) and error bars represent ranges for all dates and depths. The shaded gray bar at left spans the range of all previous observations of sulfide in the water column (Fry et al., 1991; Li et al., 2010).*

The shaded green bar at right spans expected $\delta^{34}S$ values of biosulfur (Kaplan and Rittenberg, 1964). U-14 is an unidentified organosulfur compound previously observed in Cariaco sediments.

The $\delta^{34}S$ values observed for S^0, two individual OS compounds, extractable OS fractions, and proto-kerogen are summarized in Figure 3. All of our $\delta^{34}S$ results fall below seawater sulfate $\delta^{34}S$ (~21.1‰) and that expected for biosulfur. All of the extractable and proto-kerogen OS pools have overlapping $\delta^{34}S$ ranges between 0 and 20‰, with average isotopic compositions of 8.3, 7.0, and 8.7‰ for the non-polar, polar, and strongly polar extractable OS fractions, respectively. Proto-kerogen is somewhat less ^{34}S-depleted on average (12.7‰) than the extractable OS fractions. None of these values match expectations for marine assimilatory biosulfur (18–22‰, Kaplan and Rittenberg, 1964), although individual proto-kerogen and S^0 measurements approach biosulfur-like values on some dates. The isotopic composition of S^0 ranges from -5.9 to 10.8‰ in traps below the chemocline, and reaches 18.9‰ in our 250 m sample from March 2007.

3.2 Compound-specific $\delta^{34}S$ results

Two isomers of a C_{20} isoprenoid thiophene, interpreted as the sulfurized products of phytol, are consistently observed in sediment trap extracts. These compounds match the retention times and EI mass spectra reported for C_{20} isoprenoid thiophenes in Cariaco

sediments (Raven et al., 2015) and prior published mass spectra (Brassell et al., 1986; Putschew et al., 1996). The results presented here for 'C_{20} thiophene' are for the more abundant, earlier-eluting isomer. At concentrations of up to 5.3 nmol S/g, C_{20} thiophene represents less than 1% of the non-polar extractable organic S fraction. High C_{20} isoprenoid fluxes in winter 2007 are associated with a dramatic shift toward more ^{34}S-enriched compositions relative to other investigated dates. C_{20} thiophene δ^{34}S values for March 2007 and February 2010, for example, differ by nearly 30‰. The most ^{34}S-depleted C_{20} thiophenes have δ^{34}S values near -30‰, similar to observations of dissolved sulfide in the Cariaco water column (Li et al., 2010).

We are also able to measure δ^{34}S values for the most abundant GC-amenable organosulfur compound in the intermediate-polarity fraction of 8 samples (Table 2). We previously encountered the same compound in ODP Core 1002B, collected nearby in the basin, and refer to it as "U-14" for consistency with Raven et al. (2015). Nevertheless, attempts to identify this compound are frustrated by its very low concentration relative to other, coeluting compounds, and it can not be measured in samples from winter 2007 because the intermediate-polarity fraction is extremely rich in non-sulfur bearing compounds. Measured δ^{34}S values for U-14 range from -33 to -8‰.

4. DISCUSSION

4.1 Proto-kerogen sulfur in sinking particles

Sinking organic matter in Cariaco Basin is primarily the product of phytoplankton productivity in the surface ocean (Thunell et al., 2000) and contains biosulfur predominantly as cysteine and methionine. The ratio of sulfur to carbon in fresh planktonic biomass is commonly estimated at 1.6% (Wollast et al., 1993) but was also found to range between 0.4% and 1.1% in a variety of diatoms, dinoflagellates, cyanobacteria, algae, and humic acids (Francois et al., 1987 and refs therein). Biosulfur derives from the assimilation of seawater sulfate, which has a $\delta^{34}S$ value of 21.2‰ in the Cariaco Basin (Li et al., 2010). Assimilatory sulfate reduction exhibits very little S-isotope fractionation, so fresh biomass is expected to have a $\delta^{34}S$ value between about 18 and 21.2‰ (Kaplan and Rittenberg, 1964). These ranges for the S:C ratio and $\delta^{34}S$ value of fresh biomass are compared with OM from sediment traps in Fig. 4.

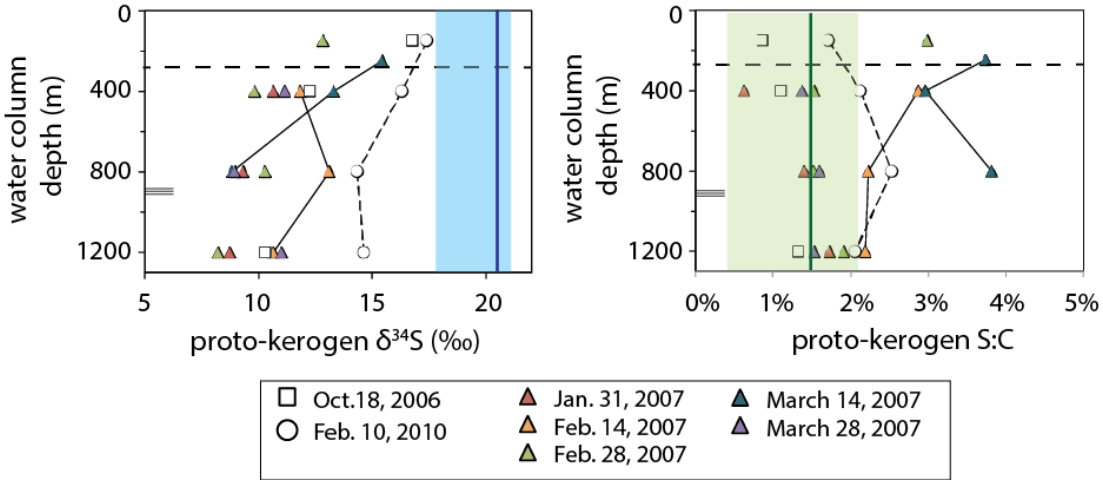

Figure 4. $\delta^{34}S$ values and S:C ratios of proto-kerogen in trap materials. *Data are from five periods in winter 2007 (triangles), February 2010 (open circles) and October 2006 (open squares). At left, the shaded region represents expected biosulfur $\delta^{34}S$ values (Kaplan and Rittenberg, 1964), and the heavy vertical line represents seawater sulfate $\delta^{34}S$. At right, the shaded region encompasses previously reported values of 'typical' S:C (mol/mol) ratios in particulates and the heavy vertical line represents the value for typical algal biomass from Wollast et al. (1993). Depth profiles connected with lines fall within the 'S-addition' field discussed below. The dashed horizontal line in both panels shows the approximate position of the chemocline in Cariaco Basin. Hash marks at ~900 m on each panel indicate the total water depth at the location of ODP Core 1002B.*

The sulfur isotopic composition of particulate proto-kerogen is more ^{34}S-depleted than the range of anticipated biosulfur in all of our samples (Fig. 4), and we find coherent patterns in $\delta^{34}S$ values by date. The most biosulfur-like $\delta^{34}S$ values for proto-kerogen (up to 17.9‰) are observed in February 2010 and above the chemocline in October 2006,

while proto-kerogen is more strongly ^{34}S-depleted below the chemocline in October 2006 and throughout winter 2007. S:C ratios of proto-kerogen are substantially higher than biomass during three of the five sampling periods in winter 2007 and in 'C' trap in February 2010. Proto-kerogen S:C ratios are in some cases more than twice those of fresh algal biomass, reaching 3.8% (Fig. 4). The average S:C ratio in Cariaco particles, 1.9%, is similar to ratios reported for a variety of OM-rich sediments, including the Cariaco Basin (mean 2.4% in the upper 100 cm, Werne et al., 2003), the Kimmeridge Clay (≤6%, mean 2.5%, Van Kaam-Peters et al., 1998), the Peru Margin (1.1% – 5.6%, Mossman et al., 1991), a salt marsh in Delaware, USA (~5% in base-extractable humic material, Ferdelman et al., 1991), and Jervis Inlet (1.1 to 1.9%, Francois, 1987). Comparable ratios were also found in particles from the Philippine Sea (Chen et al., 1996, Fig. 5). Lower S:C ratios were reported for sediments with variable OM contents off the coast of California (0.6 to 1.5%, Nissenbaum and Kaplan 1972). Although the position of the chemocline varies among these environments, their S:C ratios are reminiscent of those from sinking particles in Cariaco Basin, suggesting that rapid sulfurization – in particles, shallow sediments, or sulfidic microenvironments – may be important for OM preservation in diverse environments.

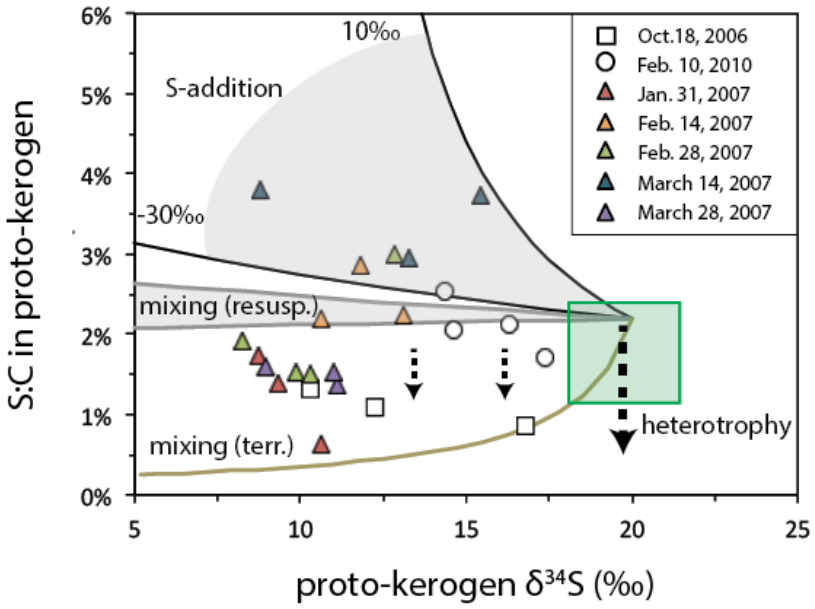

Figure 5. Processes influencing the $\delta^{34}S$ value and S:C ratio of proto-kerogen in particles. *Symbols represent all available depths for five dates in winter 2007 (triangles, key at right), October 2006 (open squares), and February 2010 (open circles). The shaded green rectangle represents expected values for fresh algal biomass. Dashed vertical arrows indicate the effect of heterotrophic remineralization. Gray shaded fields represent the effects of mixing with resuspended or terrigenous material and the addition of abiogenic organic S with a $\delta^{34}S$ value between -30‰ and +10‰.*

The S:C ratios and $\delta^{34}S$ values of particulate proto-kerogen samples are plotted in Fig. 5. Fresh biomass that sinks out of the photic zone of the ocean will undergo heterotrophic degradation, condensation reactions, and mixing with other materials (Eglinton et al., 1994), each of which will change the S:C ratio and $\delta^{34}S$ value of proto-kerogen in different but predictable ways. OM degradation is likely to decrease the S:C ratio of

proto-kerogen, especially if proteins (the main biochemical reservoir for sulfur) are preferentially remineralized relative to carbohydrates and lipids. Proteins are preferentially remineralized in the sub-oxic water column of the eastern tropical North Pacific (Van Mooy et al., 2002) but degrade at similar rates to carbohydrates and proteins in oxic and anoxic incubations (Harvey et al., 1995). S:C ratios below those of biomass were reported in sinking and suspended particles in oxic water off the California coast (S:C = 0.84% and 0.45%, respectively) and were attributed to the preferential remineralization of S-bearing proteins by heterotrophic microorganisms (Matrai et al., 1989). Similarly, the proto-kerogen S:C ratios below ~1.0% that we observe in a few samples likely reflect the heterotrophic degradation of protein-rich OM. Heterotrophy has likely influenced the S:C ratio of all of the particle samples to some extent, but it should not cause fractionation in the S isotopes of OM (vertical dashed arrows, Fig. 5).

Heterotrophy cannot, however, explain the fact that proto-kerogen is often more sulfur-rich and ^{34}S-depleted than planktonic or degraded biomass. Other potentially important processes in the Cariaco water column include mixing with terrigenous or resuspended detrital material and condensation reactions, particularly OM sulfurization. The effect of resuspension is shown on Fig. 5 as a mixing field between biomass and proto-kerogen in surface sediments from Cariaco Basin (upper 100 cm of ODP Core 1002B sediments, Werne et al., 2003). Similarly, mixing with an estimated terrigenous end-member can decrease particle proto-kerogen $\delta^{34}S$ values but fails to explain S:C ratios above about 2%. S:C ratios can be increased by OM sulfurization, which as a broad generalization

adds sulfur to proto-kerogen by replacing oxygen atoms without removing carbon. The isotopic composition of the sulfur that could be added is only weakly constrained, so the vectors representing OM sulfurization on Fig. 5 indicate a range of effects for incorporating sulfur with a $\delta^{34}S$ value between -30‰ and 10‰. Two other processes have the potential to influence proto-kerogen characteristics but are set aside in the following discussion due to a lack of available data: the hypothesized assimilation of reduced sulfur species into biomass (e.g., Canfield, 1998) and the potential for natural marine biomass to differ substantially from the limited literature data for particle S:C and $\delta^{34}S$ due to other environmental sensitivities.

Nearly all of the proto-kerogen S:C and $\delta^{34}S$ data for Cariaco particles can be explained by a combination of heterotrophy, resuspension, and sulfurization. Samples from three consecutive sampling periods in winter 2007 fall within the 'S-addition' field, which is best explained by the chemical addition of sulfur to OM (Fig. 5). Results from October 2006, on the other hand, are most consistent with mixing with terrigenous or resuspended material. For the remaining samples, including those from February 2010 and parts of winter 2007, proto-kerogen $\delta^{34}S$ values and S:C ratios could result from either mixing with detrital material or a combination of OM sulfurization and heterotrophy; combinations of these processes are likely important. In the following section, we explore what environmental conditions might have supported these different patterns using oceanographic and geochemical data from the CARIACO database (http://imars.marine.usf.edu/CAR/).

4.2 Hydrography and primary productivity during sampling

Water column profiles of potential density (σ_θ) and chlorophyll-*a* from the CARIACO time-series program for the three-month period surrounding each of our main sampling dates are shown in Fig. 6. A well-mixed water column persisted for at least two months in winter 2007, driving high productivity (chlorophyll *a*) in early February and lower productivity in March. Dates on which particulate proto-kerogen samples fall in the 'S-addition' field of Fig. 5 were thus broadly characterized by strong upwelling and high productivity in the surface ocean. In contrast, the water column in October 2006 was strongly stratified in the upper 200 m. There was also some upwelling in February 2010, but it appears to have been less intense, with a brief, strong bloom at the start of the sampling period and restratification by early March.

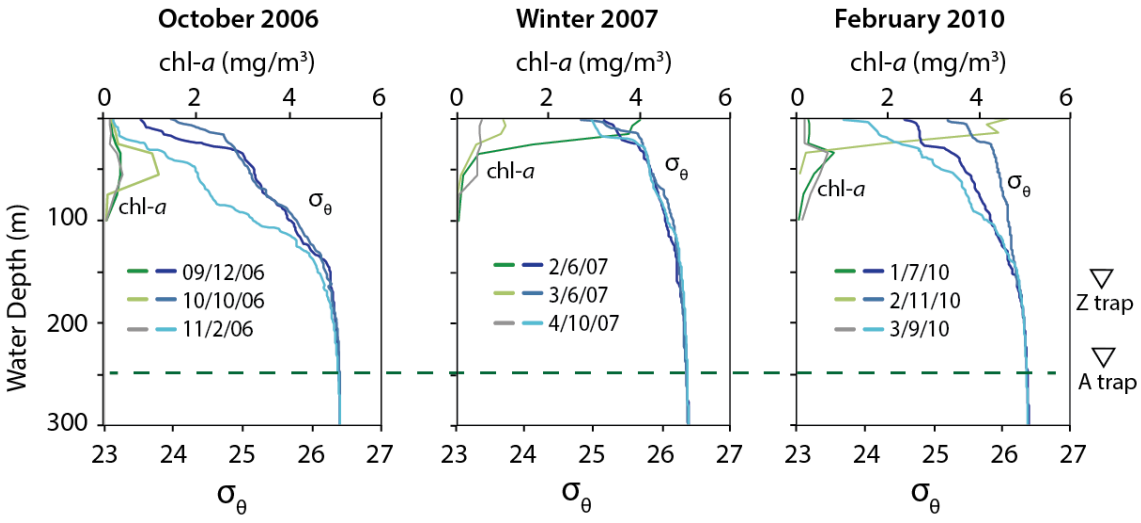

Figure 6: Density and chlorophyll-a concentrations in the Cariaco water column for three sample collection periods. *The horizontal dashed line indicates the approximate position of the chemocline. Data are from the CARIACO time series*

(http://imars.marine.usf.edu/CAR/). The approximate depths of traps Z and A are shown at right.

We next place these dates in the broader context of particle composition throughout the time-series (http://imars.marine.usf.edu/CAR/). 'Z' trap in winter 2007 contains very little terrigenous material and abundant OM, consistent with the indicators of high primary productivity at this time (Fig. 7). Relative to the rest of the seven-year time-series, winter 2007 stands out in terms of both terrestrial material and organic C flux. Fluxes of OM were unremarkable in deeper traps during winter 2007, indicating that OM remineralization during sinking was extensive; however, the remaining OM frequently falls within the 'S-addition' field of Fig. 5. Unlike winter 2007, the February 2010 and October 2006 sampling periods are similar to long-term averages in terms of both terrigenous material and organic C flux. Their differences appear to largely reflect seasonal variability, with bloom-season particles from February 2010 transporting more organic C and a lower proportion of terrestrial material than those collected during the rainy season, in October 2006. Overall, the extent of OM sulfurization appears to correlate with bloom intensity and export production, making its effects on proto-kerogen composition particularly apparent during the intense upwelling and TOC export of winter 2007. More typical upwelling periods like February 2010 may also facilitate OM sulfurization in particles, but to a lesser extent.

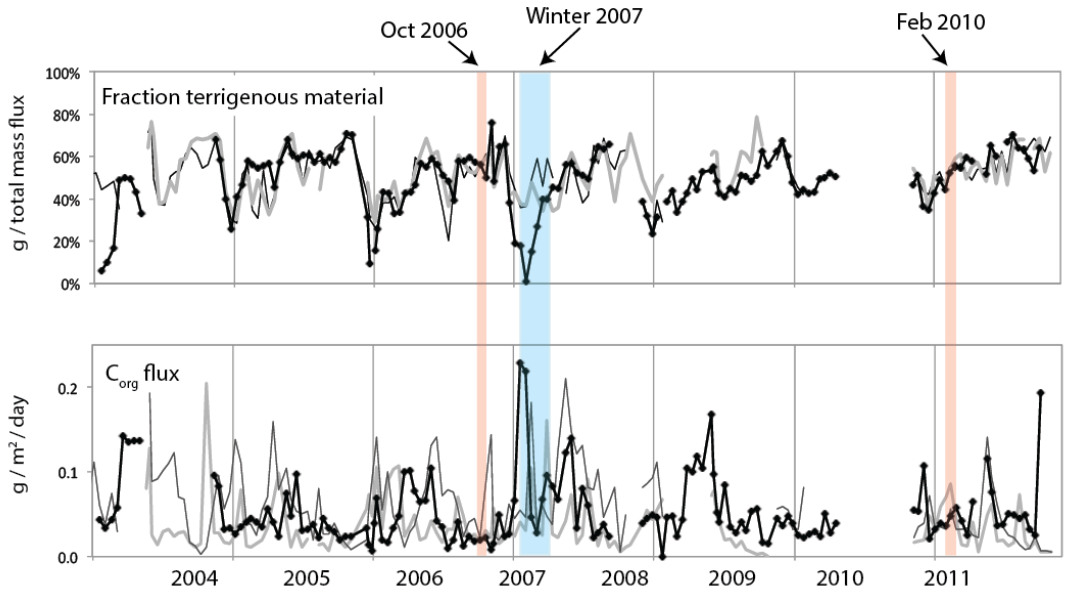

Figure 7: Contributions of terrigenous and organic material to Cariaco sediment traps. *Data shown are for Z trap (150 m, heavy line with symbols), A trap (250 m, thin black line), and C trap (880 m, grey line). Studied periods are highlighted with shading. Filled and open symbols show the fractional mass flux of terrigenous material and the total flux out of organic carbon, respectively, in g/m^2/day (http://imars.marine.usf.edu/CAR/).*

Table 3. Organosulfur compound concentrations and $\delta^{34}S$ values

Date	Trap	Depth	C_{20} thiophene		unidentified OSC (u-14)	
		m	nmol/g	$\delta^{34}S$ (‰)	nmol/g	$\delta^{34}S$ (‰)
5/6/99	B	400	0.01	--	0.12	--
	C	880	0.15	-21	0.11	--
11/18/99	B	400	0.05	--	0.04	--
	C	880	0.22	--	0.04	--
	D	1200	0.16	-29.2	0.04	--
3/23/00	B	400	0.38	-24.9	0.09	-23.2
	C	880	0.20	--	0.05	--
	D	1200	0.00	--	0.00	--
2/9/01	B	400	0.28	-14.7	0.43	-9.8
	C	880	0.42	-17.4	0.00	--
	D	1200	0.16	-22.1	0.56	-8
8/30/02	B	400	0.23	--	0.21	-30.5
	C	880	0.34	-18.2	0.21	-29.8
	D	1200	0.03	--	0.09	--
10/18/06	B	400	0.27	-27.6	0.17	-28.1
	C	880	0.07	--	0.14	--
2/10/10	B	400	0.14	-23.6	0.18	-22.3
	C	880	0.36	-27.1	0.27	-33
	D	1200	0.15	-29.9	0.20	--
Winter 2007:						
1/31/07	B	400	0.99	-11.7	--	--
	C	880	0.70	-12.5	--	--
	D	1200	0.28	-10.5	--	--
2/14/07	B	400	1.04	-0.7	--	--
	C	880	1.09	-3.3	--	--
	D	1200	1.99	-7.6	--	--
2/28/07	B	400	0.65	-11.9	--	--
	C	880	0.87	-7.4	--	--
	D	1200	0.55	-12.7	--	--
3/14/07	A	225	1.25	3.1	--	--
	B	400	5.30	-2.5	0.62	--
	C	880	2.22	-13.7	0.00	--
	D	1200	2.03	-14.1	0.00	--
3/28/07	B	400	1.12	-9.4	--	--
	C	880	2.93	-10.6	--	--
	D	1200	0.19	--	--	--

In addition to proto-kerogen, we measured the concentrations and $\delta^{34}S$ values of elemental S and the most abundant non-polar organosulfur compound extracted from trap materials, C_{20} thiophene (Table 3 and Fig. 8). S^0 and C_{20} thiophene are generally abundant, ^{34}S-rich, and isotopically variable during winter 2007. Additionally, the $\delta^{34}S$ values of S^0, C_{20} thiophene, and proto-kerogen are well correlated during winter 2007 but not with samples from other dates (Fig. 8). These patterns provide important clues about the likely mechanisms of OM sulfurization in particles.

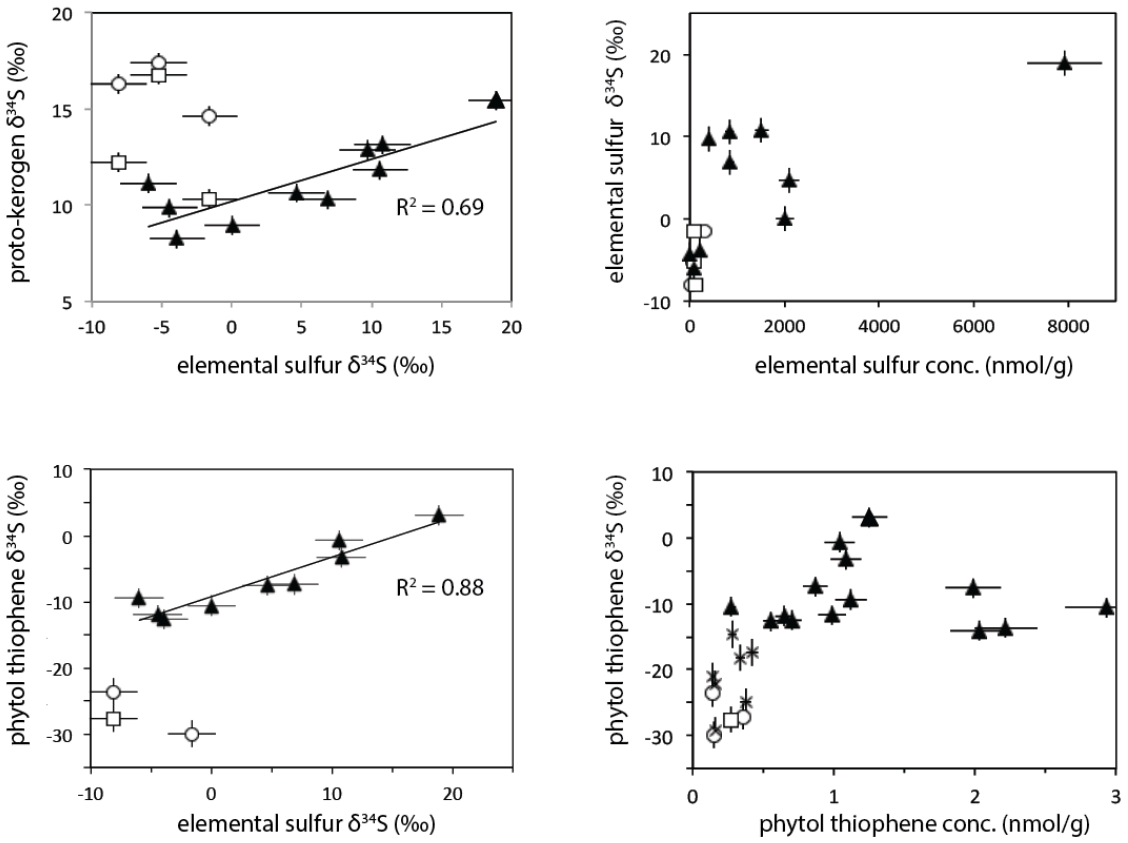

Figure 8: Correlations between $\delta^{34}S$ values and concentrations of C_{20} thiophene, S^0, and proto-kerogen S. *Symbols represent all available depths for five dates in winter*

2007 (black triangles), October 2006 (open squares), February 2010 (open circles) and all other dates (Xs, for phytol thiophene only). Lines on the left-hand panels are linear regressions of winter 2007 data.

Elemental S is central to current models for OM sulfurization because polysulfides (HS_n^-, S_n^{-2}, $n \leq 10$), which form spontaneously in the presence of dissolved sulfide and solid S^0 (Rickard and Luther, 2007), are thought to be the key reactive species in the formation of abiogenic organic sulfur (Kohnen et al., 1989; Vairavamurthy et al., 1992; Amrani and Aizenshtat, 2004b; Canfield et al., 1998; Mossman et al., 1991; Francois et al., 1987). The S_n^{2-} polysulfide species that are favored in S^0-rich systems – predominantly S_4^{-2}, S_5^{-2}, and S_6^{-2} – derive half to two-thirds of their sulfur atoms from elemental sulfur and the remainder from sulfide (Kamyshny et al., 2004; Amrani and Aizenshtat, 2004b). Polysulfide $\delta^{34}S$ values should therefore reflect mixing between particulate S^0 and water column bisulfide, which has a $\delta^{34}S$ value that is consistently near -30‰ (Li et al., 2010).

A genetic link between polysulfides and sulfurized OM during winter 2007 is evidenced by the strong correlations between S^0 $\delta^{34}S$ values and those of both proto-kerogen and C_{20} thiophene (Fig. 8), with R^2 values of 0.69 and 0.88, respectively. The slope of the regression line for S^0 and C_{20} thiophene $\delta^{34}S$ values is approximately 0.6, which would be consistent with C_{20} thiophene forming from a polysulfide pool derived from S^0 and bisulfide in an average mixing ratio between 1:1 and 3:2. If we assume that polysulfides contain equal contributions of S atoms from bisulfide and from S^0, we can estimate the

isotope effect associated with C_{20} thiophene formation. A line with a slope of 1.0 fit through the winter 2007 data has a y-intercept of ~7‰, implying an equilibrium-type isotope effect during the formation of C_{20} thiophene from polysulfide of about 7‰. A similarly sized effect was observed in laboratory sulfurization experiments (4-5‰, Amrani and Aizenshtat, 2004b), although these prior experiments relied on bulk (ir-MS) rather than compound-specific analyses. Polysulfides are thus likely reactants for OM sulfurization in Cariaco particles during winter 2007.

4.4 Potential influence of mixing with terrigenous and resuspended sediment

Proto-kerogen, S^0, and C_{20} thiophene $\delta^{34}S$ data for February 2010 and October 2006 fall off of the winter 2007 trends (Fig. 8). In February 2010, relatively ^{34}S-enriched proto-kerogen $\delta^{34}S$ values could in part reflect dilution of abiogenic OS by large fluxes of unsulfurized biomass. However, detrital (terrigenous and resuspended) material is also a potentially significant source of OS to particles, especially in October 2006 and February 2010 (Fig. 5). In a study of pyrite (Cr-reducible S) in Cariaco sediment traps, Li et al. (2011) preferred to explain relatively ^{34}S-enriched (-6 to 1‰) pyrites and abundant S^0 (27.3 μmol/g, 0.8 mg/g, trap Z) in some samples as being derived from resuspension of sedimentary pyrite and S^0 formed elsewhere in the basin (Li et al., 2011). Resuspension is also a potential source of the ubiquitous, trace concentrations of ^{34}S-depleted C_{20} thiophenes that we observe in deeper traps in October 2006, February 2010, and five additional dates (-29.9‰ to -14.7‰, Table 3). These $\delta^{34}S$ values approach those measured in ODP Core 1002B (-37.1‰ at 40 cm depth, Raven et al., 2015). In contrast,

resuspension does not appear to contribute significantly to particle OS in winter 2007, when C_{20} thiophene $\delta^{34}S$ values average –8.4‰ and proto-kerogen S:C ratios substantially exceed those measured in sediment (~2.0%).

Terrigenous material also appears to be a minor source of particle OS, despite the fact that terrigenous material accounts for about half of particle material in Cariaco Basin. The dominant sources of terrigenous material to Cariaco Basin throughout the year are local rivers, with some contribution from Saharan dust (Martinez et al., 2007). Both plant and animal terrestrial OM generally have lower $\delta^{34}S$ values than marine OM, although terrestrial OM $\delta^{34}S$ values will be largely controlled by rainwater sulfate and bedrock sulfur sources. The mixing line in Fig. 5 is based on $\delta^{34}S$ data for terrestrial OM from Bol et al. (2002), which ranged from 2 to 10‰; sulfate in rainwater falls in a similar $\delta^{34}S$ range. Because terrigenous detritus is relatively S-poor, it cannot explain the particulate S:C ratios we observe outside of October 2006. Moreover, several other geochemical proxies indicate that organic matter in Cariaco Basin particles is primarily marine rather than terrestrial in origin. Thunell et al. (2000) showed that the carbon isotopic compositions and N:C ratios of Cariaco Basin particles match expectations for marine phytoplankton ($\delta^{13}C$ = -20 ± 2‰, N:C = 16:106 = 14.7%) rather than terrestrial organic matter ($\delta^{13}C \leq$-26‰, N:C ~ 5%), and average values of $\delta^{13}C$ and N:C of Cariaco sediment trap samples have remained consistent through 2010 (http://imars.marine.usf.edu/CAR/). Biomarker studies of these sediment trap samples

also indicate that the majority of the sinking OM in Cariaco Basin is of marine origin (Goni et al., 2009).

4.5 Water column sources of organic S to sedimentary proto-kerogen

Table 4: Estimated contribution of water column sulfurization to sedimentary proto-kerogen

Sample Group	n	Total OS Flux		Abiotic OS / Total OS		Equiv. sedimentary accumulation	
		µmol/m^2/d	δ^{34}S (‰)	%	%	µmol/g	µmol/g
assumed abiotic OS δ^{34}S:				(-30‰)	(5‰)	(-30‰)	(5‰)
All samples	23	105.4	12.0	14%	48%	46	155
Figure 5 field							
'S-addition' field	6	148.7	12.8	13%	46%	60	207
all other dates	17	90.1	11.7	15%	50%	41	136
Trap depth							
Z/A (150 / 225 m)	4	69	15.6	11%	37%	23	77
B (400 m)	7	146	12.2	13%	45%	59	201
C (880 m)	6	131	10.8	16%	55%	**65**	217
D (1200 m)	6	57	10.6	17%	57%	30	100

Sedimentary OS (ODP Core 1002B)	δ^{34}S (‰)	µmol/g
5 cm	-18.9	126
10 cm	-21.2	95
75 cm	-25.0	124
155 cm	-24.5	136

We next compare the delivery of sulfurized OM from the water column to OM preservation in Cariaco sediments (ODP Core 1002B). Sediment proto-kerogen δ^{13}C values (-20 to -18‰, Fry et al., 1991) are a good match for particles, suggesting that this OM should be derived from the water column. Proto-kerogen sulfur, however, is much

more ^{34}S-depleted in sediments than in sinking particles. In both environments, proto-kerogen δ^{34}S values can be thought of as a mixture of primary productivity-derived biosulfur with a δ^{34}S value near 20‰ and a pool of abiogenic OS with a more ^{34}S-depleted isotopic composition (Eglinton et al., 1994; Anderson and Pratt, 1995). The δ^{34}S value of this abiogenic OS end member probably varies, reflecting the dynamic S-isotopic composition of S^0 in particles. We therefore select two bounding values for abiogenic OS to constrain the potential size of the abiogenic OS flux (Table 4): a δ^{34}S value of -30‰ matches sulfide in the deep Cariaco water column (Li et al., 2011), while a δ^{34}S value of 5‰ represents the sulfide that would be generated by dissimilatory sulfate reduction in the water column with a moderate isotope fractionation factor (ε) of -15‰. The implied fluxes of ^{34}S-depleted abiogenic OS are converted to equivalent sedimentary concentrations based on an estimated average mass accumulation rate of ~13.2 g/m^2/yr (Lin et al., 1997; Shipboard Scientific Party, 1997). We use the concentration of proto-kerogen S at 10 cm depth in Cariaco Basin sediments, 95 μmol S/g, as an estimate of the total accumulation of abiogenic OS from the water column and shallow (0–10 cm) sedimentary processes (Raven et al., 2015; Aycard et al., 2003). Subsets of these results are averaged in Table 4 to explore the significance of depth and water column conditions on abiogenic OS flux.

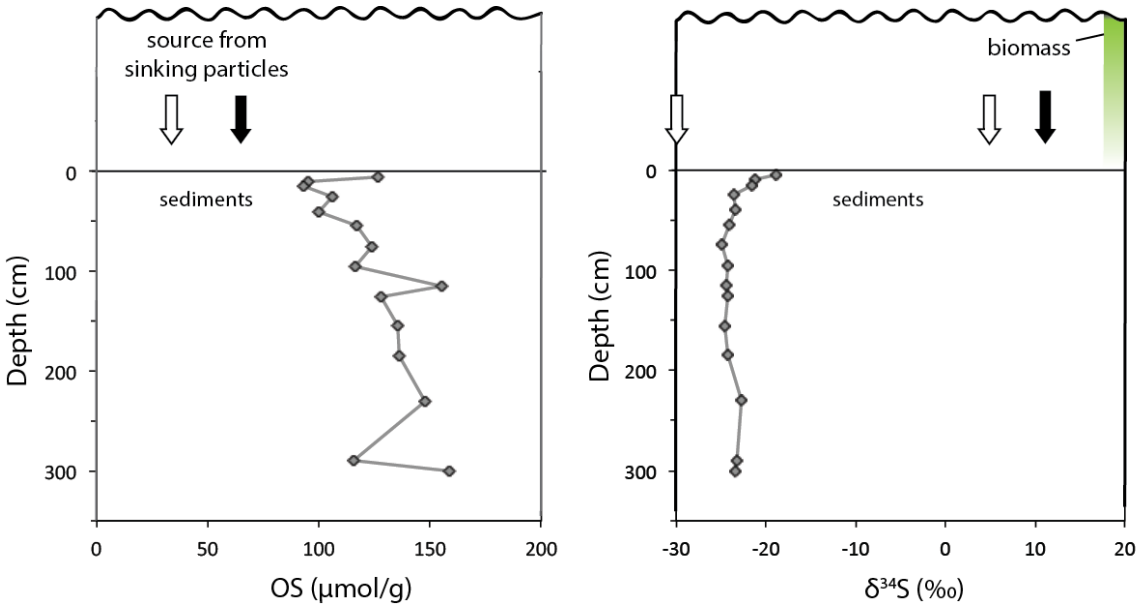

Figure 9: Comparison of water column-sourced abiotic OS and accumulated OS in Cariaco sediments. *Sediment data (diamonds) are from ODP Core 1002B, collected at ~900 m water depth (Lyons et al., 2003; Werne et al., 2003). On the left panel, the open arrow indicates the average flux for samples plotting outside of the 'S-addition' field of Fig. 5; the black arrow is the average flux for C trap; both assume abiotic OS* $\delta^{34}S$ *= -30‰. On the right panel, the open arrows indicate the bounding values used in the calculation in Table 4; the black arrow indicates the average* $\delta^{34}S$ *value of total proto-kerogen in C trap.*

The implied source of abiogenic OS from the water column based on a simple average of the available data is 46 μmol/g. A more realistic estimate may be the average of only data from C trap, which is located at 880 m and is most equivalent to delivery at the ODP 1002B core site (900 m). (Lower fluxes of OS as well as total particle mass in D trap are consistent with the long-term dataset and may be circulation and/or bathymetry-related,

see Fig. 1 and Table 1). The potential abiogenic OS accumulation based on C trap results (65 μmol/m^2/d) is equivalent to 68% of proto-kerogen S at 10 cm depth in the sediments (Fig. 9). This value, which assumes an abiogenic OS $\delta^{34}S$ value of -30‰, is a minimum estimate of the actual source. Data from February 10, 2010 and the 225 m trap on March 14, 2007 suggest that abiogenic OS may have a $\delta^{34}S$ value closer to 5‰ (Fig. 5), which would imply a larger water column source that could even exceed sedimentary concentrations (Table 4).

Below 10 cm depth in Cariaco Basin sediments, OS concentrations gradually increase by about 50% to ~150 μmol/g. Sedimentary sulfurization on this timescale (approximately 6000 years) in Cariaco Basin was described in Aycard et al. (2003) for proto-kerogen and by Werne et al. (2008) and Raven et al. (2015) for individual extractable organic compounds. Similar patterns have been found in Peru Margin sediments and elsewhere (Eglinton, 1994). However, only about one-third of the sulfur in deeper (3 m) Cariaco sediments appears to derive from these slower, diagenetic reactions. By our estimates, slightly less than half of that proto-kerogen S is delivered from the water column, with processes within the uppermost 10 cm of the sediments accounting for the remainder.

4.6 Significance of rapid OM sulfurization for carbon burial

The quantitative significance of water column-derived, abiogenic OS will depend on the frequency of periods like winter 2007, when environmental conditions appear to have

been particularly conducive to the production of abiogenic OS in the water column. Given our two-week sampling resolution, it is challenging to make more specific correlations between abiotic OS fluxes and nimble processes like phytoplankton blooms. OM export fluxes in Cariaco Basin particles have been shown to respond to surface productivity on timescales of days to weeks (Montes et al., 2012). Similarly, sulfurization intensity appears to respond dynamically to changes in circulation and surface productivity. Previous studies have found evidence for rapid OM sulfurization in a variety of environments (Sinninghe Damsté et al. 2007; Wakeham et al. 1995; Hartgers et al., 1997; Putschew et al., 1996; Canfield et al., 1998; Francois et al., 1987; Mossman et al., 1991), but it has been challenging to understand sulfurization rates near the sediment-water interface using annual-scale archives like sediments and rocks. The higher resolution record offered by sinking particles demonstrates that OM sulfurization can occur within days or less.

The vast majority of OM exported from the surface ocean is remineralized before reaching the underlying sediments. Sulfurization of OM within particles can therefore affect a much larger pool of OM than sulfurization in sediments alone. Under the right conditions, water column sulfurization could compete with remineralization for labile OM and enhance the likelihood of OM preservation in underlying sediments (Sinninghe Damsté et al., 1989; Boussafir et al., 1995). Our results thus support the conclusions of van Dongen et al. (2006) and others, who hypothesized that rapid carbohydrate sulfurization in a euxinic water column could explain the extremely high concentrations of sulfur-rich OM in the Kimmeridge Clay (≤ 34 wt%) and other OM-rich rocks. Water

column sulfurization could have played an expanded role in the carbon cycle during periods of expanded marine anoxia like the Cretaceous ocean anoxic events.

We also find some evidence that water column sulfurization may not be strictly limited to environments with measurable free sulfide in the water column. OM sulfurization was previously hypothesized to occur in micro-environments in sediments that were bathed in oxic porewater by Francois et al. (1987). The shallowest trap samples from two consecutive periods fall within the 'S-addition' field, despite being collected either just above the chemocline (A trap, 225 m) or substantially above it (Z trap, 150 m). The 'A' trap sample from March 14, 2007 is particularly notable, falling far out of the regions of Fig. 5 that can be explained by other sources. Additionally, this trap has very high fluxes of S^0 (4.7 μmol/m^2/d), polar extractable OS (5.0 μmol/m^2/d), and 1.3 nmol/g C_{20} thiophene, all of which are consistent with the operation of an active S cycle. Polysulfides may exist at redox interfaces within OM-rich particles even in the presence of low concentrations of water column O_2 (≤25 μM, Ploug et al., 2001), as typically characterize A trap (Fig. 1, Li et al., 2010). If future work confirms the activity of OM sulfurization in particles within sub-oxic (≤25 μM O_2) environments, it would greatly expand the potential significance of this process in the modern ocean to include many oxygen minimum zones. Rapid abiogenic organic S formation may also provide a mechanistic link between enhanced OM burial and environmental O_2 limitation (Hartnett et al., 1998; Devol and Hartnett, 2001) via the transformation of labile OM into more condensed, S-rich structures within sinking particles.

4.7 The S-isotope composition of rapidly sulfurized OM

The correlated S-isotopic compositions of S^0, C_{20} thiophene, and proto-kerogen indicate that polysulfides are likely the main reactive species forming abiogenic organic S in the Cariaco water column. Polysulfides are in rapid isotopic equilibrium with S^0 and sulfide (Rickard and Luther, 2007; Amrani and Aizenshtat, 2004b), and a primary control on their $\delta^{34}S$ value is the isotopic fractionation associated with dissimilatory sulfate reduction. The scale of this fractionation varies with sulfate reduction rate and substrate availability, with faster metabolic rates and higher energetic yields generally producing smaller fractionations (e.g., Sim et al., 2011a; Leavitt et al., 2013). Given abundant sulfate in the water column, sulfate reduction rate should be primarily controlled by OM lability, which decreases with water depth. Accordingly, C_{20} thiophene $\delta^{34}S$ values, which appear to reflect the $\delta^{34}S$ value of polysulfide offset by a slight equilibrium-type isotope effect, decrease with trap depth (Fig. 8b). This pattern is consistent with increasing isotopic fractionations between sulfate and sulfide (and S^0) as OM is progressively consumed. The smallest apparent fractionation factors we observe are in the shallowest traps during the winter 2007 bloom, where high sulfate reduction rates are particularly favored. On the other hand, large apparent fractionation factors for dissimilatory sulfate reduction (~50‰) are found in shallow Cariaco sediments, where the $\delta^{34}S$ value of porewater sulfide is approximately –29‰ (Werne et al., 2003) and individual organosulfur compounds have $\delta^{34}S$ values < –35‰ (Raven et al., 2015).

Like S^0, the $\delta^{34}S$ value of abiogenic organic S from the water column is likely to vary widely on the timescale of blooms. Still, we can constrain its average $\delta^{34}S$ value more tightly than the bounding values explored above (–30‰ and 5‰) based on the $\delta^{34}S$ value of proto-kerogen at 10 cm depth (–21.2‰). The abiogenic organic S formed in the sediments, which appears to represent less than one-third of total proto-kerogen S at 10 cm depth, is relatively ^{34}S-depleted. Therefore the average $\delta^{34}S$ value of water column-derived abiogenic organic S must be somewhat more ^{34}S-enriched than –21.2‰ (roughly –20 to –5‰). This estimate is consistent with the weighted average delivery of C_{20} thiophene from the water column (–9.1‰) and typical fractionation factors for dissimilatory sulfate reduction in the environment (25 to 40‰, Habicht and Canfield, 2001; Sim et al., 2011b).

5. CONCLUSIONS

Particulate OM sinking through the water column of Cariaco Basin is often more sulfur-rich and ^{34}S-depleted than typical marine biomass, especially during a period of upwelling and high productivity in winter 2007. These results are best explained by the occurrence of abiogenic OM sulfurization in particles on timescales of days or less. Correlations among the $\delta^{34}S$ values of proto-kerogen, C_{20} thiophene, and S^0 suggest a genetic link between these species, likely via polysulfides. On dates outside of winter 2007, sediment resuspension and mixing with terrestrial detritus may be relatively important processes affecting particulate OS. Although the extent of water column sulfurization appears to vary with environmental conditions like primary productivity and OM export, we roughly estimate that water column sources can account for two-thirds of proto-kerogen S at 10 cm or slightly less than half of proto-kerogen S at 3 m depth in basin sediments. Rapid, abiotic OM sulfurization in sinking particles may represent a mechanistic link between O_2-depleted environments and enhanced OM preservation in sediments.

ACKNOWLEDGEMENTS

We are grateful to Nathan Dalleska, Fenfang Wu and Guillaume Paris (Caltech) for analytical assistance, and to Eric Tappa (U. of South Carolina) for assistance with samples. We also thank the US National Science Foundation (award OCE-1258991 to R.C.T.) and Fundación La Salle de Ciencias Naturales, Estación de Investigaciones Marinas Isla Margarita (FLASA/EDIMAR) for their continuous effort in maintaining the CARIACO Ocean Time-Series program. This work was supported by NSF Award #OCE-1529120 to A.L.S. and was also funded in part by the Gordon and Betty Moore Foundation through Grant GBMF#3306 to A.L.S.. We are grateful for insightful comments from two anonymous reviewers that substantially improved the manuscript and for careful editorial handling by Joseph Werne.

REFERENCES

Amrani, A., & Aizenshtat, Z. (2004a). Reaction of polysulfide anions with α, β unsaturated isoprenoid aldehydes in aquatic media: simulation of oceanic conditions. *Organic Geochemistry*, *35*(8), 909–921.

Amrani, A., & Aizenshtat, Z. (2004b). Mechanisms of sulfur introduction chemically controlled: $\delta^{34}S$ imprint. *Organic Geochemistry*, *35*(11-12), 1319–1336. http://doi.org/10.1016/j.orggeochem.2004.06.019

Amrani, A., Sessions, A., & Adkins, J. (2009). Compound-specific $\delta^{34}S$ analysis of volatile organics by coupled GC/multicollector-ICPMS. *Anal. Chem.*, *81*, 9027–9034.

Anderson, T. F., & Pratt, L. M. (1995). Isotopic evidence for the origin of organic sulfur and elemental sulfur in marine sediments, *612*, 378–396.

Aycard, M., Aycard, M., Derenne, S., Derenne, S., Largeau, C., Largeau, C., et al. (2003). Formation pathways of proto-kerogens in Holocene sediments of the upwelling influenced Cariaco Trench, Venezuela. *Organic Geochemistry*, *34*(6), 701–718.

Blumer, M. (1957). Removal of elemental sulfur from hydrocarbon fractions. *Analytical Chemistry*, *29*(7), 1039–1041.

Bol, R., & Pflieger, C. (2002). Stable isotope (13C,15N and34S) analysis of the hair of modern humans and their domestic animals. *Rapid Commun. Mass Spectrom.*, *16*(23), 2195–2200.

Boussafir, M., Gelin, F., Lallier-Verges, E., Derenne, S., Bertrand, P., & Largeau, C. (1995). Electron microscopy and pyrolysis of kerogens from the Kimmeridge Clay Formation, UK: Source organisms, preservation processes, and origin of microcycles. *Geochimica Et Cosmochimica Acta*, *59*(18), 3731–3747.

Brassell, S. C., Lewis, C. A., De Leeuw, J. W., de Lange, F., & Damste, J. S. (1986). Isoprenoid thiophenes: novel products of sediment diagenesis? *Nature*, *320*, 160–162.

Brüchert, V., & Pratt, L. M. (1996). Contemporaneous early diagenetic formation of organic and inorganic sulfur in estuarine sediments from St. Andrew Bay, Florida, USA. *Geochimica Et Cosmochimica Acta*, *60*(13), 2325–2332.

Canfield, D. (1989). Sulfate reduction and oxic respiration in marine sediments: implications for organic carbon preservation in euxinic environments. *Deep-Sea Research*, *36*(1), 121–138.

Canfield, D. E., Boudreau, B. P., Mucci, A., & Gundersen, J. K. (1998). The early diagenetic formation of organic sulfur in the sediments of Mangrove Lake, Bermuda. *Geochimica Et Cosmochimica Acta*, *62*(5), 767–781.

Chen, C.-T. A., Lin, C.-M., Huang, B.-T., & Chang, L. F. (1996). Stoichiometry of carbon, hydrogen, nitrogen, sulfur and oxygen in the particulate matter of the western North Pacific marginalseas. *Marine Chemistry*, *54*, 179–190.

Devol, A., & Hartnett, H. E. (2001). Role of the oxygen-deficient zone in transfer of organic carbon to the deep ocean. *Limnology and Oceanography*, *46*(7), 1684–1690.

Eglinton, T. I., Irvine, J. E., Vairavamurth, Zhou, W., & Manowitz, B. (1994). Formation and diagenesis of macromolecular organic sulfur in Peru margin sediments. *Organic Geochemistry*, *22*(3), 781–799.

Emerson, S., & Hedges, J. (1988). Processes controlling the organic carbon content of open ocean sediments. *Paleoceanography*, *3*(5), 621–634.

Ferdelman, T., Church, T. M., & Luther, G. I. (1991). Sulfur enrichment of humic substances in a Delaware salt marsh sediment core. *Geochimica Et Cosmochimica Acta*, *55*, 979–988.

Francois, R. (1987). A study of sulphur enrichment in the humic fraction of marine sediments during early diagenesis. *Geochimica Et Cosmochimica Acta*, *51*, 17–27.

Fry, B., Jannasch, H. W., Molyneaux, S. J., Wirsen, C. O., Muramoto, J. A., & King, S. (1991). Stable isotope studies of the carbon, nitrogen and sulfur cycles in the Black Sea and the Cariaco Trench. *Deep Sea Research Part a. Oceanographic Research Papers*, *38*(Supplement 2), S1003–S1019.

Gelin, F., Kok, M. D., De Leeuw, J. W., & Damsté, J. S. S. (1998). Laboratory sulfurisation of the marine microalga Nannochloropsis salina. *Organic Geochemistry*, *29*(8), 1837–1848.

Goni, M. A., Aceves, H., Benitez-Nelson, B., Tappa, E., Thunell, R., Black, D. E., et al. (2009). Oceanographic and climatologic controls on the compositions and fluxes of biogenic materials in the water column and sediments of the Cariaco Basin over the Late Holocene. *Deep Sea Research Part I: Oceanographic Research Papers*, *56*(4), 614–640.

Habicht, K. S., & Canfield, D. E. (2001). Isotope fractionation by sulfate-reducing natural populations and the isotopic composition of sulfide in marine sediments. *Geology*, *29*(6), 555–558.

Hartnett, H. E., Keil, R. G., Hedges, J. I., & Devol, A. (1998). Influence of oxygen exposure time on organic carbon preservation in continental margin sediments. *Nature*, *391*(6667), 572–575.

Harvey, H. R., Tuttle, J. H., & Bell, J. T. (1995). Kinetics of phytoplankton decay during simulated sedimentation: changes in biochemical composition and microbial activity under oxic and anoxic conditions. *Geochimica Et Cosmochimica Acta*, *59*(16), 3367–3377.

Hulthe, G., Hulth, S., & Hall, P. (1998). Effect of oxygen on degradation rate of refractory and labile organic matter in continental margin sediments. *Geochimica Et*

Cosmochimica Acta, 62(8), 1319–1328.

Kaplan, I. R., & Rittenberg, S. C. (1964). Microbiological fractionation of sulphur isotopes. *Journal of General Microbiology*, *34*(2), 195–212.

Keil, R. G., Neibauer, J., Biladeau, C., van der Elst, K., & Devol, A. H. (2015). A multiproxy approach to understanding the "enhanced" flux of organic matter through the oxygen deficient waters of the Arabian Sea. *Biogeosciences Discussions*, *12*(20), 17051–17092.

Kohnen, M., Damste, J. S., Haven, ten, H. L., & De Leeuw, J. W. (1989). Early incorporation of polysulfides in sedimentary organic matter. *Nature*, *341*, 640–641.

Kohnen, M., Sinninghe, Dalen, A. K.-V., & De Leeuw, J. W. (1991). Di- or polysulphide-bound biomarkers in sulphur-rich geomacromolecules as revealed by selective chemolysis. *Geochimica Et Cosmochimica Acta*, *55*, 1375–1394.

Kok, M., Schouten, S., & Damste, J. S. (2000). Formation of insoluble, nonhydrolyzable, sulfur-rich macromolecules via incorporation of inorganic sulfur species into algal carbohydrates. *Geochimica Et Cosmochimica Acta*, *64*(15), 2689–2699.

Krein, E. B., & Aizenshtat, Z. (1994). The formation of isoprenoid sulfur compounds during diagenesis: simulated sulfur incorporation and thermal transformation. *Organic Geochemistry*, *21*(10), 1015–1025.

Leavitt, W. D., Halevy, I., Bradley, A. S., & Johnston, D. T. (2013). Influence of sulfate reduction rates on the Phanerozoic sulfur isotope record. *Proceedings of the National Academy of Sciences*, *110*(28), 11244–11249.

Lee, C. (1992). Controls on organic carbon preservation: the use of stratified water bodies to compare intrinsic rates of decomposition in oxic and anoxic systems. *Geochimica Et Cosmochimica Acta*, *56*, 3323–3335.

Li, X., Cutter, G. A., Thunell, R. C., Tappa, E., Gilhooly, W. P., III, Lyons, T. W., et al. (2011). Particulate sulfur species in the water column of the Cariaco Basin. *Geochimica Et Cosmochimica Acta*, *75*(1), 148–163.

Li, X., Gilhooly, W. P., III, Zerkle, A. L., Lyons, T. W., Farquhar, J., Werne, J. P., et al. (2010). Stable sulfur isotopes in the water column of the Cariaco Basin. *Geochimica Et Cosmochimica Acta*, *74*(23), 6764–6778.

Lin, H.-L., Peterson, L., Overpeck, J., Trumbore, S., & Murray, D. (1997). Late Quaternary climate change from δ18O records of multiple species of planktonic foraminifera: High-resolution records from the anoxic Cariaco Basin, Venezuela. *Paleoceanography*, *12*(3), 415–427.

Lyons, T. W., Werne, J. P., Hollander, D. J., & Murray, R. W. (2003). Contrasting sulfur geochemistry and Fe/Al and Mo/Al ratios across the last oxic-to-anoxic transition in the Cariaco Basin, Venezuela. *Chemical Geology*, *195*(1-4), 131–157.

Martinez, N., Murray, R., Thunell, R., Peterson, L. C., Muller-Karger, F., Astor, Y., et al. (2007). Modern climate forcing of terrigenous deposition in the tropics (Cariaco

Basin, Venezuela). *Earth and Planetary Science Letters*, *264*(3-4), 438–451.

Matrai, P. A., & Eppley, R. W. (1989). Particulate organic sulfur in the waters of the southern California bight. *Global Biogeochemical Cycles*, *3*(1), 89–103.

Montes, E., Muller-Karger, F., Thunell, R., Hollander, D., Astor, Y., Varela, R., et al. (2012). Vertical fluxes of particulate biogenic material through the euphotic and twilight zones in the Cariaco Basin, Venezuela. *Deep-Sea Research Part I*, *67*, 73–84.

Mossman, J. R., Aplin, A. C., Curtis, C. D., & Coleman, M. L. (1991). Geochemistry of inorganic and organic sulphur in organic-rich sediments from the Peru Margin. *Geochimica Et Cosmochimica Acta*, *55*, 3581–3595.

Muller-Karger, F., Bohrer, R., Walsh, J. J., Varela, R., Capelo, J., Astor, Y., et al. (2001). Annual cycle of primary production in the Cariaco Basin- Response to upwelling and implications for vertical export. *Journal of Geophysical Research*, *106*(C3), 4527–4542.

Nissenbaum, A., & Kaplan, I. R. (1972). Chemical and isotopic evidence for the in-situ origin of marine humic substances. *Limnology and Oceanography*, *17*, 570–582.

Paris, G., Adkins, J. F., Sessions, A. L., & Subhas, A. (2013). MC-ICP-MS measurement of δ34S and Δ33S in small amounts of dissolved sulfate. *Chemical Geology*, *345*, 50–61.

Shipboard Scientific Party (1997). Site 1002. In *Proceedings of the Ocean Drilling Program, Initial Reports* (Vol. 165). College Station, TX.

Ploug, H. (2001). Small-scale oxygen fluxes and remineralization in sinking aggregates. *Limnology and Oceanography*, *46*(7), 1624–1631.

Putschew, A., Scholz-Böttcher, B. M., & Rullkötter, J. (1996). Early diagenesis of organic matter and related sulphur incorporation in surface sediments of meromictic Lake Cadagno in the Swiss Alps. *Organic Geochemistry*, *25*(5-7), 379–390.

Raven, M. R., Sessions, A. L., Fischer, W. W., & Adkins, J. F. (2016). Sedimentary pyrite $\delta^{34}S$ differs from porewater sulfide in Santa Barbara Basin: Proposed role of organic sulfur. *Geochimica Et Cosmochimica Acta*, *186*, 120–134.

Raven, M. R., Adkins, J. F., Werne, J. P., Lyons, T. W., & Sessions, A. L. (2015). Sulfur isotopic composition of individual organic compounds from Cariaco Basin sediments. *Organic Geochemistry*, *80*, 53–59.

Rowland, S., Rockey, C., Al-Lihaibi, S. S., & Wolff, G. A. (1993). Incorporation of sulphur into phytol derivatives during simulated early diagenesis. *Organic Geochemistry*, *20*(1), 1–5.

Schimmelmann, A., & Kastner, M. (1993). Evolutionary changes over the last 1000 years of reduced sulfur phases and organic carbon in varved sediments of the Santa Barbara Basin, California. *Geochimica Et Cosmochimica Acta*, *57*(1), 67–78.

Sim, M. S., Ono, S., Donovan, K., Templer, S. P., & Bosak, T. (2011a). Effect of electron donors on the fractionation of sulfur isotopes by a marine Desulfovibrio sp. *Geochimica Et Cosmochimica Acta*, *75*(15), 4244–4259.

Sim, M. S., Bosak, T., & Ono, S. (2011b). Large sulfur isotope fractionation does not require disproportionation. *Science*, *333*, 74–77.

Sinninghe Damsté, J.S., Rijpstra, I., Coolen, M., Schouten, S., & Volkman, J. (2007). Rapid sulfurisation of highly branched isoprenoid (HBI) alkenes in sulfidic Holocene sediments from Ellis Fjord, Antarctica. *Organic Geochemistry*, *38*(1), 128–139.

Sinninghe Damsté, J. S., & De Leeuw, J. W. (1990). Analysis, structure and geochemical significance of organically-bound sulphur in the geosphere: state of the art and future research. *Organic Geochemistry*, *16*(4), 1077–1101.

Sinninghe Damsté, J. S., Irene, W., Rijpstra, C., De Leeuw, J. W., & Schenck, P. A. (1988). Origin of organic sulphur compounds and sulphur-containing high molecular weight substances in sediments and immature crude oils. *Organic Geochemistry*, *13*(4), 593–606.

Thunell, R. C., Varela, R., Llano, M., Collister, J., Muller-Karger, F., & Bohrer, R. (2000). Organic carbon fluxes, degradation, and accumulation in an anoxic basin: Sediment trap results from the Cariaco Basin. *Limnology and Oceanography*, 300–308.

Tribovillard, N., Riboulleau, A., Lyons, T., & Baudin, F. (2004). Enhanced trapping of molybdenum by sulfurized marine organic matter of marine origin in Mesozoic limestones and shales. *Chemical Geology*, *213*(4), 385–401.

Vairavamurthy, A., Mopper, K., & Taylor, B. (1992). Occurrence of particle-bound polysulfides and significance of their reaction with organic matters in marine sediments. *Geophysical Research Letters*, *19*(20), 2043–2046.

van Dongen, B. E., Schouten, S., & Sinninghe Damsté, J. S. (2006). Preservation of carbohydrates through sulfurization in a Jurassic euxinic shelf sea: Examination of the Blackstone Band TOC cycle in the Kimmeridge Clay Formation, UK. *Organic Geochemistry*, *37*(9), 1052–1073.

van Dongen, B. E., Schouten, S., Baas, M., Geenevasen, J. A. J., & Sinninghe Damsté, J. S. (2003). An experimental study of the low-temperature sulfurization of carbohydrates. *Organic Geochemistry*, *34*(8), 1129–1144.

Van Kaam-Peters, H. M., Schouten, S., Köster, J., & Damsté, J. S. S. (1998). Controls on the molecular and carbon isotopic composition of organic matter deposited in a Kimmeridgian euxinic shelf sea: Evidence for preservation of carbohydrates through sulfurisation. *Geochimica Et Cosmochimica Acta*, *62*(19), 3259–3283.

Van Mooy, B., Keil, R. G., & Devol, A. H. (2002). Impact of suboxia on sinking particulate organic carbon: Enhanced carbon flux and preferential degradation of amino acids via denitrification. *Geochimica Et Cosmochimica Acta*, *66*(3), 457–465.

Vandenbroucke, M., & Largeau, C. (2007). Kerogen origin, evolution and structure. *Organic Geochemistry*, *38*(5), 719–833.

Wakeham, S., Damste, J. S., Kohnen, M., & De Leeuw, J. W. (1995). Organic sulfur compounds formed during early diagenesis in Black Sea sediments. *Geochimica Et Cosmochimica Acta*, *59*(3), 521–533.

Werne, J., Hollander, D., Behrens, A., Schaeffer, P., Albrecht, P., & Damste, J. (2000). Timing of early diagenetic sulfurization of organic matter: A precursor-product relationship in early Holocene sediments of the anoxic Cariaco Basin, Venezuela. *Geochimica Et Cosmochimica Acta*, *65*(10), 1741–1751.

Werne, J., Lyons, T., Hollander, D., Formolo, M., & Damste, J. (2003). Reduced sulfur in euxinic sediments of the Cariaco Basin: sulfur isotope constrains on organic sulfur formation. *Chemical Geology*, *195*, 159–179.

Werne, J., Lyons, T., Hollander, D., Schouten, S., Hopmans, E., & Damste, J. (2008). Investigating pathways of diagenetic organic matter sulfurization using compound-specific sulfur isotope analysis. *Geochimica Et Cosmochimica Acta*, *72*, 3489–3502.

Wollast, R., Mackenzie, F., & Lei, C. (1993). *Interactions of C, N, P, and S biogeochemical cycles and global change.* NATO ASI Series Vol. I 4, Springer-Verlag Berlin Heidelberg.

C h a p t e r 4

SEDIMENTARY PYRITE $\delta^{34}S$ DIFFERS FROM POREWATER SULFIDE IN SANTA BARBARA BASIN:

PROPOSED ROLE OF ORGANIC SULFUR

Raven M.R., Sessions A.L., Fischer W.F., Adkins J.F. (2016). "Sedimentary pyrite $\delta^{34}S$ differs from porewater sulfide in Santa Barbara Basin: Proposed role of organic sulfur." *Geochimica et Cosmochimica Acta* (in press).

ABSTRACT

Santa Barbara Basin sediments host a complex network of abiotic and metabolic chemical reactions that knit together the carbon, sulfur, and iron cycles. From a 2.1-m sediment core collected in the center of the basin, we present high-resolution profiles of the concentrations and isotopic compositions of all the major species in this system: sulfate, sulfide ($\sum H_2S$), elemental sulfur (S^0), pyrite, extractable organic sulfur (OS), proto-kerogen S, total organic and dissolved inorganic carbon, and total and reducible iron. Below 10 cm depth, the core is characterized by low apparent sulfate reduction rates (<0.01 mM/yr) except near the sulfate-methane transition zone. Surprisingly, pyrite forming in shallow sediments is ~30‰ more ^{34}S-depleted than coexisting $\sum H_2S$ in porewater. S^0 has the same strongly ^{34}S-depleted composition as pyrite where it forms near the sediment–water interface, though not at depth. This pattern is not easily explained by conventional hypotheses in which sedimentary pyrite derives from abiotic reactions with porewater $\sum H_2S$ or from the products of S^0 disproportionation. Instead, we

propose that pyrite formation in this environment occurs within sulfate reducing microbial aggregates or biofilms, where it reflects the isotopic composition of the immediate products of bacterial sulfate reduction. Porewater $\sum H_2S$ in Santa Barbara Basin may be more ^{34}S-enriched than pyrite due to equilibration with relatively ^{34}S-enriched OS. The difference between OS and pyrite $\delta^{34}S$ values would then reflect the balance between microbial sulfide formation and the abundance of exchangeable OS. Both OS and pyrite $\delta^{34}S$ records thus have the potential to provide valuable information about biogeochemical cycles and redox structure in sedimentary paleoenvironments.

1. INTRODUCTION

Pyrite burial in sediments represents one of the largest fluxes in the global sulfur cycle (Bottrell and Newton, 2006). Records of the sulfur-isotopic composition of sedimentary pyrite have informed studies of the evolution of major metabolic pathways (Canfield and Teske, 1996; Bontognali et al., 2013), the size of the marine sulfate reservoir (Habicht et al., 2002; Canfield, 2004), and the redox balance of the planet (Berner and Raiswell, 1983; Leavitt et al., 2013). In these applications, pyrite $\delta^{34}S$ is typically assumed to record the sulfur isotopic composition of porewater sulfide ($\sum H_2S$) (e.g., Anderson and Pratt, 1995; Johnston et al., 2005; Leavitt et al., 2013). Nevertheless, we have only a partial understanding of the microbial and abiotic processes affecting the $\delta^{34}S$ values of pyrite, $\sum H_2S$, and other sedimentary sulfur pools in modern environments.

Pyrite is the product of one of two reactions that involve sulfide either directly (as S^{2-}) or indirectly (via polysulfides).

$$Fe^{2+} + HS^- \rightarrow [FeS] + H^+ \qquad (1)\ \text{(rapid)}$$

$$[FeS] + S_n^{2-} \rightarrow FeS_2 + S_{(n-1)}^{2-} \qquad (2a)$$

$$[FeS] + H_2S \rightarrow FeS_2 + H_2 \qquad (2b)$$

Both reactions have been demonstrated experimentally (Butler et al., 2004), and their relative importance depends on pH and the details of polysulfide speciation in any

particular environment. In either case, however, pyrite takes on the sulfur-isotope composition of its source with less than 1‰ fractionation (Wilkin and Barnes, 1996; Bottcher et al., 1998; Butler et al., 2004). In the following discussion, we refer to that source as '$\sum H_2S$', which can also be thought of as total inorganic S(-II).

Microbial sulfate reduction (MSR) is the dominant mechanism of organic matter remineralization and sulfide production in anoxic marine sediments (Froelich et al., 1979; Jorgensen, 1982; Bottrell and Newton, 2006). For over three decades it was thought that fractionations associated with MSR (ε_{MSR}) did not exceed 48‰ (Rees, 1973; Goldhaber and Kaplan, 1975; Fry et al., 1991; Detmers et al., 2001). It has since been established that MSR alone is capable of generating large fractionations of >70‰ (Brunner and Bernasconi, 2005; Johnston et al., 2007; Canfield et al., 2010; Sim et al., 2011). Still, there are large discrepancies between experimentally measured MSR fractionation factors for natural microbial communities and the $\delta^{34}S$ values of pyrite from the same environment (Habicht and Canfield, 2001), highlighting our limited understanding of the complexity of the sulfur cycle in many natural systems.

In modern marine sediments, the vast majority of $\sum H_2S$ produced by MSR can be reoxidized (Jorgensen, 1982; Canfield, 1989; Brüchert et al., 2000) both biotically and abiotically by a variety of potential electron acceptors, including oxygen, nitrate, and ferric iron (Canfield, 2001). These reactions produce S^0 and other sulfur intermediates that are slightly more ^{34}S-depleted than the initial $\sum H_2S$ (Poser et al., 2014), and

subsequent disproportionation of these intermediate compounds could generate very strongly ^{34}S-depleted $\sum H_2S$ (Kaplan and Rittenberg, 1964; Fry et al., 1986). The combination of MSR, $\sum H_2S$ oxidation and disproportionation has been hypothesized to drive the $\delta^{34}S$ difference between $\sum H_2S$ and pyrite to exceed the fractionation from MSR (Canfield and Thamdrup, 1994). Moreover, the distribution of ^{34}S in sediments can be influenced by other microbial and abiological reactions, including organic matter sulfurization (Sinninghe Damste et al., 1989; Bruchert et al., 2000), isotopic exchange between different pools (Dale et al., 2009), and enhanced biogeochemical cycling associated with the sulfate-methane transition zone (SMTZ).

To evaluate *in situ* biogeochemical cycling and help constrain how marine sediments acquire and modify their sulfur isotope signatures through organic diagenesis, we collected new sediment cores from the center of the Santa Barbara Basin and measured the major S, C, and Fe pools with very high (2.5-cm) stratigraphic resolution. We employed a new approach to measure $\delta^{34}S$ values of very small samples by multicollector inductively-coupled plasma mass spectrometry (ICP-MS) (Paris et al., 2013). This technique enabled high-resolution depth profiles of both major and minor sulfur species throughout a 2.1-m-long core. We find that the sulfur isotopic composition of porewater $\sum H_2S$ is remarkably different from that of both pyrite and S^0, challenging conventional explanations for their formation. These $\delta^{34}S$ records constrain the possible sources of pyrite sulfur and porewater $\sum H_2S$ and provide new insights into the biogeochemical processes operating in these anoxic sediments.

2. METHODS

2.1 Site Background

Sediment cores were taken from the deepest point (~590 m) of Santa Barbara Basin, a silled basin off the coast of southern California that has been extensively studied to take advantage of its high sedimentation rate and annual varves (Soutar and Crill, 1977; Reimers et al., 1990; Schimmelmann et al., 1990; Schimmelmann et al., 2013). Bottom water O_2 concentrations are typically low (<0.1 mL/L; <10 μM) at depths below the western sill of the basin (475 m) except during spring inflow events (Sholkovitz, 1973; Reimers et al., 1996; Moffitt et al., 2014). Sediments in the basin are rich in organic matter and contain up to 4% TOC (Schimmelmann and Kastner, 1993). Shallow sediments are characterized by a dynamic sulfur cycle driven by communities of microorganisms, including both extensive microbial sulfate reduction (MSR) and $\sum H_2S$ reoxidation by widespread *Beggiatoa* mats at the sediment-water interface (Schimmelmann and Kastner, 1993; Kuwabara et al., 1999).

Santa Barbara Basin sediments overlie hydrocarbon-rich sedimentary bedrock that releases methane and other light hydrocarbons. Both thermogenic and biogenic methane may diffuse upward to the sulfate methane transition zone (SMTZ), where enough sulfate is available to drive anaerobic oxidation of methane (AOM). The depth of the SMTZ in Santa Barbara Basin has been reported at as little as 15 cm in seep-type environments

(Orphan et al., 2001) and at 120-150 cm in non-seep environments (Berelson et al., 2005; Harrison et al., 2009; Li et al., 2009).

2.2 Porewater Sample Collection

Santa Barbara Basin cores were collected in early October 2013 as part of *R/V Atlantis* cruise AT26-06. Triplicate multicores ('M', 'R', and 'A') and a longer gravity core were collected from approximately the same location in the basin on consecutive days. Immediately after collection, multicore 'M' and the gravity core were extruded and sliced into 2.5-cm-thick discs. Solids were isolated by squeezing in a benchtop, N_2-flushed apparatus (after Reeburgh, 1967) and immediately frozen at -40°C. Porewater was also collected at 2-cm resolution using Rhizon samplers (Rhizosphere Research Products) in multicore 'R' in a 2°C cold room. Porewater aliquots from both the gravity core and multicore 'R' were aliquotted via disposable syringe into vials for sulfate, sulfide, and DIC analyses. Sulfate vials were acidified with high-purity Seastar HCl to volatilize dissolved sulfide. Sulfide vials contained 1 M zinc acetate to trap sulfide as solid ZnS, and an untreated aliquot without headspace was retained for DIC. All porewater samples were stored frozen (-40°C) until analysis. DIC concentrations and $\delta^{13}C$ values were measured by combustion elemental analyzer – isotope ratio mass spectrometry (EA-IRMS, Costech EA, Thermo Delta V+ with Gasbench II) and have estimated uncertainties of ~2% and 0.21‰ (1σ), respectively. Zinc sulfides were washed with milli-Q water and oxidized to sulfate with hydrogen peroxide (90°C, 24 hrs). Porewater sulfate and sulfide were analyzed as sulfate by ICP-MS (see below).

The multi-core preserved the sediment-water interface; the gravity core did not. Initial field observations of the gravity core suggested overpenetration of ~35 cm. Our revised estimate of ~13 cm overpenetration is based on the linear extrapolation of DIC and sulfate concentrations to seawater values at the sediment-water interface. We also present data from one box core sample (0–10 cm) that was collected at approximately the same location on a prior cruise to Santa Barbara Basin in 2004, as described in Li et al. (2009). This material was frozen without squeezing in heavy-duty Ziploc bags at –40°C until sub-sampling.

2.3 Sample Preparation and Sulfur Analyses

Sediment samples were freeze-dried and then subjected to sequential organic and acid extractions (Fig. 1). Sediments were first microwave-extracted twice with 9:1 dichloromethane (DCM):methanol (MeOH) at 100°C for 15 minutes (MARS 5, CEM Corp). The total lipid extract was separated into fractions by silica gel chromatography, eluting with 4:1 hexane:DCM for non-polar OS, DCM for intermediate-polarity OS (not discussed further here), and 1:1 DCM:MeOH for polar OS. S^0 represents the vast majority of the sulfur in the non-polar extractable organic fraction. A split of this fraction was treated with activated elemental Cu to remove S^0 (Blumer, 1957) and account for the small quantity of non-polar organosulfur compounds in this fraction. Aliquots of the polar OS and treated and untreated non-polar OS fractions were dried and then oxidized in 30% H_2O_2 at 90° C for 24 hours. Solvent-extracted sediments were washed twice with

Milli-Q water to remove any residual porewater sulfate and then leached in 1 N nitric acid for 12 days at room temperature to oxidize mineral sulfides, predominantly pyrite, to sulfate (Schimmelmann and Kastner, 1993). This 'pyrite' fraction may include a minor amount of other metal disulfides and oxidizable, non-solvent-extractable organosulfur compounds, but not acid-volatile components, including most mineral monosulfides (Rickard and Morse, 2005). Leached sediments were washed twice with 0.5 N HCl and freeze-dried for residual organic matter analysis.

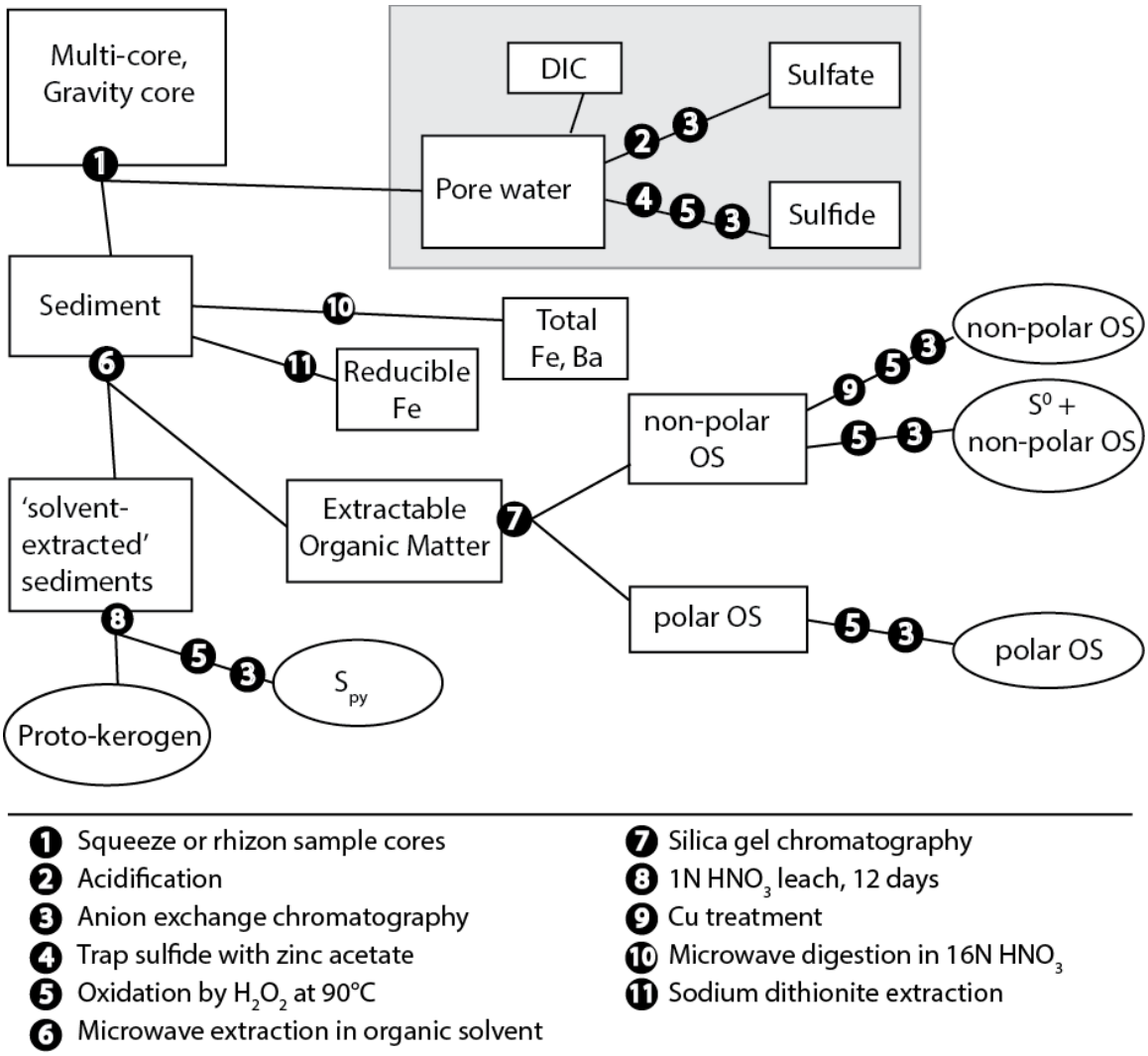

Figure 1. *Sample analysis workflow (see text for methodological details).*

Oxidized pyrite, S^0, and extractable OS fractions were then purified on AG1-X8 anionic exchange resin (Paris et al., 2013). Resin was washed with ten column volumes (CV) 10% HNO_3, conditioned with 10 CV 10% HCl and 10 CV 0.5% HCl, loaded in trace

HCl, and washed with 3x5 CV MQ H_2O before sulfate was eluted in 0.5N HNO_3. Sulfate samples were stored dry in Teflon vials until analysis.

Pyrite, S^0, extractable OS fractions, sulfate and porewater sulfide were quantified as sulfate by ion chromatography (IC, Dionex ICS-2000) with an AS-19 anion column and AERS 500 ion regeneration. The reproducibility of IC concentration measurements was better than 2% (1σ), and external standard replicates, reflecting sample purification, workup, and analysis, had a long-term error of ±10% relative. Concentrations were used to intensity-match samples and the required Na^+ supplement for analysis by inductively coupled plasma – mass spectrometry (ICP-MS, Thermo Neptune$^+$) (Paris et al., 2013). Samples were injected into the plasma torch with a desolvating nebulizer (Aridus) and bracketed with a $NaSO_4$ standard solution with a $\delta^{34}S$ value of –1.5‰. The Neptune was operated in medium resolution ($M/\Delta M \sim 8000$) to fully resolve oxygen interferences on mass 34. Sample $\delta^{34}S$ reproducibility was typically better than ±0.2‰. Sulfur in residual material, which we refer to as proto-kerogen, was measured as SO_2 by EA-IRMS (Carlo Erba NC 2500 EA connected to a Delta+ XL, ThermoQuest, via the Thermo Conflo III interface). Proto-kerogen concentrations and $\delta^{34}S$ data have estimated uncertainties based on standard replicates of ± 2.5% and ± 0.5‰, respectively.

2.4 Iron Analyses

A separate aliquot of freeze-dried sediment was weighed and microwave-digested in 16 N reagent-grade HNO_3 (15 min, 1200W) for analysis of total iron (Fe_T) and barium. A

0.5-g aliquot was extracted by the dithionite method to determine 'reducible' iron (Fe_R) primarily in the form of iron (oxy)hydroxides (Raiswell et al., 1994). Sediments (0.5 g) were buffered in 20 mL of 0.35 acetic acid / 0.2 N sodium citrate solution and extracted with 1 g sodium dithionite at room temperature for two hours. Fe_T, Ba and Fe_R were analyzed by inductively coupled plasma optical emission spectrometry (ICP-OES, Perkin-Elmer Optima 7300DV) at the UC Riverside Environmental Sciences Research Laboratory. Uncertainties for Fe_T and Fe_R based on standard replicates are ≤ 2.0%.

2.5 Electron microscopy

To image authigenic pyrite in the Santa Barbara Basin sediments, representative dried sediment samples (from 1, 6, 16, 26, 61, and 215 cm depths) were pressed onto carbon tape, carbon coated, and imaged using a Zeiss 1550VP Field Emission SEM equipped with an Oxford X-Max 80mm^2 SDD EDS system housed at Caltech (12 mm working distance; 120 μm aperture). High-resolution images of the sediment were taken using secondary electron detector and backscatter detector imaging modes to enhance compositional contrast. Energy-dispersive X-ray spectroscopy was used to confirm elemental compositions with accuracy typically better than 5% relative.

3. RESULTS

We discuss our results in terms of three 'zones' representing major features of the dataset. Zone 1 includes the shallowest 10 cm of sediments near the sediment-water interface, and is represented only in multicore data. Zone 2 is present in both the multicore and gravity core between 45 – 55 cm below seafloor, and captures an inflection point in the profiles of some sulfur species. Zone 3 is present only in the gravity core and contains the apparent sulfate-methane transition zone (SMTZ) at 165 – 190 cm depth. Results for the concentration and isotopic composition of dissolved and solid-phase pools are provided in Supplementary Tables 1 and 2, respectively. We compare our multicore and gravity core data with other samples collected in approximately the same area of Santa Barbara Basin, including a box core sample from 2004 (Li et al., 2009) and ODP Hole 893A, which was drilled to 191 m depth (~160,000 yrs) in November 1992 (Bruchert et al., 1995).

Concentration profiles of DIC, sulfate, and sulfide in the gravity core are generally consistent with previously published data (Sholkovitz, 1973; Schimmelmann and Kastner, 1993; Reimers et al., 1996; Kuwabara et al., 1999; Li et al., 2009). These porewater species have distinctly different profiles in the multicores, however, potentially reflecting spatial heterogeneity in the basin. Santa Barbara Basin is characterized by occasional, meter-scale topographic features that could affect sediment accumulation (as observed during Jason ROV operations). Alternatively, the multicore coring site could have been disturbed, either by a recent depositional event or during core collection. To

assess potential disruption at the multicore coring site, we split multicore 'A' in half while still frozen and polished the exposed surface. We observed a distinct, firm, light-toned layer at 5–8 cm within zone 1 that may represent a recent, discrete depositional event associated with a sediment gravity flow. Between 20 and 45 cm depth, the sediment is characterized by mm-scale laminations that are consistent with previous observations (Fleischer, 1972; Soutar and Crill, 1977; Schimmelmann et al., 1990; Schimmelmann and Lange, 1996). Laminations are thicker between 10 and 20 cm and are apparently folded due to subcoring of multicore 'A'. Despite the apparent deformation of these layers, minimally deformed laminae at 8.5 and ~20 cm and substantial gradients of DIC, sulfide, and sulfate across this interval indicate that porewater mixing was not extensive during core collection. In zone 2 and below of multicore 'A', sediments are massive, potentially indicating a period of rapid sedimentation at the multicore sampling site ~100 years ago. Because porewater concentration profiles in the multicore and gravity core may reflect different depositional conditions at each coring site, we did not merge the two cores into a single combined record, but rather discuss them separately in the following discussion.

3.1 Carbon Pools

Total organic carbon (TOC) concentrations, shown in Fig. 2, range from 2.58 to 4.52 mmol C/g dry weight and average 3.29 mmol C/g (4.0 wt.%), with analytical uncertainties of 0.32 mmol C/g. The $\delta^{13}C$ value of this pool averages -22.0‰ and ranges from -22.7 to -21.5‰, with an analytical uncertainty of ±0.1‰. The distributions of TOC values from the gravity core and multicores are comparable in mean and variance,

although $\delta^{13}C$ profiles do not match point for point between cores with the current alignment. In pore water, DIC concentration profiles in the multicore and gravity core (above zone 3) have distinctly different slopes of 0.18 mM/cm and 0.086 mM/cm, respectively. DIC concentrations cease their linear increase in zone 3 and below, where they average 31.4 ± 1.0 mM (1σ). Zone 3 also contains minimum values of DIC $\delta^{13}C$, averaging -24.55 ± 0.45‰ (1σ).

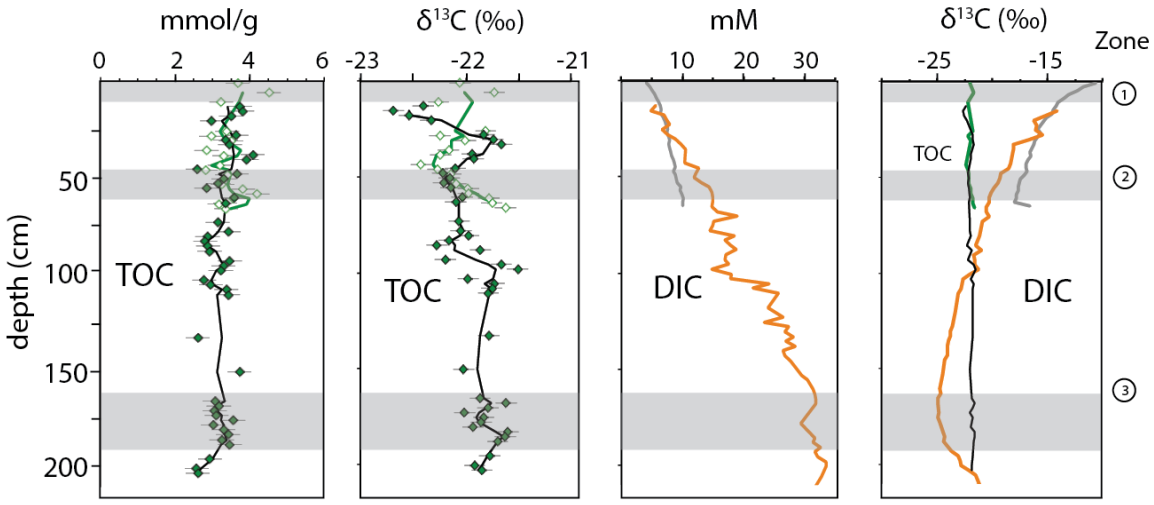

Figure 2: Concentrations and isotopic compositions of total organic carbon (TOC) and dissolved inorganic carbon (DIC). *Shaded bands refer to zones (1-3, at right) discussed in text. TOC $\delta^{13}C$ values are repeated in panel D for comparison. Filled symbols represent gravity core results, and open symbols represent multicore results. Lines on TOC plots show three-point running averages. Porewater DIC results for the multi- and gravity cores are shown in light (grey) and darker (orange) lines, respectively. DIC concentration uncertainties are approximately ±2%. Uncertainties for DIC $\delta^{13}C$ data are less than the line width.*

Total Fe concentrations in Santa Barbara Basin sediments, shown in Fig. 3, average 307 μmol Fe/g and are similar in both cores. As much as 39% of this Fe is present as reducible iron oxy-hydroxides (ferrihydrite, goethite, lepidocrocite, hematite) near the surface. Dithionite-reducible iron (Fe_R) concentrations average 99.5 ± 2.0 μmol Fe/g in zone 1 (0–10 cm) and decline smoothly to zone 2, where 27.2 μmol Fe_R/g represents only about 10% of total iron. Fe_R concentrations drop more gradually below zone 2, reaching an average of 14.4 μmol Fe/g in zone 3.

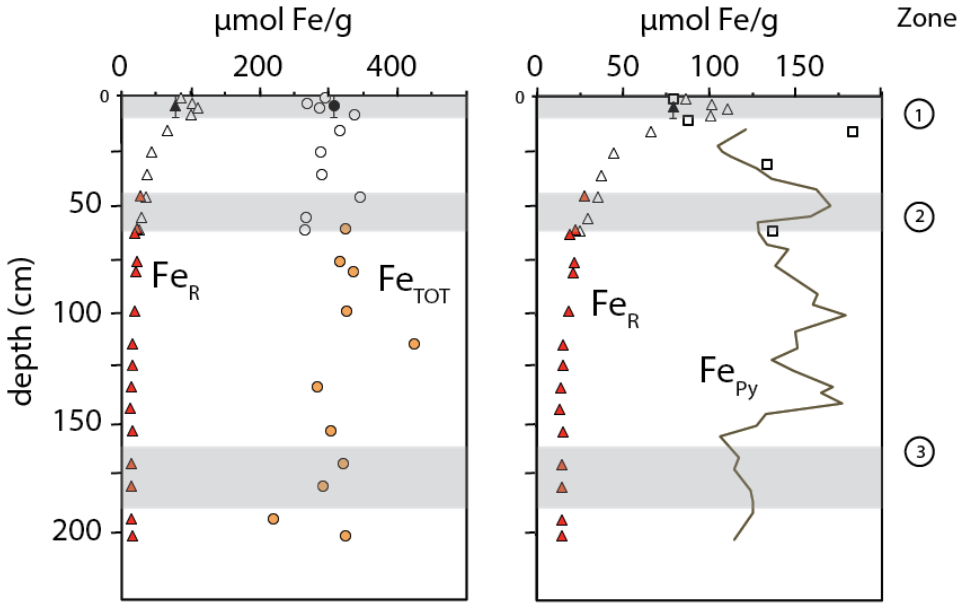

Figure 3: Concentrations of iron pools in Santa Barbara Basin sediments*. Total iron (Fe_{TOT}), reducible iron (Fe_R), and a running 3-point average of pyrite (Fe_{Py}) iron are shown as circles, triangles, and a thin line, respectively. Fe_{Py} data from the multicore are*

shown as open squares. Open triangles represent multi-core data; filled triangles are from the gravity core and filled black symbols with vertical error bars are from the box core. Fe_{Py} is calculated from S_{py} results assuming an ideal 2:1 S:Fe stoichiometry. Shaded bands indicate zones discussed in the text. The right panel shows the same Fe_R data as at left but with expanded x-axis for clarity. Error bars for Fe_T and Fe_R are smaller than symbols.

3.3 Dissolved Sulfur Pools

Porewater sulfate and sulfide exhibit very different behaviors in the two cores (Fig. 4). In the gravity core, concentrations of sulfate and sulfide are relatively noisy, likely due to the imprecise method of aliquotting porewaters shipboard (analytical standards were much more precise), but nevertheless show roughly linear changes throughout. Sulfate concentrations drop from a maximum concentration of 27.8 mM in the shallowest available sediments to 3.2 mM in zone 3. Over this interval, sulfate becomes increasingly ^{34}S-enriched with a slope of 0.25‰/cm, with a maximum $\delta^{34}S$ value of 61.8‰ at 163 cm. Standards processed along with sulfate samples from 100 to 160 cm were inaccurate for unknown reasons, and so these data are not reported. Reoxidation of porewater sulfides during squeezer sampling from the gravity core is likely responsible for the convergence of sulfate and sulfide $\delta^{34}S$ values as well as the nonzero sulfate concentrations below zone 3. Accordingly, sulfide concentrations in the gravity core are minimum estimates. Measured sulfide concentrations are near zero (~ 0.05 mM) above 22 cm depth and increase to ~2 mM in zone 3. The sulfur-isotopic composition of this sulfide averages -

14‰ in zones 1–2. Below zone 2, sulfide $\delta^{34}S$ increases in parallel with that of sulfate to a maximum value of 22.9‰ at the base of zone 3.

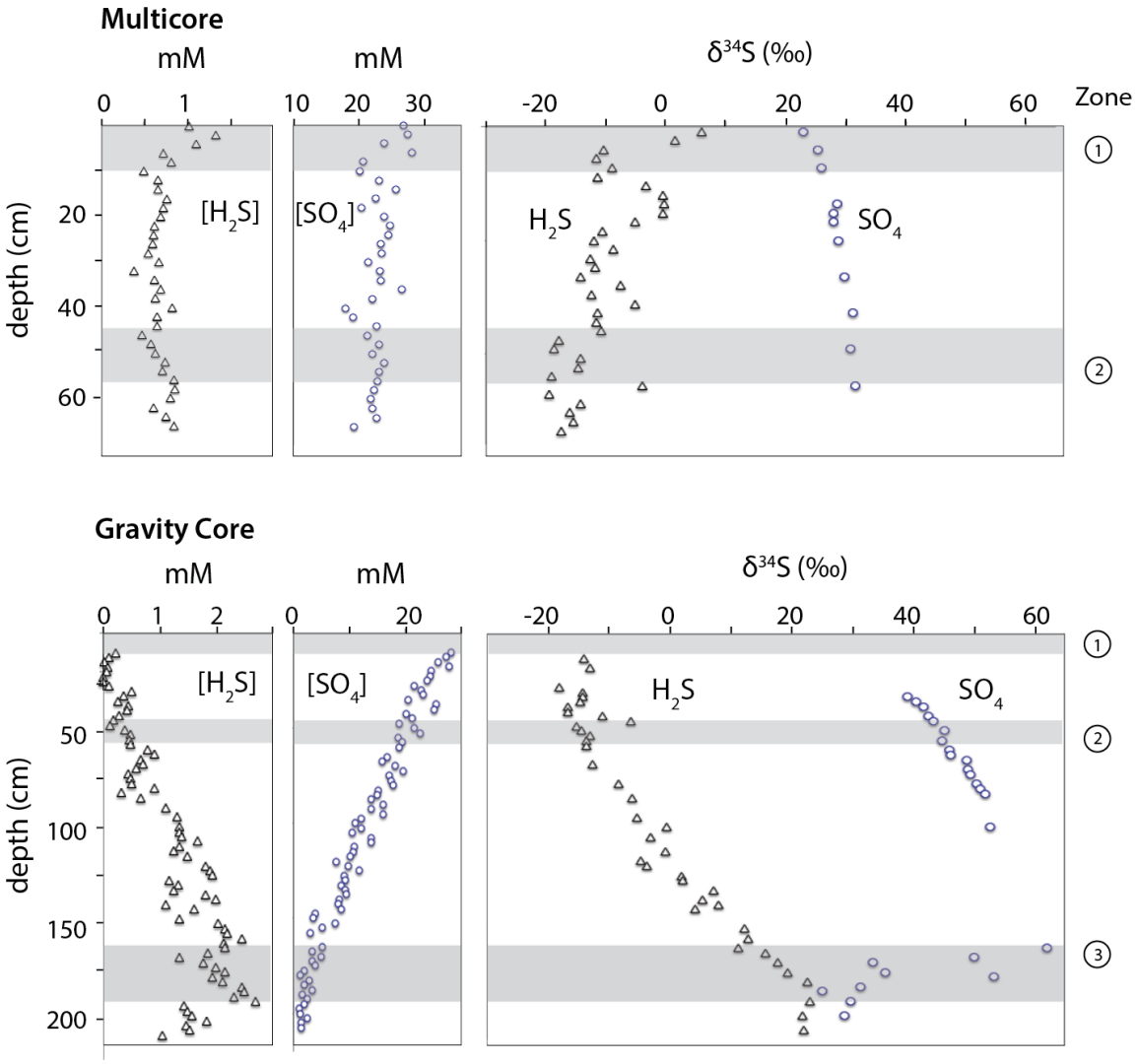

Figure 4: Concentrations and isotopic compositions of sulfate and sulfide in porewater from the multicore (top) and gravity core (bottom). *$\delta^{34}S$ values are relative to VCDT,*

and have analytical uncertainties smaller than symbols. Shaded bands (labeled at right) indicate zones discussed in the text.

Porewater profiles of sulfate and sulfide in the multicore differ from both the gravity core and previously published profiles (Reimers et al., 1996; Kuwabara et al., 1999) from the Santa Barbara Basin. Below zone 1, sulfate concentrations in the multicore are steadily 22.5 ± 1.9 mM (1σ). Sulfate $\delta^{34}S$ values increase with depth gradually, with a slope of only 0.13‰/cm. In a closed (i.e., Rayleigh-type) system, this change would be equivalent to less than 0.5% consumption of the porewater sulfate reservoir by a reaction with a fractionation factor similar to the offset between porewater sulfate and sulfide at this depth (~30‰). Another surprising difference between the multicore and prior work is the presence of 1.3 mM sulfide in porewater near the sediment-water interface. Below zone 1 in the multicore, the concentration of porewater sulfide is relatively constant at 0.66 ± 0.11 mM (1σ). Over the same interval, however, sulfide $\delta^{34}S$ values exhibit several shifts with amplitudes of roughly 10‰. Below zone 2, sulfide $\delta^{34}S$ is much less variable and increases linearly toward a value of 20‰ in zone 3.

3.4 Solid Sulfur Pools

Concentrations of the major pools of solid-phase sulfur in Santa Barbara Basin sediments are shown in Fig. 5. In general, the concentration and $\delta^{34}S$ profiles of these solid-phase pools are consistent between the multicore and gravity core for the current alignment. Near the sediment-water interface, the pyrite sulfur (S_{py}) pool is slightly larger than the

proto-kerogen S (OS_{pk}) pool while the pool of elemental sulfur (S^0) is about half as large. The $\delta^{34}S$ profiles of all three solid sulfur pools share some features, including $\delta^{34}S$ minima within zone 2 and higher $\delta^{34}S$ values in zone 3.

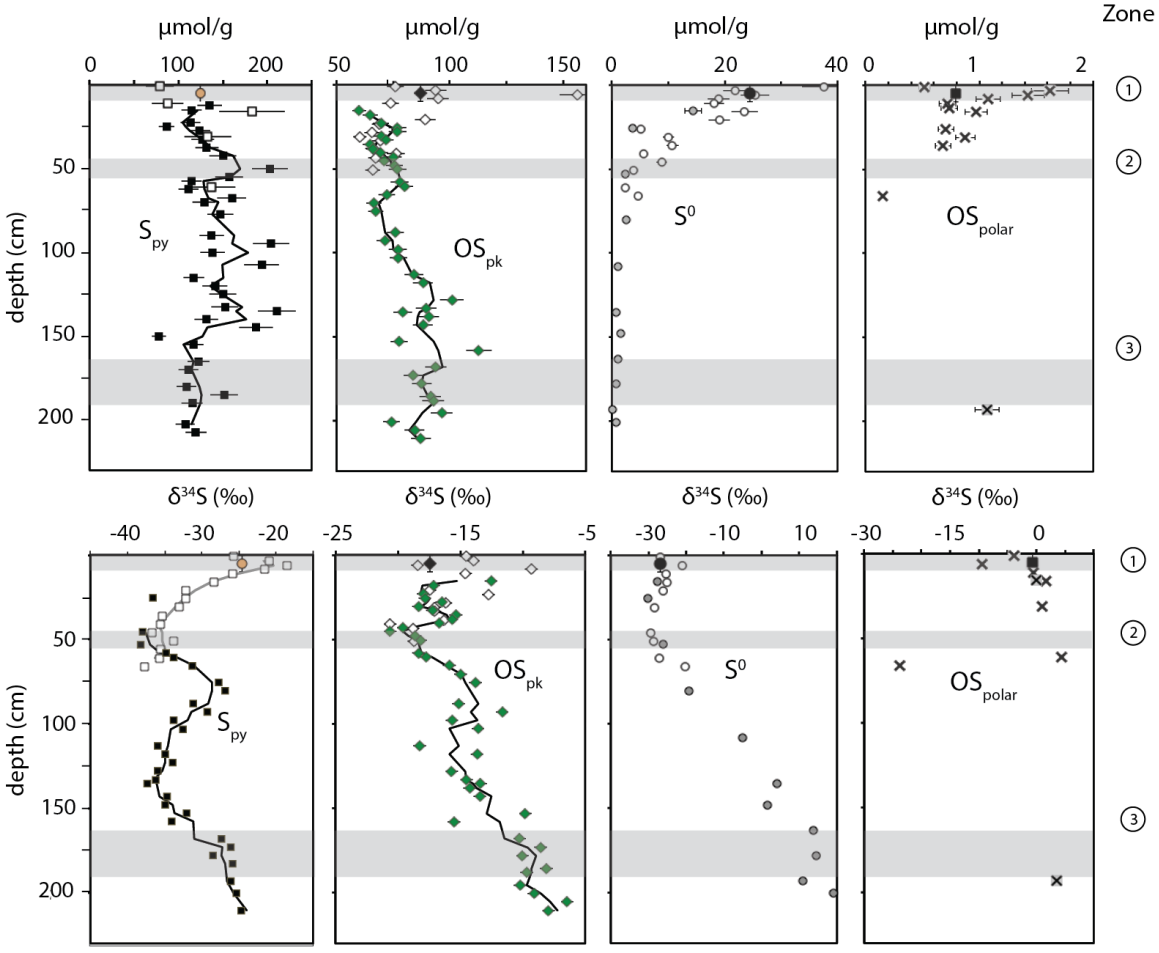

Figure 5: Concentrations and isotopic compositions of solid-phase sulfur pools in Santa Barbara Basin sediments*, including pyrite (S_{py}), proto-kerogen (OS_{pk}), elemental S (S^0), and polar extractable OS. Shaded bars, labeled at right, indicate zones discussed in the text. Open symbols represent multicore data; filled symbols represent gravity core*

data, and filled symbols at 5 cm are from the box core. Three-point running averages are shown for gravity core S_{py} and OS_{pk} (black lines) and multicore S_{py} (grey line).

Pyrite concentrations increase with depth from an average of 84 μmol S/g (zone 1) to approximately 135 μmol/g in the deeper multicore or 170 μmol/g in zone 2 of the gravity core. Below zone 2, pyrite concentrations are broadly constant except for a shift toward lower concentrations near the SMTZ (zone 3). Pyrite concentrations in the gravity core average 146 ± 35 μmol S/g between zones 2 and 3 and only 119 ± 15 μmol S/g in zone 3 and below. The isotopic composition of pyrite varies from –20.9 to –38.2‰ and shows complex variation with depth. Pyrite $\delta^{34}S$ values in the multicore decrease dramatically between zones 1 and 2 and have a second minimum at the top of zone 3 in the gravity core.

The highest S^0 concentrations are near the sediment-water interface (zone 1), where they reach 38 ± 4 μmol/g. They decline with depth over the multicore to 5.0 ± 0.5 μmol/g in zone 2. S^0 concentrations in the gravity core also decline with depth, from 2.3 μmol/g in zone 2 to 0.8 ± 0.1 μmol/g in zone 3. The small amounts of S^0 in deeper sediments have sulfur isotopic compositions that become increasingly ^{34}S-enriched with depth, approaching the composition of dissolved sulfide.

Proto-kerogen S concentrations in the multicore are consistent with depth, averaging 74.5 ± 11.3 μmol/g. This value excludes one extremely OS-rich sample at 6 cm depth

containing 156.4 ± 4 μmol/g. In contrast, the gravity core has a depth trend in proto-kerogen S, increasing from a multi-core-like concentration in zone 2 to an average concentration of 89.9 ± 4.1 μmol/g in zone 3. A linear regression of this data yields a slope of approximately 0.12 μmol S/g/cm (R^2 = 0.52). Paired with a less significant decrease in TOC of –2.2 μmol/g/cm (R^2 = 0.13), the molar S:C ratio of proto-kerogen increases from about 1.8% to 3.2% between zones 2 and 3 of the gravity core. Minimum $\delta^{34}S$ values for proto-kerogen S are found in zone 2, where they average –18.8 ± 1.1‰ (1σ). Proto-kerogen $\delta^{34}S$ values increase with depth to an average of –9.3‰ ± 0.9‰ in zone 3. In both cores, proto-kerogen $\delta^{34}S$ values are consistently around 15-20‰ more ^{34}S-enriched than those of coexisting pyrite. The size of this offset is not correlated with solid phase $\delta^{34}S$ values, TOC, or proto-kerogen S:C ratio.

4. DISCUSSION

4.1 Apparent rates of microbial sulfate reduction (MSR)

A fundamental control on the sedimentary sulfur cycle is the rate of microbial sulfate reduction (MSR), which generates the reduced sulfur required for organic S and pyrite formation as well as sulfide-oxidizing metabolisms. Gross rates of MSR may significantly exceed net rates because microbial communities commonly reoxidize the majority of sulfide produced by MSR (Jorgensen, 1979; Walker and Brimblecombe, 1985; Zerkle et al., 2009). MSR rates have been reported previously for Santa Barbara

Basin based on experiments using $^{35}SO_4$ (Reimers et al., 1996), which yielded estimates of 2 to 10 mM/yr in the upper 10 cm and approximately 0.4 mM/yr below ~22 cm depth. In the following section, we constrain the rates of net and gross MSR in our cores based on changes in the abundance and isotopic composition of sedimentary sulfur pools, reducible iron (Fe_R), and DIC. This analysis yields MSR rates that are comparable with those of Reimers et al. in the upper 10 cm but slower in deeper sediments. We convert sediment depths to approximate ages using an age model based on density profiles and varve counts from Schimmelmann et al. (1990; 2013) and visual observation of laminae in multicore 'A.'

Sediments in zone 1 (0–10 cm) show evidence for extensive MSR. Our shallowest porewater sample (0–2 cm) contains substantially more abundant and more ^{13}C-depleted DIC (4.1 mM, -10.7‰) than seawater (2.2 mM, ~0‰), indicating extensive remineralization of organic matter. Due to low concentrations of O_2 in Santa Barbara Basin bottom waters (<10 μM, (Sholkovitz, 1973; Moffitt et al., 2015)), we attribute the majority of this DIC to the respiration of organic carbon by MSR with potential smaller contributions from anaerobic heterotrophy using nitrate, iron, or manganese (porewater nitrate concentrations are <80μM, (Reimers et al., 1996)) and fermentation. Surface sediments also contain 228 ± 23 μmol/g solid-phase reduced sulfur, including pyrite, proto-kerogen, polar extractable OS, and S^0. Each of these phases can act as 'traps' for the $\sum H_2S$ produced by MSR. If delivery from the water column is assumed to be negligible and zone 1 sediments contain an average of 82 wt% water, this concentration

of reduced S solids would represent a sink of approximately 2.6 mmol S/cm^3/yr, equivalent to 3.1 mM/yr dissolved $\sum H_2S$. This rate estimate neglects any $\sum H_2S$ that diffuses out of the sediments or is reoxidized to sulfate. It is not possible to assign strict limits on the extent of sulfide reoxidation to sulfate near the sediment-water interface without data for bottom water O_2 and nitrate concentrations. However, the net rate of solid-phase S change is a minimum estimate of the gross rate of $\sum H_2S$ production. Estimates of minimum MSR rates in zone 1 (at the multicore site) of >2.6 mM/yr are consistent with prior estimates of 2 to 10 mM/yr (Reimers et al., 1996).

Below zone 1, sulfate in porewater reflects the balance of MSR, the reoxidation of reduced S species to sulfate, and net downward diffusion. Neither the multicore nor the gravity core sulfate concentration profiles have any discernable curvature. This is consistent with either an entirely diffusion-controlled regime in which net MSR rates are near zero in sediments between zones 1 and 3 (the SMTZ) or highly efficient sulfur cycling (i.e., MSR followed by complete reoxidation of sulfide back to sulfate). In the absence of O_2, sulfide oxidation may be coupled to the reduction of ferric iron, manganese oxides, or nitrate. Nitrate concentrations were observed to drop toward zero within a few cm of the surface throughout the Santa Barbara Basin (Reimers et al., 1996), so Fe(III)-bearing phases likely represent the primary electron acceptors for sulfide reoxidation below zone 1. The pool we quantify as Fe_R is functionally defined to include easily reducible iron species that have been shown to react with sulfide on a timescale of hours to days. The Fe in silicates, which makes up the majority of our Fe_T pool, is thought to have a half life of hundreds to tens of thousands of years in reaction with

sulfide (Canfield et al., 1992; Raiswell and Canfield, 1998). Therefore, we assume that Fe_R is the most significant electron acceptor below zone 1 in Santa Barbara Basin sediments.

In the multicore, Fe_R concentrations drop from 99.5 μmol/g (18 μmol/cm^3) in zone 1 to 32.3 μmol/g (8.4 μmol/cm^3) in zone 2. Fe_R loss at a rate of 80 nmol/cm^3/yr is balanced by the accumulation of Fe in pyrite, and we tuned the shallow age model to equate these values. Full oxidation of sulfide to sulfate requires the transfer of eight electrons, or eight equivalents of Fe^{3+} reduction. If $\sum H_2S$ is fully oxidized to sulfate, Fe_R loss between zones 1 and 2 is therefore capable of powering the stoichiometric oxidation of $\sum H_2S$ at a rate of 10 nmol/cm^3/yr, equivalent to approximately 13 μM/yr of dissolved $\sum H_2S$ assuming sediment contains 77 wt% water. Partial oxidation of $\sum H_2S$ (e.g., to S^0) could also consume Fe_R without regenerating sulfate, although there is little evidence for S^0 formation below zone 1. Active turnover of the shrinking S^0 pool might be expected to make S^0 $\delta^{34}S$ values more similar to that of actively forming pyrite, while instead we observe S^0 $\delta^{34}S$ values are steady through this interval. The primary biogeochemical role of S^0 in multicore sediments is more likely as a metabolic substrate, as it is lost at a rate of 42 nmol/cm^3/yr.

Based on the availability of oxidants, the rates of MSR in multicore sediments are quite low in sediments below zone 1 (on the order of 0.01 mM/yr). In the gravity core, the abundance of Fe_R declines at an even slower rate (10 nmol/cm^3/yr) and can only account

for the oxidation of around 1 μM/yr of sulfide to sulfate. These rates are several orders of magnitude slower than the several-mM/yr rates implied in zone 1. The linear sulfate concentration profiles in these sediments thus appear to reflect very low MSR rates and a diffusive flux of sulfate down toward the SMTZ (zone 3). Linear DIC profiles are also consistent with a diffusion-controlled porewater regime. The low MSR rates we infer would not generate any observable curvature in the DIC concentration profile, as DIC will diffuse upward from the SMTZ (assuming a diffusion constant of ~1 x 10^{-5} cm^2/sec) at approximately 45 μmol/cm^2/yr.

Low MSR rates between zones 1 and 3 are surprising given the availability of sulfate in pore fluids. MSR in this environment is apparently limited by the availability of electron donors (H_2 or OM) or nutrients (e.g., iron, Sim et al., 2012) rather than electron acceptor (sulfate). Although OM limitation in the presence of 4 wt.% TOC may appear paradoxical, it may instead speak to the importance of OM stabilization near the sediment-water interface. Throughout both cores, OM contains an average of 6.4 wt.% S (molar S:C ratio of 2.4%). We speculate that this S-rich proto-kerogen material may be substantially more resistant to microbial hydrolysis and thus indigestible to heterotrophic sulfate reducers, limiting their growth. Alternatively, sulfate reducers may simply be outcompeted by fermentative organisms that are better at consuming polymeric organic matter.

4.2 Pyrite Formation in Santa Barbara Basin

Pyrite in Santa Barbara Basin sediments appears to form most rapidly near the sediment-water interface, where it is present at an average concentration of 84 μmol S/g. In zone 1, which is only captured in the multi-core, pyrite concentrations are equivalent to ~55% of the concentrations in zone 2. Pyrite $\delta^{34}S$ values in surface sediments are very similar to those of S^0, suggesting that pyrite and S^0 are either genetically related or equilibrate with one another *in situ*. Although rates of pyrite accumulation drop below zone 1, pyrite formation appears to remain an important sink for both sulfur and Fe_R until the base of zone 2, at least in the multi-core. Over this interval, the $\delta^{34}S$ value of pyrite shifts from -25.7‰ to -37.7‰ while porewater $\sum H_2S$ $\delta^{34}S$ values are substantially higher, ranging from 5.9‰ to –19.5‰ (± 0.2‰, Fig 6). In the shallowest sediment sample, the difference between pyrite and $\sum H_2S$ $\delta^{34}S$ values is more than 30‰. Porewater $\sum H_2S$ remains more ^{34}S-enriched than pyrite throughout the gravity core (Fig. 7). Assuming the precipitation process generates small to zero fractionation from its sulfur source (Wilkin and Barnes, 1996; Bottcher et al., 1998), the S-isotopic composition of pyrite cannot be inherited directly from that of porewater $\sum H_2S$ as measured.

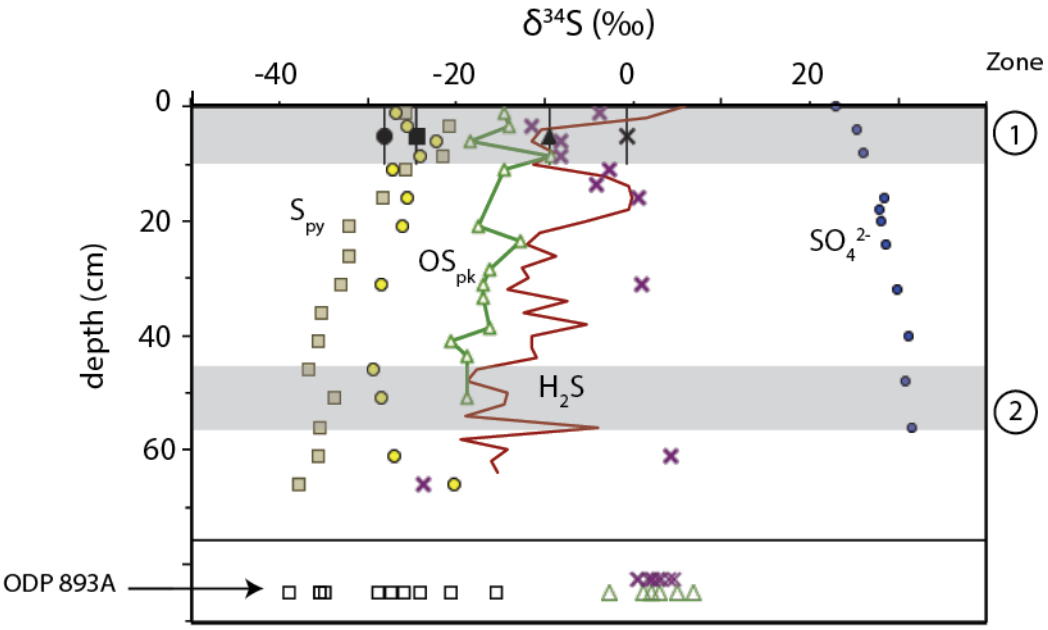

Figure 6: $\delta^{34}S_{VCDT}$ relationships among reduced sulfur pools in multicore sediments and ODP Hole 893A. *Solid black symbols at 5 cm depth represent data for the box core. Symbols represent pyrite (S_{py}, squares), elemental S (S^0, open circles), proto-kerogen (OS_{pk}, triangles), porewater sulfide ($\sum H_2S$, red line); polar extractable OS (Xs), and porewater sulfate (SO_4^{2-}, small filled circles). ODP Hole 893A samples were collected between 0.9 and 192 m below sea floor; data from (Bruchert et al., 1995). Grey bands, numbered at right, correspond to zones discussed in the text.*

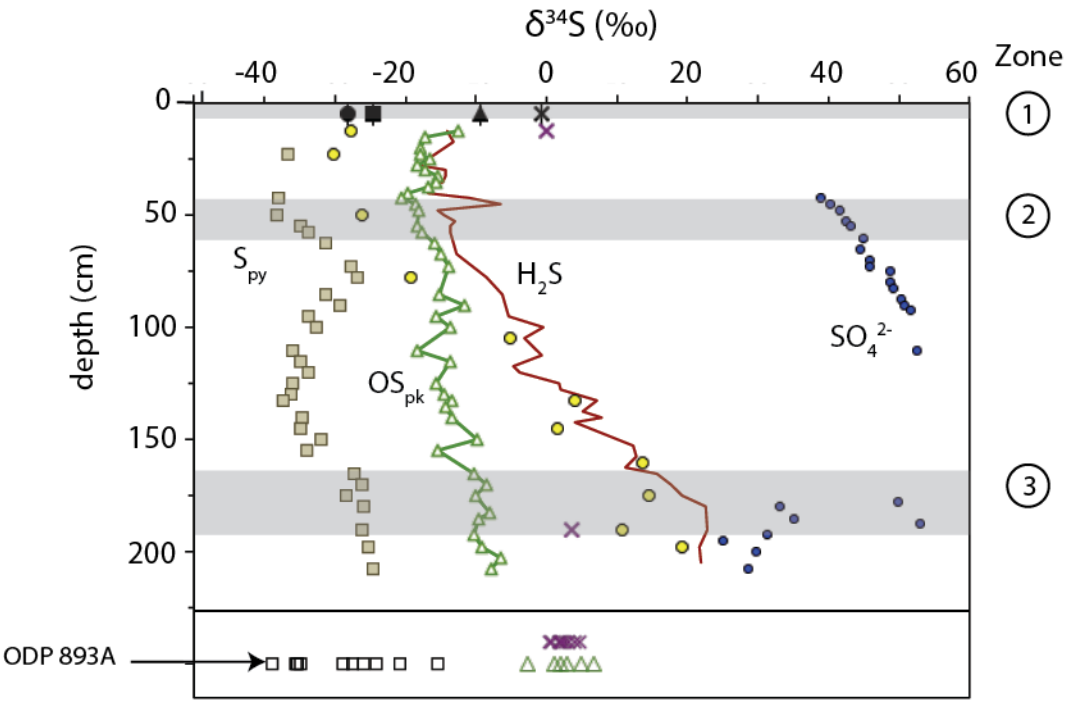

Figure 7: $\delta^{34}S_{VCDT}$ relationships among reduced sulfur pools in gravity core sediments and ODP Hole 893A. *Solid black symbols at 5 cm depth represent data for the box core. Symbols represent pyrite (S_{py}, squares), elemental S (S^0, open circles), proto-kerogen (OS_{pk}, triangles), porewater sulfide ($\sum H_2S$, red line); polar extractable OS (Xs), and porewater sulfate (SO_4^{2-}, small filled circles). ODP Hole 893A samples were collected between 0.9 and 192 m below sea floor; data from (Bruchert et al., 1995).*

Similar isotopic relationships between porewater sulfide and sedimentary pyrite are common in the literature. Kaplan et al (1963), working on shallow (<4 m) sediments from the California Borderland Basins, recorded pyrite that was an average of 24‰ depleted in ^{34}S relative to porewater "free sulfide" and 10‰ depleted relative to "acid volatile sulfide" (AVS). Canfield et al (1992) reported a ^{34}S depletion of fine-grained

pyrite relative to porewater "H_2S" of 5-15‰ over 2.5 m of sediment core from Long Island Sound (the FOAM site). Similarly, pyrite was ≥10‰ more ^{34}S-depleted than porewater sulfide in sediments from Cape Lookout Bight (Chanton and Martens, 1987). Bruchert et al (1996) reported 10-40‰ depletions of pyrite relative to AVS over the nearly 200 m of core from ODP Hole 893A, Santa Barbara Basin. In shallow sediments of St. Andrew's Bay, Florida, Bruchert and Pratt (1996) measured $\delta^{34}S$ values for pyrite that were 0-3‰ more negative than those of $\sum H_2S$, one of the few examples of similar $\delta^{34}S$ values for pyrite and sulfide. Canfield et al (1998) reported a 12-15‰ depletion of "chromium reducible sulfur" (presumed to be mainly pyrite) relative to AVS over 50 cm in Mangrove Lake, Bermuda. Habicht and Canfield (2001) studied shallow (0 – 20 cm) sediments from seven different coastal environments, and obtained direct measurements of sulfide produced by MSR via incubation experiments. The sulfide $\delta^{34}S$ values were uniformly more positive than those of coexisting pyrite, by 5–30‰. In Cariaco Basin, Werne et al (2003) measured pyrite $\delta^{34}S$ values that were 3-5‰ more negative than coeval H_2S, although here the relationship is complicated by water column precipitation of pyrite. Dale et al (2009) studied the upper 5 m of sediment from the Namibian Margin, and found pyrite $\delta^{34}S$ values that are similar to those of porewater H_2S, but in an environment of intense sulfide re-oxidation.

The pattern of ^{34}S-depleted pyrite relative to porewater $\sum H_2S$ that we observe in Santa Barbara Basin thus appears to be common in anoxic marine sediments. Such a pattern is conventionally interpreted as evidence for sulfide oxidation to elemental S, which has a minimal isotope effect, coupled to sulfur disproportionation, which generates sulfide that

is 5–16‰ further ^{34}S-depleted and precipitates as pyrite (e.g. Canfield and Thamdrup, 1994; Habicht and Canfield, 2001). A limitation of this hypothesis is the necessity of somehow separating, in time or space, the sulfide produced by MSR from that produced by sulfur disproportionation. If they mixed prior to forming pyrite, then measurements of porewater $\sum H_2S$ should reveal an isotopic composition similar to pyrite.

Our new dataset from Santa Barbara Basin presents several difficulties for this conventional explanation. First, pyrite and S^0 have similar $\delta^{34}S$ values while porewater sulfide is 33‰ heavier than either solid-phase S pool. Thus S^0 at the sediment surface does not appear to be a direct product of porewater sulfide oxidation, and may instead have the same source as pyrite. Moreover, the disproportionation of S^0 produces fractionations >5‰ (Fry et al., 1986; Canfield, 2001) rather than the <1‰ difference from pyrite we observe in surface sediments. Disproportionation does not therefore appear to play a significant role in controlling pyrite $\delta^{34}S$ in Santa Barbara Basin surface sediments. Last but not least, the high spatial and temporal resolution of our dataset reveals that at no point does the $\delta^{34}S$ value of porewater $\sum H_2S$ approach that of pyrite, eliminating precipitation at shallower levels as a viable explanation.

As an alternative to disproportionation to explain the offset between porewater sulfide and pyrite $\delta^{34}S$, we propose the following hypothesis: the porewater $\sum H_2S$ that we sample is ^{34}S-enriched relative to that produced by MSR, which forms pyrite. The ^{34}S-depleted sulfide generated by MSR could be segregated from bulk porewater sulfide

within biological structures like cells (and their sheaths), microbial aggregates, or biofilms. The ε_{MSR} values of $\leq$ 80‰ that are implied by the $\delta^{34}S$ difference between porewater sulfate and accumulating pyrite in Santa Barbara Basin sediments are high but within known limits (Brunner and Bernasconi, 2005) and are similar to some values reported for ε_{MSR} at low sulfate reduction rates (Canfield et al., 2010; Sim et al., 2011).

Sulfur-cycling biofilms and aggregates are favorable locations for pyrite mineralization because they can both act as sources of $\sum H_2S$ and enhance rates of iron sulfide formation by several orders of magnitude (Frankel and Bazylinski, 2003). Biologically induced mineralization is increasingly seen as having an important role in the precipitation of various iron sulfide minerals, including pyrite (Canfield et al., 1998), pyrrhotite, mackinawite, and greigite (Neal et al., 2001; Schoonen, 2004), although the significance of biologically induced pyrite formation in marine sediments remains essentially unknown. Cell membrane surfaces promote reactions between the FeS* intermediate and S_n^{-2} because their negatively charged surfaces bind metal cations like Fe^{2+} and then stabilize the monosulfide intermediate, promoting crystal nucleation. Pyrite mineralization has been observed in association with enrichment cultures of both sulfur disproportionating and sulfate reducing bacteria. The marine S-disproportionating bacteria *Desulfocapsa* can induce rapid pyrite formation (Canfield et al., 1998) and the sulfate-reducing firmicute *Desulfotomaculum* is capable of mineralizing a bilayer of pyrite on the inside and outside of its cell membrane (Donald and Southam, 1999). Both organisms produce intracellular sulfide that equilibrates in natural systems to form both

S_n^{-2} and S^{2-} (Rickard and Luther, 2007). Additionally, many sulfur cycling microorganisms accumulate solid elemental S^0 (Frigaard and Dahl, 2009), which promotes the formation of reactive polysulfide species. Thus, many sulfur-cycling microorganisms provide a particularly favorable environment for biologically induced pyrite mineralization.

Direct inspection of pyrite grains supports the hypothesis of biologically induced pyrite mineralization in Santa Barbara Basin sediments. Sediment from seven depths were investigated by scanning electron microscopy (SEM), using high backscatter (QBSD) and elemental analysis by energy dispersive spectroscopy (EDS) to image and identify pyrite. At all depths, pyrite phases are exclusively present as sub-micron (~0.3 μm) equidimensional and equimorphic crystals, often aggregated into framboids. Examples are shown in Fig. 8. Although pyrite framboids have been shown to form abiotically at elevated temperatures (60 to 350° C) (MacLean et al., 2008), no laboratory studies have yet generated framboids abiotically at lower temperatures (Ohfuji and Rickard, 2005). Recent work by MacLean et al. (2008) provides evidence for the formation of framboidal pyrite on organic templates within microbial biofilms (Wacey et al., 2014). The pyrites observed in Santa Barbara Basin sediments are therefore consistent with biologically induced pyrite mineralization in association with sulfate-reducing microbial communities. We propose that the highly ^{34}S-depleted sulfide produced by MSR reacts to form pyrite within relatively isolated microbial biofilm environments and that the $\sum H_2S$ that diffuses away from this environment into porewater can subsequently become more

^{34}S-enriched via additional processes (discussed below). A key aspect of this hypothesis is that it can account for S^0 with $\delta^{34}S$ values similar to pyrite. We further note that generation of ^{34}S-depleted sulfide by MSR and sulfur disproportionation are not mutually exclusive, and both could contribute to pyrite formation.

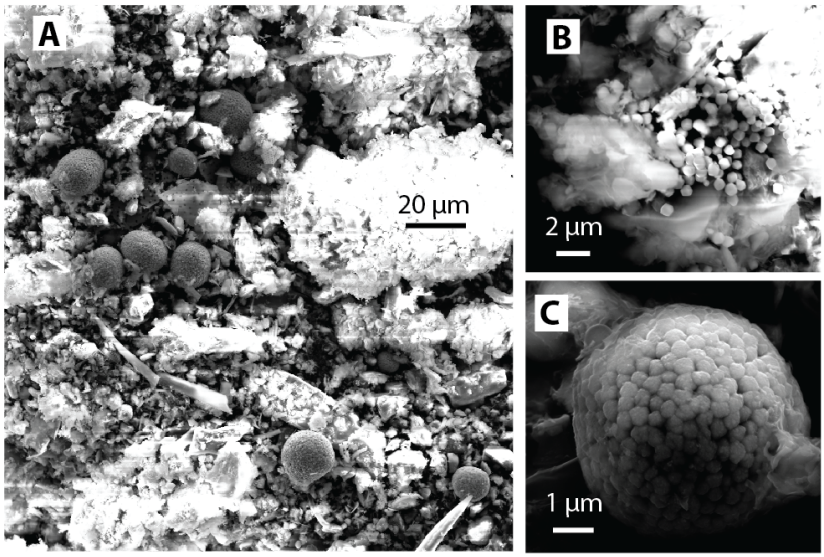

Figure 8: *Secondary electron photomicrographs of authigenic pyrites within siliciclastic Santa Barbara Basin sediments. Samples are stuck on carbon tape and carbon-coated; bright contrast in the foreground of A is due to charging. Phase identifications were confirmed using EDS. A: Cluster of ~10 µm diameter framboidal pyrites (26 cm sample); B: Individual pyrite crystals within an amorphous matrix (26 cm sample); C: Typical framboid morphology (215 cm sample).*

4.3 Potential controls on porewater sulfide $\delta^{34}S$

What additional processes might explain the consistent ^{34}S-enrichment of porewater sulfide relative to pyrite, proto-kerogen S, and S^0? We propose that isotopic exchange with organic sulfur is a prime candidate. Porewater $\sum H_2S$ and proto-kerogen have very similar $\delta^{34}S$ values in the upper 35 cm of the gravity core (within ~2‰). Below this depth, $\sum H_2S$ $\delta^{34}S$ values increase approximately linearly (Fig. 7), likely reflecting the upward flux of $\sum H_2S$ produced near the SMTZ (zone 3). The S-isotope composition of proto-kerogen partially follows that of porewater $\sum H_2S$ throughout deeper sediments and into the ODP core. In the presence of low MSR rates, these patterns suggest isotopic equilibration between these pools, especially in the upper part of the core. In Santa Barbara Basin, equilibration can drive particularly large $\delta^{34}S$ offsets between pyrite and proto-kerogen because proto-kerogen S is highly abundant while rates of $\sum H_2S$ production are low. Therefore, the equilibrium $\delta^{34}S$ value of the $\sum H_2S$ + OS system should be buffered by the proto-kerogen pool rather than by $\sum H_2S$. In environments with higher MSR rates and less abundant proto-kerogen S, equilibration would lead to smaller offsets between pyrite and proto-kerogen. In either case, phases precipitating within MSR-hosting microenvironments (e.g., pyrite) should trap the most strongly ^{34}S-depleted $\sum H_2S$, while $\sum H_2S$ that diffuses out of microenvironments into porewater can undergo isotopic exchange with abundant, ^{34}S-enriched organic matter and become more ^{34}S-enriched.

Dale et al. (2009) found similar evidence for equilibration between porewater $\sum H_2S$ and proto-kerogen in Namibian shelf sediments, where TOC and proto-kerogen S

concentrations are comparable to those in Santa Barbara Basin. Their model suggested that ~70% of proto-kerogen S and a similar proportion of S_{py} were exchangeable. However, with nearly 18 mM porewater $\sum H_2S$ (130 cm depth), isotopic equilibration between porewater $\sum H_2S$ and some proto-kerogen S in Namibian shelf sediments has a strong effect on the $\delta^{34}S$ value of the organic matter but a negligible effect on porewater $\sum H_2S$ (Dale et al., 2009), which is opposite the situation in Santa Barbara Basin. Also unlike that study, we find no evidence for isotopic exchange between porewater sulfide and pyrite in our samples. This difference may reflect different conditions of pyrite formation in Santa Barbara Basin and the Namibian Shelf, where rates of sulfate reduction are much higher and pyrite formation occurs deeper in the sediments.

Even more so than for proto-kerogen, polar extractable OS $\delta^{34}S$ values track $\sum H_2S$ $\delta^{34}S$ in the shallow multicore. Both the extractable OS and porewater $\sum H_2S$ multicore $\delta^{34}S$ profiles reproduce a sharp shift from values near -10‰ at 10 cm depth to around 0‰ at 20 cm. Equilibration between OS and porewater sulfide is a potential mechanism to maintain this strong of an isotopic gradient despite ongoing diffusion. Although the quantity of sulfur in polar extractable OS alone is insufficient to control the $\delta^{34}S$ value of porewater sulfide, polar extractable OS may be representative of the portion of proto-kerogen S that is exchangeable. Essentially, we propose that sulfide $\delta^{34}S$ values in shallow sediments are buffered by local exchange with OS, including polar extractable OS and part of the larger proto-kerogen pool. In this interpretation, the large (~10‰) shifts in the shallow multicore porewater $\sum H_2S$ profile represent a primary depositional

signal in exchangeable OS $\delta^{34}S$, likely controlled by the sediment gravity flow recorded at 5–8 cm depth. These sediments are also characterized by peak concentrations of FeR, TOC, and proto-kerogen OS and relatively ^{34}S-enriched pyrite and S^0.

Porewater sulfide $\delta^{34}S$ could also be influenced by fractionations associated with metabolic sulfide oxidation. For example, porewater $\sum H_2S$ $\delta^{34}S$ values are 4.3‰ more ^{34}S-enriched than even polar extractable OS in the shallowest multicore sample, which could result from the preferential reoxidation of ^{32}S by sulfide oxidizing microorganisms. Sulfide oxidation coupled to O_2 is associated with a fractionation factor of about –5.2‰ (Fry et al., 1988), while sulfide oxidation coupled to nitrate reduction imparts a similar fractionation of –1.3 to –4.3‰ (Poser et al., 2014). In either case, sulfide oxidation is therefore expected to leave the residual sulfide pool relatively ^{34}S-enriched, which is the pattern we observe in the shallowest 5 cm of the multicore. Given the complicating factors of diffusion, exchange, variable bottom water oxidant concentrations, and a potential flood layer in the shallowest part of the multicore, we cannot estimate rates of sulfide oxidation in zone 1 with certainty. Regardless, if we assume that porewater $\sum H_2S$ has an 'initial' $\delta^{34}S$ value matching extractable OS and is removed only by oxidation with a fractionation factor of -1.3 or –4.3‰, the approximately 5‰ enrichment we observe in our shallowest multicore sample could be achieved by reoxidation of approximately 98% or 69%, respectively, of the $\sum H_2S$ pool. Below zone 1, sulfide oxidation is likely oxidant-limited and constrained to low rates by Fe_R concentration data (Section 4.1).

4.4 The generation of sedimentary sulfur isotope records

Pyrite $\delta^{34}S$ values are often interpreted in terms of their formation under idealized closed-system or open-system conditions, following Jorgensen (1979). In the first case, $\sum H_2S$ is diffusion-limited and pyrite $\delta^{34}S$ values reflect progressive distillation of the $\sum H_2S$ reservoir, generating relatively heterogeneous and ^{34}S-enriched pyrite (e.g., Gautier, 1986). In the open-system case, $\sum H_2S$ can be thought of as an infinite reservoir, and pyrite forms with a relatively low and invariant isotopic composition (e.g., Lyons, 2003). Sedimentary environments like central Santa Barbara Basin are particularly poorly suited to these idealized models because the chemocline is located near the sediment-water interface, where the local environments hosting pyrite precipitation may be fairly restricted while dissolved species are strongly affected by diffusive and advective processes. Pyrite $\delta^{34}S$ values in this environment may be particularly sensitive to secular changes in the precise position of the chemocline, which is likely to respond dynamically to changes in bottom water chemistry and sediment supply. If the deep water column becomes sufficiently suboxic (e.g., Ploug, 2001), it is possible that large particles could host MSR and act as an episodic source of pyrite or abiogenic OS to surface sediments. Additionally, changes in the O_2 content of bottom waters or fluxes of labile organic matter could affect the rate of MSR and by extension, its fractionation factor and the $\delta^{34}S$ value of the $\sum H_2S$ recorded as pyrite.

The pyrite and organic S generated in shallow sediments represent potential archives of information about depositional conditions and biogeochemical cycling, with the usual

caveat regarding the extent to which their $\delta^{34}S$ values are preserved during later sediment diagenesis. Pyrite $\delta^{34}S$ values from our shallow cores as well as ODP Hole 893A appear to reflect temporal variability in sediment deposition and redox conditions. Both profiles have no simple trends with depth and share a $\delta^{34}S$ range of -39.0 to -15.4‰ (Figs. 6 and 7, Bruchert et al., 1995). Proto-kerogen $\delta^{34}S$ profiles are smoother and Hole 893A data are less variable, reflecting the influence of S exchange with other pools. However, this exchange does not continue indefinitely. Outside of zone 1, polar extractable OS $\delta^{34}S$ values from the multi-, gravity, and box cores are remarkably consistent with Hole 893A (Bruchert et al., 1995), suggesting that equilibration between polar extractable OS and $\sum H_2S$ does not continue below surface sediments. Moreover, porewater $\sum H_2S$ and proto-kerogen $\delta^{34}S$ values diverge below zone 2 in the gravity core, suggesting that proto-kerogen becomes more stable and resistant to exchange at this point in the diagenetic sequence. Nevertheless, some amount of OS apparently continues to exchange below the SMTZ, because proto-kerogen in ODP Hole 893A is more ^{34}S-enriched than any proto-kerogen in our core (Figs. 6 and 7). Diagenetic reactions may change the dominant type of S-bearing organic matter structure over time and reduce the exchangeability of OS, for example as thiol groups convert to more stable sulfides, thiophenes, and/or polysulfide bridges (Kohnen et al., 1989; Damsté and De Leeuw, 1990; Vairavamurthy et al., 1994). Proto-kerogen $\delta^{34}S$ values will be affected by exchange processes and biogeochemical sulfur cycling as long as a significant proportion of OS remains exchangeable.

The $\delta^{34}S$ difference between proto-kerogen and pyrite may contain useful information for reconstructing paleoenvironments. In our hypothesis, the degree of ^{34}S enrichment of OS relative to pyrite should be related to the relative abundances of OS versus $\sum H_2S$. At sites with high rates of MSR, OS should be more similar to locally forming pyrite because abundant porewater $\sum H_2S$ dominates the exchangeable sulfur reservoir. In contrast, if the flux of $\sum H_2S$ to porewater is relatively low, we predict OS should retain a more ^{34}S-enriched composition reflecting the influence of biosulfur. In Santa Barbara Basin, the location of the chemocline at the sediment-water interface encourages the formation of abundant OS that appears to survive with minimal degradation over the next several hundred years, potentially limiting MSR. This environment is particularly conducive to $\sum H_2S$ – OS exchange and generates a relatively large (>15‰) $\delta^{34}S$ difference between coexisting pyrite and proto-kerogen. Further work is clearly warranted to help us interpret records of pyrite and OS $\delta^{34}S$ as well as their difference in naturally dynamic sedimentary environments.

5. CONCLUSIONS

Pyrite formation is a complex process that occurs at the intersection of multiple microbial metabolisms, abiotic reactions, and physical processes in sediments. We studied the distribution of ^{34}S among all the major dissolved and solid sulfur species to constrain the

pathways of pyrite formation in Santa Barbara Basin. Consistent with previous work, we find evidence for the accumulation of pyrite with very low $\delta^{34}S$ values of -30 to -40‰ throughout the upper part of the core, where porewater $\sum H_2S$ has $\delta^{34}S$ values ranging from 5.9 to -19.5‰. However, our observation that S^0 has $\delta^{34}S$ values matching those of pyrite, not $\sum H_2S$, largely rules out sulfur disproportionation as a possible reason for this isotopic disparity. From electron microscopy, sub-micron pyrite crystals are very consistent in size and shape, intergrown with amorphous materials, and commonly agglomerated into framboids—morphologies that are consistent with pyrite forming in association with organic structures, cell walls and biofilms. We therefore propose that pyrite is the product of the sulfide generated by microbial sulfate reduction (MSR) within biofilms or aggregates. In Santa Barbara Basin, only a small flux of $\sum H_2S$ then diffuses into porewater, where it is exposed to a relatively large pool of organic sulfur (OS) that is at least partially exchangeable. Sulfur isotopic exchange between porewater $\sum H_2S$ and OS would tend to enrich the smaller $\sum H_2S$ pool in ^{34}S, potentially explaining the isotopic composition of these pools in our shallow core (zones 1 and 2). In deeper sediments, porewater $\sum H_2S$ and other dissolved species appear to be controlled primarily by diffusion related to processes at the SMTZ (zone 3) at ~165–190 cm depth.

These results illustrate the complexity of the sulfur cycle in organic-rich marine sediments and support a significant role for microbially-driven microenvironments in pyrite formation. Despite this complexity, if pyrite is indeed recording the isotopic composition of the $\sum H_2S$ produced by MSR, it can represent a relatively straightforward

and potentially powerful archive of paleoenvironmental information. Complementary information about the relative abundance of $\sum H_2S$ and OS can also be recorded in the $\delta^{34}S$ difference between OS and pyrite in marine sediments.

ACKNOWLEDGEMENTS

We gratefully acknowledge the science team and crew of *R/V Atlantis* cruise AT26-06, especially the efforts of Katherine S Dawson (Caltech), David L. Valentine, Karin Lemkau, and Alex Phillips (UC Santa Barbara). This work benefitted from helpful discussions with Victoria J. Orphan and Guillaume Paris, analytical support from David Lyons (UC Riverside) and Fenfang Wu (Caltech), and assistance with sediment extractions from Emilia S. Hernandez. Funding was provided by the National Science Foundation award OCE1436566 to A.L.S. and the Gordon and Betty Moore Foundation through Grant GBMF#3306 to A.L.S.. This manuscript was much improved by insightful reviews from David Fike (Washington U. in St. Louis), Maya Gomes (Harvard), and Matt Hurtgen (Northwestern U.) and the careful editorial handling of Claire Rollion-Bard.

REFERENCES

Anderson T. F. and Pratt L. M. (1995) Isotopic evidence for the origin of organic sulfur and elemental sulfur in marine sediments. *ACS Symposium Series* **612**, 378–396.

Berelson W. M., Prokopenko M., Sansone F. J., Graham A. W., McManus J. and Bernhard J. M. (2005) Anaerobic diagenesis of silica and carbon in continental margin sediments: Discrete zones of TCO_2 production. *Geochimica et Cosmochimica Acta* **69**, 4611–4629.

Berner R. A. and Raiswell R. (1983) Burial of organic carbon and pyrite sulfur in sediments over Phanerozoic time: a new theory. *Geochimica et Cosmochimica Acta* **47**, 855–862.

Bontognali T. R., Sessions A. L., Allwood A. C., Fischer W. W., Grotzinger J. P., Summons R. E., Eiler J. M. (2012) Sulfur isotopes of organic matter preserved in 3.45-billion-year-old stromatolites reveal microbial metabolism. *Proceedings of the National Academy of Sciences* **109**, 15146–15151.

Bottcher M., Smock A. and Cypionka H. (1998) Sulfur isotope fractionation during experimental precipitation of iron(II) and manganese(II) sulfide at room temperature. *Chemical Geology* **146**, 127–134.

Bottrell S. and Newton R. (2006) Reconstruction of changes in global sulfur cycling form marine sulfate isotopes. *Earth Science Reviews* **75**, 59–83.

Bottrell S. H. and Raiswell R. (2000) Sulphur isotopes and microbial sulphur cycling in sediments. In *Microbial Sediments*, eds. Riding R. E. and Awramik S.M., 96–104.

Bruchert V., Pratt L. M., Anderson T. F. and Hoffmann S. R. (1995) Abundance and isotopic composition of organic and inorganic sulfur species in laminated and bioturbated sediments from Hole 893A, Santa Barbara Basin eds. J. P. Kennett, J. G. Baldauf, and M. Lyle. *Proceedings of the Ocean Drilling Program, Scientific Results* **146**, 219–230.

Brunner B. and Bernasconi S. (2005) A revised isotope fractionation model for dissimilatory sulfate reduction in sulfate reducing bacteria. *Geochimica et Cosmochimica Acta* **69**, 4759–4771.

Butler I. B., Böttcher M. E., Rickard D. and Oldroyd A. (2004) Sulfur isotope partitioning during experimental formation of pyrite via the polysulfide and hydrogen sulfide pathways: implications for the interpretation of sedimentary and hydrothermal pyrite isotope records. *Earth and Planetary Science Letters* **228**, 495–509.

Canfield D. (2004) The evolution of the earth surface sulfur reservoir. *American Journal of Science* **304**, 839–861.

Canfield D. and Teske A. (1996) Late Proterozoic rise in atmospheric oxygen concentration inferred from phylogenetic and sulphur-isotope studies. *Nature* **382**, 127–132.

Canfield D. E. (2001) Biogeochemistry of Sulfur Isotopes. *Reviews in Mineralogy and Geochemistry* **43**, 607–636.

Canfield D. E. and Thamdrup B. (1994) The production of 34S-depleted sulfide during bacterial disproportionation of elemental sulfur. *Science* **266**, 1973.

Canfield D. E., Raiswell R. and Bottrell S. H. (1992) The reactivity of sedimentary iron minerals toward sulfide. *American Journal of Science* **292**, 659–683.

Canfield D. E., Thamdrup B. and Fleischer S. (1998) Isotope fractionation and sulfur metabolism by pure and enrichment cultures of elemental sulfur-disproportionating bacteria. *Limnology and Oceanography* **43**, 253–264.

Canfield D., Farquhar J. and Zerkle A. (2010) High isotope fractionations during sulfate reduction in a low-sulfate euxinic ocean analog. *Geology* **38**, 415–418.

Canfield D., Olesen C. and Cox R. (2006) Temperature and its control of isotope fractionation by a sulfate-reducing bacterium. *Geochimica et Cosmochimica Acta* **70**, 548–561.

Chanton and Martens C. (1987) Biogeochemical cycling in an organic-rich coastal marine basin. 8. A sulfur isotopic budget balanced by differential diffusion across the sediment-water interface. *Geochimica et Cosmochimica Acta* **51**, 1201–1208.

Dale A. W., Bruchert V., Alperin M. and Regnier P. (2009) An integrated sulfur isotope model for Namibian shelf sediments. *Geochimica et Cosmochimica Acta* **73**, 1924–1944.

Damsté J. S. S. and De Leeuw J. W. (1990) Analysis, structure and geochemical significance of organically-bound sulphur in the geosphere: state of the art and future research. *Organic Geochemistry* **16**, 1077–1101.

Detmers J., Bruchert V., Habicht K. and Kuever J. (2001) Diversity of sulfur isotope fractionations by sulfate-reducing prokaryotes. *Applied and Environmental Microbiology* **67**, 888–894.

Donald R. and Southam G. (1999) Low temperature anaerobic bacterial diagenesis of ferrous monosulfide to pyrite. *Geochimica et Cosmochimica Acta* **63**, 2019–2023.

Fleischer P. (1972) Mineralogy and sedimentation history, Santa Barbara Basin, California. *Journal of Sedimentary Petrology* **42**, 49–58.

Frankel R. B. and Bazylinski D. A. (2003) Biologically induced mineralization by bacteria. *Reviews in Mineralogy and Geochemistry* **54**, 95–114.

Frigaard N. U. and Dahl C. (2009) Sulfur metabolism in phototrophic sulfur bacteria. In *Advances in Microbial Physiology*, ed. Poole R. K.. London: Academic Press, 103-200.

Froelich P. N., Klinkhammer G. P., Bender M. L., Luedtke N. A., Heath G. R., Cullen D. and Dauphin P. (1979) Early oxidation of organic matter in pelagic sediments of the eastern equatorial Atlantic: suboxic diagenesis. *Geochimica et Cosmochimica Acta* **43**, 1075–1090.

Fry B., Cox J., Gest H. and Hayes J. M. (1986) Discrimination between ^{34}S and ^{32}S during bacterial metabolism of inorganic sulfur compounds. *Journal of Bacteriology* **165**, 328–330.

Fry B., Jannasch H. W., Molyneaux S. J., Wirsen C. O., Muramoto J. A. and King S. (1991) Stable isotope studies of the carbon, nitrogen and sulfur cycles in the Black Sea and the Cariaco Trench. *Deep Sea Research Part A, Oceanographic Research Papers* **38**, S1003–S1019.

Fry B., Ruf W., Gest H. and Hayes J. M. (1988) Sulfur isotope effects associated with oxidation of sulfide by O2 in aqueous solution. *Chemical Geology: Isotope Geoscience Section* **73**, 205–210.

Gautier, D. L. (1987). Isotopic composition of pyrite: relationship to organic matter type and iron availability in some North American Cretaceous shales. *Chemical Geology: Isotope Geoscience Section*, **65**, 293–303.

Goldhaber M. B. and Kaplan I. R. (1975) Controls and consequences of sulfate reduction rates in recent marine sediments. *Soil Science* **119**, 42–55.

Habicht K. S. and Canfield D. E. (2001) Isotope fractionation by sulfate-reducing natural populations and the isotopic composition of sulfide in marine sediments. *Geology* **29**, 555–558.

Habicht K., Gade M., Thamdrup B., Berg P. and Canfield D. (2002) Calibration of sulfate levels in the Archean ocean. *Science* **298**, 2372–2374.

Harrison B., Zhang H., Berelson W. and Orphan V. (2009) Variations in archaeal and bacterial diversity associated with the sulfate-methane transition zone in continental margin sediments (Santa Barbara Basin, California). *Applied and Environmental Microbiology* **75**, 1487–1499.

Johnston D., Wing B., Farquhar J., Kaufman A., Strauss H., Lyons T., Kah L. and Canfield D. (2005) Active microbial sulfur disproportionation in the Mesoproterozoic. *Science* **310**, 1477–1479.

Johnston D., Farquhar J., Canfield D. (2007) Sulfur isotope insights into microbial sulfate reduction: When microbes met models. *Geochimica et Cosmochimica Acta* **71**, 3929–3947.

Jorgensen B. B. (1979) A theoretical model of the stable sulfur isotope distribution in marine sediments. *Geochimica et Cosmochimica Acta* **43**, 363–374.

Jorgensen B. B. (1982) Mineralization of organic matter in the sea bed-the role of sulphate reduction. *Nature* **296**, 643–645.

Kaplan I. R. and Rittenberg S. C. (1964) Microbiological fractionation of sulphur

isotopes. *Journal of General Microbiology* **34**, 195–212.

Kohnen M., Damste J. S., ten Haven H. L. and De Leeuw J. W. (1989) Early incorporation of polysulfides in sedimentary organic matter. *Nature* **341**, 640–641.

Kuwabara J. S., van Geen A., McCorkle D. C. and Bernhard J. M. (1999) Dissolved sulfide distributions in the water column and sediment pore waters of the Santa Barbara Basin. *Geochimica et Cosmochimica Acta* **63**, 2199–2209.

Leavitt W. D., Halevy I., Bradley A. S. and Johnston D. T. (2013) Influence of sulfate reduction rates on the Phanerozoic sulfur isotope record. *Proceedings of the National Academy of Sciences*.

Li C., Sessions A. L., Kinnaman F. S. and Valentine D. L. (2009) Hydrogen-isotopic variability in lipids from Santa Barbara Basin sediments. *Geochimica et Cosmochimica Acta* **73**, 4803–4823.

MacLean L., Tyliszczak, Gilbert P., Zhou D., Pray T. J., Onstott T. C. and Southam G. (2008) A high-resolution chemical and structural study of framboidal pyrite formed within a low-temperature bacterial biofilm. *Geobiology* **6**, 471–480.

Moffitt S. E., Hill T. M., Ohkushi K., Kennett J. P. and Behl R. J. (2014) Vertical oxygen minimum zone oscillations since 20 ka in Santa Barbara Basin: A benthic foraminiferal community perspective. *Paleoceanography* **29**, 44–57.

Moffitt S. E., Moffitt R. A., Sauthoff W., Davis C. V., Hewett K. and Hill T. M. (2015) Paleoceanographic Insights on Recent Oxygen Minimum Zone Expansion: Lessons for Modern Oceanography ed. Y. Hong. *PLOS ONE* **10**, e0115246.

Neal A. L., Techkarnjanaruk S., Dohnalkova A., McCready D., Peyton B. M. and Geesey G. G. (2001) Iron sulfides and sulfur species produced at hematite surfaces in the presence of sulfate-reducing bacteria. *Geochimica et Cosmochimica Acta* **65**, 223–235.

Ohfuji H. and Rickard D. (2005) Experimental syntheses of framboids—a review. *Earth Science Reviews* **71**, 147–170.

Orphan V. J., Hinrichs K. U., Ussler W., Paull C. K., Taylor L. T., Sylva S. P., Hayes J. M. and Delong E. F. (2001) Comparative Analysis of Methane-Oxidizing Archaea and Sulfate-Reducing Bacteria in Anoxic Marine Sediments. *Applied and Environmental Microbiology* **67**, 1922–1934.

Paris G., Adkins J. F., Sessions A. L. and Subhas A. (2013) MC-ICP-MS measurement of $\delta^{34}S$ and $\Delta^{33}S$ in small amounts of dissolved sulfate. *Chemical Geology* **345**, 50–61.

Poser, A., Vogt, C., Knöller, K., Ahlheim, J., Weiss, H., Kleinsteuber, S., & Richnow, H.-H. (2014). Stable Sulfur and Oxygen Isotope Fractionation of Anoxic Sulfide Oxidation by Two Different Enzymatic Pathways. *Environmental Science and Technology*, **48**, 9094–9102.

Raiswell R. and Canfield D. (1998) Sources of iron for pyrite formaiton in marine sediments. *American Journal of Science* **298**, 219–245.

Raiswell R., Canfield D. E. and Berner R. A. (1994) A comparison of iron extraction methods for the determination of degree of pyritisation and the recognition of iron-limited pyrite formation. *Chemical Geology* **111**, 101–110.

Rees C. E. (1973) A steady-state model for sulphur isotope fractionation in bacterial reduction processes. *Geochimica et Cosmochimica Acta* **37**, 1141–1162.

Reimers C. E., Lange C. B., Tabak M. and Bernhard J. M. (1990) Seasonal spillover and varve formation in the Santa Barbara Basin, California. *Limnology and Oceanography* **35**, 1577–1585.

Reimers C. E., Ruttenberg K. C., Canfield D. E., Christiansen M. B. and Martin J. B. (1996) Porewater pH and authigenic phases formed in the uppermost sediments of the Santa Barbara Basin. *Geochimica et Cosmochimica Acta* **60**, 4037–4057.

Rickard D. and Luther G. I. (2007) Chemistry of Iron Sulfides. *Chemical Reviews* **107**, 514–562.

Rickard, D., & Morse, J. (2005). Acid volatile sulfide (AVS). *Marine Chemistry*, **97**, 141–197.

Schimmelmann A. and Kastner M. (1993) Evolutionary changes over the last 1000 years of reduced sulfur phases and organic carbon in varved sediments of the Santa Barbara Basin, California. *Geochimica et Cosmochimica Acta* **57**, 67–78.

Schimmelmann A. and Lange C. B. (1996) Tales of 1001 varves: a review of Santa Barbara Basin sediment studies. *Geological Society, London, Special Publications* **116**, 121–141.

Schimmelmann A., Hendy I. L., Dunn L., Pak D. K. and Lange C. B. (2013) Revised ~2000-year chronostratigraphy of partially varved marine sediment in Santa Barbara Basin, California. *GFF* **135**, 258–264.

Schimmelmann A., Lange C. B. and Berger W. H. (1990) Climatically controlled marker layers in Santa Barbara Basin sediments and fine-scale core-to-core correlation. *Limnology and Oceanography* **35**, 165–173.

Schoonen M. (2004) Mechanisms of sedimentary pyrite formation eds. J. Amend, K. Edwards, and T. W. Lyons. *GSA Special Papers* **379**, 117–134.

Sholkovitz E. (1973) Interstitial water chemistry of the Santa Barbara Basin sediments. *Geochimica et Cosmochimica Acta* **37**, 2043–2073.

Sim M. S., Bosak T. and Ono S. (2011a) Large sulfur isotope fractionation does not require disproportionation. *Science* **333**, 74–77.

Sim M. S., Ono S., Donovan K., Templer S. P., Bosak T. (2011b) Effect of electron donors on the fractionation of sulfur isotopes by a marine *Desulfovibrio* sp.. *Geochimica et Cosmochimica Acta* **75**, 4244–4259.

Soutar A. and Crill P. A. (1977) Sedimentation and climatic patterns in the Santa Barbara Basin during the 19th and 20th centuries. *Geological Society of America Bulletin* **88**,

1161–1172.

Vairavamurthy A., Zhou W., Eglinton T. and Manowitz B. (1994) Sulfonates: a novel class of organic sulfur compounds in marine sediments. *Geochimica et Cosmochimica Acta* **58**, 4681–4687.

Wacey D., Kilburn M. R., Saunders M., Cliff J. B., Kong C., Liu A. G., Matthews J. J. and Brasier M. D. (2014) Uncovering framboidal pyrite biogenicity using nano-scale CNorg mapping. *Geology* **43**, 27–30.

Walker J. C. G. and Brimblecombe P. (1985) Iron and sulfur in the pre-biologic ocean. *Precambrian Research* **28**, 205 – 222.

Wilkin R. T. and Barnes H. L. (1996) Pyrite formation by reactions of iron monosulfides with dissolved inorganic and organic sulfur species. *Geochimica et Cosmochimica Acta* **60**, 4167–4179.

Zerkle A., Farquhar J., Johnston D., Cox R. and Canfield D. (2009) Fractionation of multiple sulfur isotopes during phototrophic oxidation of sulfide and elemental sulfur by a green sulfur bacterium. *Geochimica et Cosmochimica Acta* **73**, 291–306.

Chapter 5

SULFUR ISOTOPE EXCHANGE BETWEEN ORGANIC MATTER AND POLYSULFIDES

Raven M.R., Sessions A.L., Adkins J.F., et al. 'Sulfur isotope exchange between organic matter and polysulfides. (*in prep*).

ABSTRACT

Sedimentary organic sulfur (OS) is rarely considered in global biogeochemical models, which traditionally assume that reduced S is effectively buried as pyrite. In reality, however, OS preserves a different S-isotope composition than pyrite and likely has different roles in the sedimentary environment. For example, OS may exchange with porewater sulfide, affecting its S-isotope composition. We investigate the exchangeability of OS with sulfide and polysulfides by exposing OS-rich sediments, cysteine, humic acids, and low-molecular-weight (di)sulfide compounds to ^{34}S-labelled sulfide–polysulfide solutions. Cysteine takes on some of the ^{34}S label within days, at which point polysulfide δ^{34}S values look like a mixture of cysteine and initial polysulfide S. We propose that this exchange proceeds through cysteine–polysulfide structures that mature via chain-rearrangement reactions to shorter chain lengths over several days. These organic polysulfides could facilitate the incorporation of primary biogenic S into proto-kerogen. Additionally, after a two-week incubation, the δ^{34}S difference between sulfide and proto-kerogen from Santa Barbara Basin sediments dropped from 302‰ to 16‰, indicating sulfide–OS exchange. At the end of the experiment, the S-isotope composition

of dissolved sulfide primarily reflected that of proto-kerogen S, not the initial sulfide source, which is consistent with our observations in shallow Santa Barbara Basin sediments (Chapter 4). The rate and/or extent of sulfide–OS exchange appears to decline in older sediments, but at least some of the S in proto-kerogen appears to remain exchangeable for thousands of years. Sulfide–OS exchange may be a primary driver of the large difference between pyrite and OS $\delta^{34}S$ values in Santa Barbara Basin sediments and an important process affecting the distribution of S isotopes in sulfidic marine sediments.

1. INTRODUCTION

1.1 Sedimentary burial of organic and inorganic sulfur

Sulfur burial in marine sediments is a long-term control on the oxidation state of the surface earth (Berner, 1984). Inorganic S burial as pyrite has been the focus of most work in the field and is commonly treated as representative of the total sink of reduced sedimentary S (Berner, 1987; Canfield, 2005; Halevy et al., 2012). The S-isotope composition of pyrite is often used to understand biogeochemical processes and their changes over Earth history. At the same time, both pyrite and organic matter (OM) burial can be major sinks for sedimentary S (Mossman et al., 1991; Eglinton et al., 1994), and they may respond differently to environmental conditions.

Pyrite and organic sulfur (OS) have consistently different S-isotope compositions despite the fact that both phases derive from dissolved reduced S species, which we call $\sum S^{\leq 0}$. One potential means to explain this offset is for kerogen to contain large amounts of primary biogenic S (~24%), which has an S-isotope composition near seawater sulfate at 21‰ (Anderson and Pratt, 1995). Sulfur in biomass is predominantly in the forms of cysteine and methionine in proteins, which are relatively valuable substrates for heterotrophs and may even be preferentially remineralized during OM diagenesis (Van Mooy et al., 2002; Matrai et al., 1989). The preservation of large amounts of biogenic S thus appears to be at odds with the high remineralization potential of S in proteins. Another theory to explain the $\delta^{34}S$ difference between pyrite and kerogen is that Fe^{3+} in

some minerals outcompetes organic functional groups for sulfide, leading to earlier pyritization and later organic matter sulfurization. Because porewater sulfide typically becomes increasingly ^{34}S-enriched with depth, later-forming OS would have higher $\delta^{34}S$ values than more rapidly forming pyrite (Hartgers et al., 1997; Werne et al., 2003). In most modern environments, however, pyrite and organic sulfur appear to form concurrently (e.g., Ferdelman et al., 1991; Bruchert and Pratt, 1996; Chapters 3 and 4) or at least sedimentary OS is added during very early processes (Mossman et al, 1991, Francois et al., 1987). Another theory posited that pyrite could be the product of sulfide recycling via S^0 disproportionation (Canfield and Thamdrup, 1994; Bruchert, 1998), which requires pyrite formation to occur preferentially from disproportionation-derived sulfide but not the immediate, more ^{34}S-enriched products of microbial sulfate reduction, which are perhaps reflected in OS. As described in Chapter 4, however, the $\delta^{34}S$ patterns we observe in Santa Barbara Basin are inconsistent with this model.

To explain the basic features of $\delta^{34}S$ profiles in Santa Barbara Basin sediments, we proposed that pyrite formation may be particularly favorable within biofilms, where microorganisms are actively generating sulfide. Sulfide that does not precipitate locally can diffuse into porewater, where its $\delta^{34}S$ value can be modified by a variety of processes, notably exchange with OS. S-isotope exchange between OS and sulfide was proposed previously to explain $\delta^{34}S$ profiles from the Namibian Shelf (Dale et al., 2009). Exchange between aldehydes and polysulfides has been demonstrated experimentally

(Amrani et al., 2008), and thiol–disulfide exchange reactions are well known from enzyme biochemistry (Gilbert, 1995).

The experiments described here are intended to test the idea that there are S-exchange reactions between natural OM and sulfide that can help explain $\delta^{34}S$ profiles in sediments. We incubate standard compounds and sediments from Santa Barbara Basin with ^{34}S-labeled sulfide–polysulfide solutions and generate some initial constraints on the rates, mechanisms, and quantitative significance of sulfide–OS exchange.

1.2 Polysulfide chemistry and analysis

These exchange experiments rely on our ability to measure the concentrations and $\delta^{34}S$ values of the various pools of dissolved S in our experiments, which include sulfide, polysulfides, elemental S (S^0), and sometimes OS. Our polysulfide solutions are saturated with respect to S^0 and buffered at pH 8.5 in 50 mM Tris solution (2-amino-2-hydroxymethyl propane-1,3-diol). Under these conditions, sulfide is easily oxidized to an array of polysulfides with oxidation states between 0 and –1, generating roughly equal concentrations of total polysulfides and HS^- (Fig. 1). Polysulfides have been the target of a substantial amount of experimental work because they are highly reactive and have important roles in a variety of sedimentary and industrial processes. Still, they are notoriously challenging to handle analytically because sulfur exchange and chain rearrangement within the polysulfide pool can occur on timescales of seconds

(Kamyshny et al., 2003). The current 'gold standard' method for measuring individual polysulfide species takes advantage of the rapid kinetics of methylation by methyl triflate (trifluoromethansulfonate) to stabilize polysulfide chains for analysis by LC. Based on this work, the most abundant polysulfides are mid-chain dianions S_5^{2-}, S_6^{2-}, and S_4^{2-} (Fig. 1). Dianionic polysulfide chains with 2, 3, 7, 8, and 9 sulfur atoms as well as the monoanionic radicals derived from splitting of longer polysulfide chains are also present in smaller amounts (Steudel, 2003).

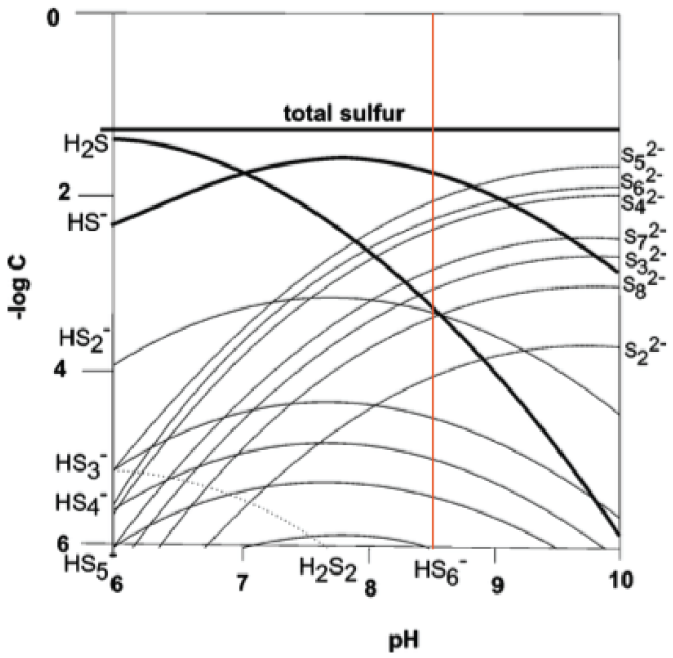

Fig. 1: Concentration vs. pH diagram for dissolved sulfur species in the presence of excess S^0. *Taken from Rickard and Luther (2007) and based on data from Kamyshny et al., 2004. The working pH for our experiments is highlighted with an orange line.*

Polysulfides are only stable at high pH and spontaneously break down in the presence of acid by the reaction (e.g.) $2S_5^{2-} + H_2S \rightarrow \alpha\text{-}S^8 + 2H_2S$, generating S^0 and sulfide. This reaction subdivides the polysulfide pool according to its net oxidation state. Previous research has used acidification to investigate polysulfides, including their isotopic behavior. Amrani and Aizenshtat used acid dissociation of polysulfides to demonstrate that these species exhibit complete isotopic mixing of their H_2S and S^0 atoms. They recovered S^0 that was consistently ~4.4‰ ^{34}S-enriched relative to evolved H_2S, which was interpreted as an equilibrium isotope fractionation factor (Amrani and Aizenshtat, 2004).

A variety of other methods have been used to quantify total polysulfides, including cyclic voltammetry (Boyd and Druschel, 2003, Brendel and Luther, 1995, Glazer et al., 2006), UV-absorption (Teder, 1969), Raman spectroscopy (Badoz-Lambling et al., 1976, Hagen et al., 2013) and UV-Vis spectroscopy (Li et al., 2008). None of these techniques, however, allow for $\delta^{34}S$ analysis. In Section 2.2, we describe a combination of chemical separation methods that make it possible to compare the $\delta^{34}S$ values of five dissolved sulfur pools.

2. METHODS

2.1 Experimental design

We present data for a series of experiments that explored the reactivity and exchangeability of different types of organic S with sulfide and polysulfides, which together we call $\sum S^{\leq 0}$. In the first experiment, four different types of organic S were incubated with a ^{34}S-labeled polysulfide solution for two days. In experiment #2, cysteine was incubated with ^{34}S-labeled polysulfides and sampled in high temporal resolution. Subsequent experiments exposed natural sediments from Santa Barbara Basin to ^{34}S-labeled polysulfide solutions for 1 and 30 days (experiment #3), and for 2 days (experiment #4). Dissolved S fractions were also successfully measured as part of experiment #4. In experiment #5, polysulfide incubations of natural sediments were sampled in high temporal resolution with dissolved S analysis throughout, similar to experiment #2 for cysteine.

Experiment #1 investigated whether S atoms from $\sum S^{\leq 0}$ would appear in different types of OS after 48 hours of exposure. The OS materials we investigated were Sigma Aldrich humic acid (lot BCBN1711V), cysteine, a combination of two, low-molecular-weight organic (di)sulfides (dodecyl sulfide, Aldrich #222801, lot 10318DH; and benzyl disulfide, Aldrich #B21805, lot 01225EC), and Santa Barbara Basin (SBB) sediment (0–10 cm). SBB sediment was collected from 590 m water depth in June 2004 by box coring and frozen until it was subsampled, freeze-dried, soaked overnight in formic acid solution (2.5% in PBS), and washed three times in MQ–buffer solution (pH 8.5, Tris). Each OS

material was weighed into vials for duplicate incubations with polysulfides and a polysulfide-free control. OS materials were sealed with butyl stoppers in pH 8.5 buffer solution (10 mL for sediments, 15 mL for others) under N_2. A ^{34}S-labeled polysulfide solution (Table 1) was added by syringe (10 mL for sediment, 5 mL for others). Twice as much polysulfide solution was added to the sediment samples than to the amino acid samples to ensure that all of the polysulfides were not consumed by precipitation with iron (see discussion below). Vials were stirred at room temperature in the dark for 48 hours.

Table 1. Characteristics of polysulfide spikes used in incubation experiments.

Exp. #	Samples	[polysulfide S^0 + Zn-rx sulfide] mM	$\delta^{34}S$ Zn-rx sulfide (‰)	$\delta^{34}S$ polysulfide S^0 (‰)
1	cysteine, sediment, etc.	11.9	376.5	379.4
2	cysteine	10.3	311.7	314.1
3	SBB sediments	8.6	279.4	287.7
4	SBB sediment	11.9	376.5	379.4
5	SBB sediment	12.7	285.3	285.6

Experiment #3 was conducted similarly to experiment #1 but focused on sedimentary OM. Separate vials were prepared for five replicates each of two different SBB sediments: the box core material from 0–10 cm, and a deeper multi-core sediment sample (30 cm, 'M24' from Chapter 4). Sediments were prepared in the same way as for experiment #1 except it was not treated with formic acid (this experiment was conducted prior to the others). Four of the replicates of each sediment were incubated with polysulfides (Table 1), and the fifth replicate was incubated with a ^{34}S-labeled, 20-mM

sulfate solution as a polysulfide-free control. Two replicates were collected after one day of incubation, and two were collected after 30 days.

Experiment #4 replicated the procedures from experiment #3 with a few modifications. Only one sediment (0–10 cm SBB box core) was investigated, and its preparation included an overnight formic acid solution soak. Dissolved S fractions were also collected successfully and reported below. The duration of the incubation was two days.

Experiments #2 and #5 included repeated sampling of cysteine and SBB sediment incubations to gain better constraints on the rates of exchange and other processes. Accordingly, they required stronger protections against O_2 contamination and were conducted entirely in an anaerobic chamber under an N_2/H_2 atmosphere. Shallow SBB sediment and cysteine were each weighed into triplicate serum vials, including two incubations with polysulfides (Table 1) and a polysulfide-free control in buffer solution only. In each case, one replicate bottle was sampled repeatedly after polysulfide addition, at 10 minutes, 2 hours, 8 hours, and 1, 3, and 14 days. The second replicate was sampled at 1 and 14 days. Both dissolved S fractions and solids (as slurry) were collected via syringe at each time point. Additionally, aliquots were collected after 14 days from the cysteine incubations and control for cysteine derivatization and analysis by GC-MS. The sediment incubations were scaled up four-fold to a total volume of 80 mL each, while the other bottles contained 20 mL as before.

In this study, our goal is to understand the large-scale speciation and S-isotope composition of different dissolved sulfur pools in experimental systems with organic sulfur. To this end, we operationally define five pools of dissolved (<0.2 μm) sulfur, listed in Table 2 and illustrated in Fig. 2.

Table 2. Summary of methods for separating dissolved sulfur pools

Working Name	Target Species	Separation Method
total	all dissolved (<0.2μm) S	no treatment
neutral S^0	α-S_8, nanoparticulate S^0	after 30 min. with ZnAc, extract 3x in ether
polysulfide S^0	neutral S^0 + zero-valent S_x^{2-}	after acidification with HCl, extract 3x in ether
aqueous	SO_4^{2-}, $S_2O_3^{2-}$, cysteine, humic acids	acidify with HCl, wash with ether
Zn-rx sulfide	HS^-, H_2S, sulfhydryl S_x^{2-}	precipitate with ZnAc, wash with ether and H_2O

The five dissolved S pools we measure derive from three initial aliquots of sample, all of which are filtered at 0.2 μm. One aliquot is left untreated for analysis of total dissolved sulfur. The other two treatments each divide this total dissolved sulfur pool into three parts, as illustrated on Fig. 2. One aliquot is reacted with 1 M zinc acetate, which traps HS^- and the sulfhydryl groups of polysulfides as ZnS(s). Zero-valent S from the polysulfides stays attached to the Zn solid during extraction with diethyl ether. After

extraction, the remaining solution is discarded. The Zn solid is washed with MQ water (pH <6), which causes the polysulfides to dissociate, leaving only S from polysulfide sulfhydryl groups and sulfide in the solid phase. We refer to the fractions generated from this aliquot as 'Zn-reactive sulfide' (Zn-rx sulfide) and 'neutral S^0' (Table 2). The third aliquot contains N_2-sparged 0.5 N HCl, which causes polysulfides to immediately disassociate into H_2S and S^0. In this case, both bisulfide and the sulfhydryl groups of polysulfides will degas from solution as H_2S, which was encouraged by swirling the solution under N_2 gas. In this idealized model, the S lost from the acid aliquot as H_2S is the same as that measured as Zn-reactive sulfide. After at least 30 minutes under N_2, non-polar compounds are extracted in diethyl ether, which separates the 'polysulfide S^0' and 'aqueous' fractions. The polysulfide S^0 fraction is composed primarily of zero-valent S from dissociated polysulfides but also includes 'neutral S^0.' Sulfur in the 'aqueous' pool should be in the form of acid-soluble organics (humic acids, amino acids) and/or ionic salts (sulfate, sulfite, thiosulfate).

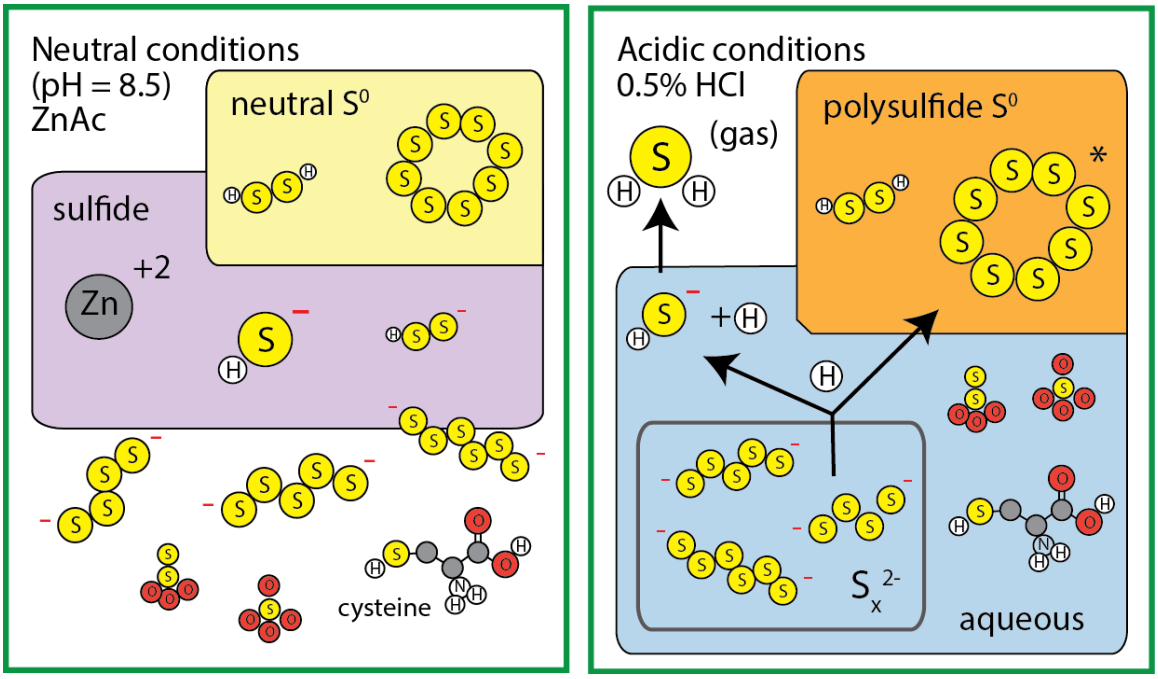

Fig. 2. Distribution of dissolved sulfur among operationally defined pools. *The asterix associated with S_8 in the polysulfide S^0 fraction is intended to emphasize that this S_8 includes α–S^0 and nanoparticulates from the 'neutral S^0' fraction as well as zero-valent S from polysulfide dissociation.*

Composition of polysulfide solutions – We compare the relative abundances of S in each of these five fractions with expectations based on thermodynamic data (Kamyshny et al., 2004; Fig. 1). At pH 8.5, the sulfide–polysulfide solution should be approximately half bisulfide and half total polysulfides (Kamyshny, 2009). The dominant polysulfides should be the mid-chain species S_4^{-2}, S_5^{-2}, and S_6^{-2}, which have an average ratio of 3:2 S^0:sulfhydryl atoms. Therefore, we expect roughly 60% of polysulfide S atoms to be recovered in the polysulfide S^0 pool (along with nanoparticulate and α-S^0) and 40% to

either volatilize as H_2S or be recovered in the Zn-reactive sulfide pool (along with HS^-), depending on pH. As shown in Fig. 3, measured concentrations of sulfur pools in a ~13 mM polysulfide solution are consistent with these simple theoretical predictions. The 'neutral S^0' fraction contains an order of magnitude less S than the 'polysulfide S^0' fraction, which supports the interpretation that ZnAc treatment traps the sulfhydryl groups of polysulfides without causing immediate dissociation (as was assumed in Li et al., 2008). Zero-valent S from polysulfides remains associated with the Zn solid during ether extraction but is removed during washing with MQ water.

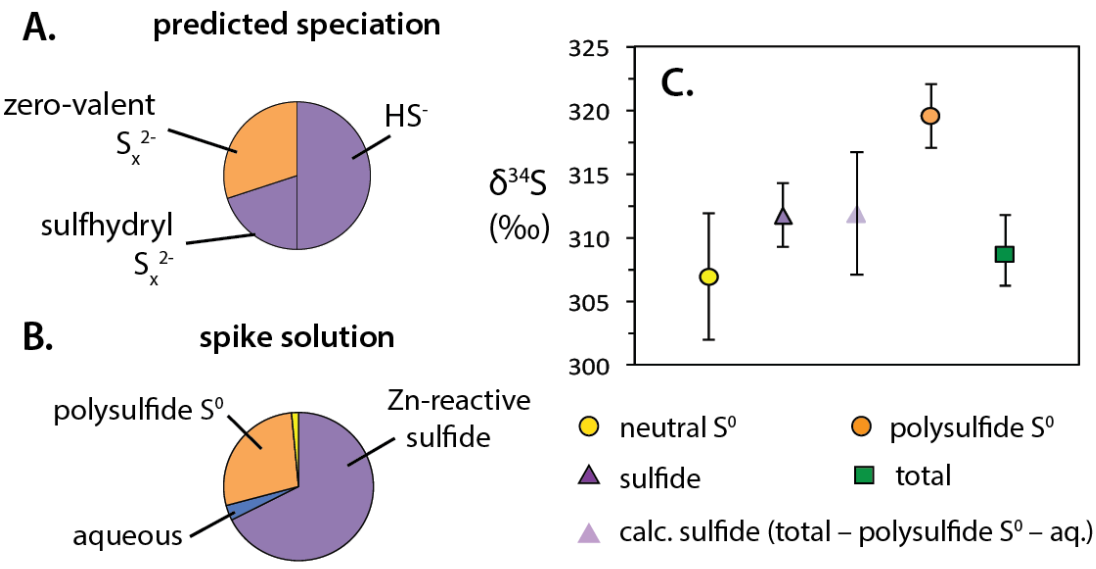

Fig. 3: ***Distribution of dissolved sulfur in polysulfide solutions.*** *Chart (a) shows the relative abundances different sulfur types anticipated in an S^0-saturated polysulfide solution at pH 8.5. Chart (b) shows the measured relative abundances of dissolved sulfur pools in a polysulfide solution ('spike 5'). Neutral S^0 is subtracted from polysulfide S^0 and illustrated separately (yellow). The $\delta^{34}S$ values (in ‰ VCDT) of these pools are*

compared in (c). Each symbol represents the average of 2–6 replicates, and error bars span the estimated 1σ reproducibility of each measurement based on typical replicates.

The $\delta^{34}S$ values of sulfur pools from the polysulfide solution are generally consistent with expectations from the literature. Zero-valent polysulfide S (polysulfide S^0) should be a few per mil heavier than sulfhydryl polysulfide S (Amrani and Aizenshtat 2004), and we see a difference of 7.8 ± 6‰ that is consistent with that observation albeit less precise (polysulfide S^0 replicates suffered from relatively poor reproducibility, likely arising from inconsistency in the manual liquid-liquid separation). Confidence in our method is also gained by the good agreement between direct measurements of sulfide and calculation of sulfide loss by subtracting the polysulfide S^0 and aqueous pools from total dissolved S (Fig. 3C). The relatively large uncertainty for this point derives from the uncertainty in recovery during oxidation with H_2O_2, which is typically 78–95%, with some phases (ZnS) working better than others (hydrophobic OM). Typical observed recoveries for oxidized fractions, using polysulfide spike #5 as an example, are shown in Table 3.

Table 3. Typical replicate concentration measurements for dissolved sulfur pools (μM), used to assign methodological uncertainty to our experimental results

Repl.	spike #5				10 mM sulfide	
#	polysulfide S^0	aqueous	neutral S^0	Zn-rx sulfide	total	Zn-rx sulfide
1	4055	571	195	8672	9351	8327
2	3909	326	187	8204	8340	8868
3	3216	364			8799	9153
4	3282	474				
5	3711	434				
ave.	3634	434	191	8438	8830	8783
1σ	10.3%	22.2%	2.7%	3.9%	5.7%	4.8%

Sulfide and polysulfide S^0 represent the vast majority of S in the polysulfide spike solutions (Fig. 3). Roughly 20 times less S is recovered in the neutral S^0 fraction than in the polysulfide S^0 fraction. The neutral S^0 pool is expected to contain multiple forms of S^0, ranging from true S_8 (α-S_8) through nanoparticulate S_8^0 to solid crystalline S^0. The solubility of α-S_8 is very low at about ~0.31 μM at 25°C (Kamyshny 2009), so the neutral S^0 pool is likely composed largely of nanoparticulate S^0. Polysulfides can accelerate the formation of nanoparticulate S_8^0 by acting as nucleophiles to open α-S_8 rings (Boyd and Druschel, 2003).

Samples from different rounds of the experiments were subjected to increasingly intensive methods for O_2 exclusion, in part as an attempt to reduce the amount of S recovered from polysulfide solutions in the aqueous pool, which we initially interpreted as resulting from oxidation during sampling. Regardless, polysulfide solutions from

different iterations of benchtop and anaerobic chamber experiments all contain at least ~ 250 μM aqueous S (after blank correction), which would be equivalent to ~3% of the polysulfide solution if it were simply the result of oxidation during sampling. However, the S-isotope composition of the aqueous pool is typically much lower than the rest of the spike solution, suggesting that products of (poly)sulfide oxidation are mixed with a variably-sized blank with a $\delta^{34}S$ value near natural abundance. The most likely source of this blank is laboratory glassware, which is a particular issue for aqueous fractions because they contain HCl. Hydrogen peroxide reactivity is enhanced at low pH and is a more intense cleaning reaction than the 3.3 N HCl soak used to prepare the vials.

Equilibration within the polysulfide solution – Polysulfides are generated by combining buffered NaHS solution and solid S^0 in pH 8.5 buffer. Fig. 4 shows the evolution of neutral S^0 and Zn-reactive sulfide $\delta^{34}S$ values in a polysulfide solution over time. Although it takes about 20 days for the solution to fully equilibrate with the solid S^0, equilibration within the solution is much faster (Fig. 4b). In all of the samples collected between 1 and 26 days, measured sulfide $\delta^{34}S$ values in the polysulfide solution were consistently 11.5‰ ± 1.8‰ (1σ) lower than neutral S^0 $\delta^{34}S$ values, even though the absolute $\delta^{34}S$ values of both pools were steadily changing due to gradual $^{34}S^0(s)$ dissolution. Zn-reactive sulfide, neutral S^0, and by extension polysulfide S^0 thus appear to equilibrate within hours in our polysulfide solutions. Solutions were stirred for at least 21 days before being used in experiments to ensure that they were fully equilibrated with $S^0(s)$.

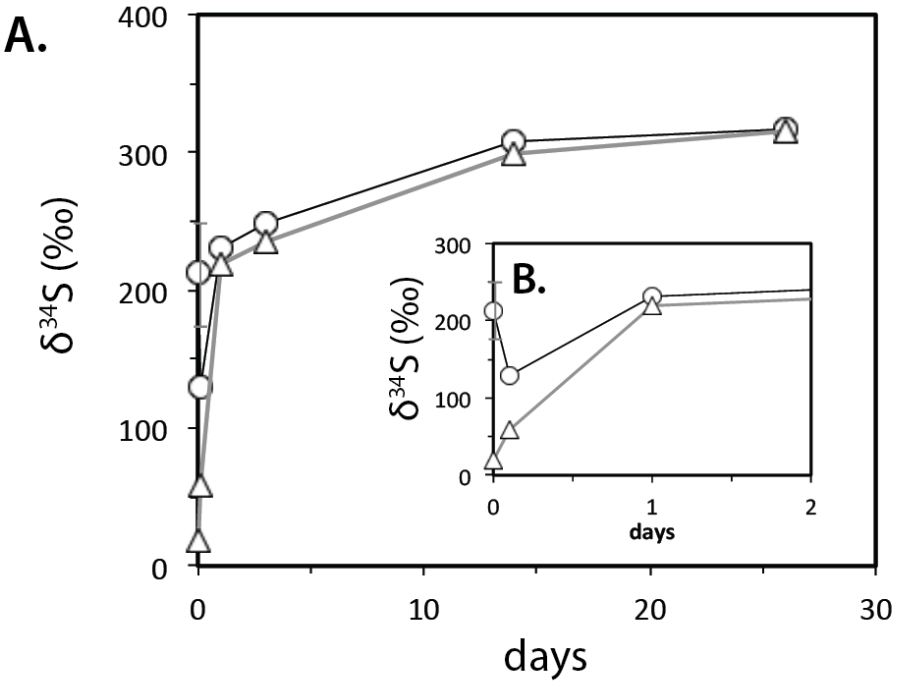

Fig. 4. S-isotope equilibration in solutions with sulfide and S^0(s). *Circles and squares show the $\delta^{34}S$ values for neutral S^0 and Zn-reactive sulfide, respectively, as defined in the text. Most symbols represent the average result from duplicate bottles. Inset (b) reproduces the first three time points on an expanded x-axis for clarity. Results are in per mil, relative to VCDT. Replicates and analytical uncertainties are smaller than symbols except where shown (neutral S^0 replicates, 10 minutes). Sulfide data (by EA) and neutral S^0 data (by ICP-MS) have an estimated inter-calibration uncertainty in this $\delta^{34}S$ range of 5‰.*

Polysulfide-free experimental controls – Some of the following experiments investigate water-soluble OS materials, so we tested whether these standards could be effectively recovered in our analytical scheme for dissolved S fractions. As shown in Table 4,

cysteine was effectively recovered in the aqueous fraction. (We note that less cysteine was recovered in the total fraction than in the aqueous fraction. Total S recoveries were typically 5–10% lower than other pools at the time these tests were run, although in later work, sealed–vial peroxide addition largely resolved this discrepancy). Humic acid was recovered predominantly in the aqueous fraction, but about 10% of humic acid S hydrolyzed in 0.5 N HCl and was recovered as polysulfide S^0. Hydrophobic organosulfur compounds were recollected by ether-washing the reaction vial after collecting dissolved sulfur aliquots. On a basic level, we conclude it is reasonable to use the aqueous fraction as a measure of cysteine, and (to a lesser extent) humic acids. The contributions of cysteine, organic sulfides, and humic acid to the Zn-reactive sulfide, polysulfide S^0, and neutral S^0 fractions are minor relative to the polysulfide spike.

Table 4. Sulfur in dissolved fractions for polysulfide-free controls

	total	Zn-rx sulfide	aqueous	polysulfide S^0	neutral S^0	extractable OS
	mM	mM	mM	mM	mM	mM
cysteine	1.19	0.08	1.26	0.07	≤ 0.02	--
organic sulfides	0.03	0.06	0.06	≤ 0.02	≤ 0.02	0.72
humic acid	0.67	≤ 0.02	0.51	0.06	≤ 0.02	--
sediment	0.11	≤ 0.02	0.11	≤ 0.02	≤ 0.02	0.019

For each sulfide–polysulfide solution of interest, we collected three parallel, 1 mL aliquots of solution through a 0.2 μm syringe filter, working under N_2. One aliquot was added to 1 mL N_2-sparged 1 M zinc acetate in a 50 mL Falcon tube, one was added to 1 mL N_2-sparged, 0.5% Seastar high-purity HCl in a glass VOA, and a third was collected into an empty VOA. After at least 30 minutes, the ZnAc and HCl-containing vials were each washed with 5 mL diethyl ether three times. After ether-extraction, the tubes containing ZnAc were centrifuged, and the solids were separated from the aqueous phase and washed twice with milli-Q water. Sulfur in all five fractions was oxidized to sulfate using 3 mL reagent-grade 30% H_2O_2 (90°C, 24 hrs). Peroxide addition by syringe through the VOA cap septa (rather than by opening the cap) significantly increased the amount and consistency of S recovery, particularly from the total fraction. Oxidation blanks from H_2O_2 were typically ~ 20 nmol S.

Aliquots for cysteine derivatization from experiment #2 were reacted with a solution of acetyl chloride and methanol (1 hr, 70° C) to methylate the amino acid group. After drying, they were dissolved in methyl tert-butyl ether (MTBE) and acetylated with trifluoroacetic anhydride to add a $COCF_3$ group to the nitrogen atom. The thiol group was not targeted for derivatization. Products were dissolved in MTBE and analyzed by GC-MS (Thermo DSQ-II with Trace GC Ultra).

In experiments #1, 3, and 4, sediments were collected after sampling the dissolved pool by opening the serum vial and transferring its contents to a 50-mL Falcon tube. In experiment #5, solid slurries were sampled by syringe (4 mL yielding 80–90 mg dry sediment) directly into centrifuge tubes. All sediment samples were washed with MQ water and freeze-dried. Dry sediments were microwave-extracted (MARS 5, CEM Corp.) into 9:1 dichloromethane (DCM):methanol at 100° for 15 minutes. Extracts were dried, transferred in 4:1 hexane:DCM, and separated by silica gel chromatography. Elemental sulfur from the polysulfide solution that might have been loosely associated with and extracted from the sediments was removed from the lipid extract by elution with 4:1 hexane:DCM, and a subsequent intermediate polarity fraction (DCM) was discarded. Polar extractable OM was eluted in 1:1 DCM:methanol. After drying, polar extractable OM samples were oxidized in 3 mL H_2O_2 (90°, 24 hrs).

Solvent-extracted sediments were washed with MQ water and leached with 1M nitric acid at 20° C for ten days (Schimmelmann and Kastner, 1993) to oxidize pyrite and hydrolysable organic matter. We refer to the remaining sulfur, which is not soluble in organic solvent, water, or nitric acid, as 'proto-kerogen'. Proto-kerogen abundance and $\delta^{34}S$ values were measured by combustion elemental analyzer – isotope ratio mass spectrometry (EA-IRMS, a Carlo Erba NC 2500 EA connected to a Delta+ XL ThermoQuest via the Thermo Conflo III interface). Proto-kerogen concentrations and $\delta^{34}S$ data have estimated uncertainties based on standard replicates of ± 2.5% and ± 0.5‰, respectively.

Oxidized samples of extractable OS and dissolved S pools were purified and analyzed for concentration and $\delta^{34}S$ value according to the methods detailed in Chapters 3 and 4, which are based on Paris et al. (2013). Sulfate was separated from other ions on AG1-X8 anionic exchange resin. Resin was washed with ten column volumes (CV) 10% HNO_3^-, conditioned with 10 CV 10% HCl and 10 CV 0.5% HCl, loaded in .05% HCl, and washed with 3x5 CV MQ H_2O before sulfate was eluted in 0.5 N HNO_3. Sulfate samples were stored dry in Teflon vials until analysis. The sulfur content of each OS fraction was measured as sulfate by ion chromatography (IC, Dionex ICS-2000) with an AS-19 anion column and AERS 500 ion regeneration. Concentrations were used to intensity-match samples and the required Na^+ supplement for analysis using a Thermo Neptune$^+$ multicollector inductively coupled plasma mass spectrometer (ICP-MS) (Paris et al., 2013). Samples were injected into the plasma torch with a desolvating nebulizer (Aridus) and bracketed with known $\delta^{34}S$ $NaSO_4$ standards. The Neptune was operated in medium resolution ($M/\Delta M \sim 8000$) to resolve oxygen interferences on mass 34. Sample reproducibility for $\delta^{34}S$ was typically better than ±0.2‰.

3. EXPERIMENTAL RESULTS AND DISCUSSION

3.1 Polysulfides + model organic S compounds (experiment #1)

Four different types of organic sulfur at concentrations of approximately 1.5 mM were incubated with ~1.5 mM $\sum S^{\leq 0}$ (Zn-reactive sulfide + polysulfide S^0) for two days (25° C, stirred). For incubations with cysteine, organic sulfides, and humics, sulfide and polysulfide S^0 were recovered at roughly the same concentrations that were added in the spike, but much less $\sum S^{\leq 0}$ was recovered following incubations with sediment. The $\delta^{34}S$ of OS recovered in all four incubations changed in response to incubation with ^{34}S-labelled $\sum S^{\leq 0}$. Different patterns in the $\delta^{34}S$ values of the dissolved S pools (Fig. 5) suggest that several different types of reactivity are important in these experiments.

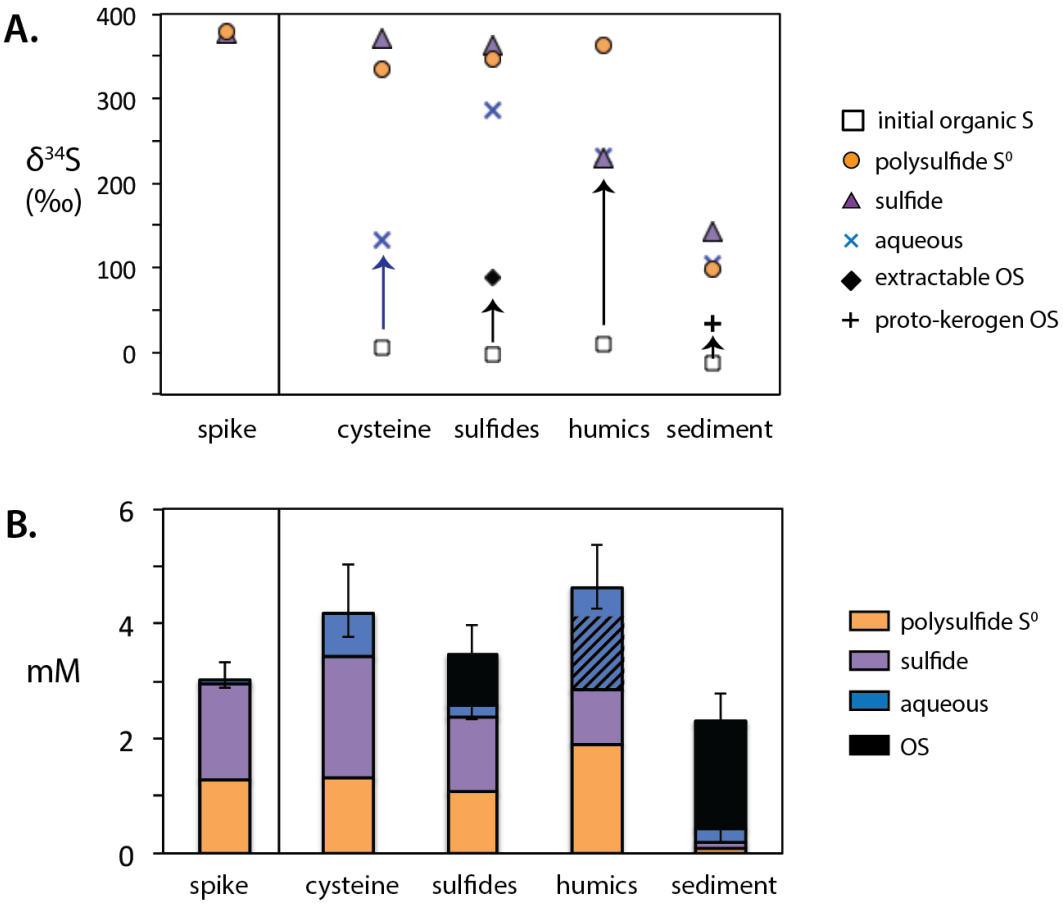

Fig. 5: Results of a two-day polysulfide incubation with different types of OS. *Arrows in chart (a) highlight the change in the $\delta^{34}S$ value of the organic S reactant before and after incubation. The hashed area for humic acids in (b) indicates the added aqueous sulfur relative to the control.*

Cysteine – Cysteine is recovered in the aqueous fraction (Table 2), which is substantially more ^{34}S-enriched after incubation, at 127‰ relative to an initial $\delta^{34}S$ value of 5.6‰. This change is mirrored in the $\delta^{34}S$ value of polysulfide S^0, which drops by 45‰ relative to the spike value. Surprisingly, however, this change is not also observed in sulfide

despite expectations that polysulfides – which disassociate into both of these pools – should be in internal isotopic equilibrium. We return to this question in greater detail in the following Section.

Organic Sulfides – We selected two organic sulfide standard compounds to test for their exchangeability with $\sum S^{\leq 0}$: a dialkyl monosulfide (C_{12}-S-C_{12}) and benzyl disulfide (Ph–S–S–Ph). These compounds are not miscible in aqueous buffer solution and were visible floating on the surface of the liquid throughout the experiment. They were recovered by extracting the reaction vial with diethyl ether after sampling for the dissolved sulfur fractions. The ether extracts were exposed to activated copper for an hour and then split into aliquots for oxidation and GC-MS analysis. The bulk (oxidized) ether-extracted pool was nearly 90‰ more ^{34}S-enriched following incubation with ^{34}S-labeled polysulfides than the control. This δ^{34}S change is complemented by drops in the δ^{34}S values of polysulfide S^0 from 379‰ to 347‰ and of sulfide from 377‰ to 363‰. By mass balance, the change we observe in bulk organic sulfide δ^{34}S would be equivalent to one quarter of the S atoms in the (di)sulfide mix having exchanged with polysulfides. Conceptually, this could represent either one-quarter exchange of all S atoms, complete exchange of only one quarter of the S atoms, or something in between. This single time point after two days likely does not represent the final state of the system, especially given the potential kinetic limitations from phase immiscibility. Still, it appears that at least some organic sulfides can exchange with polysulfides. We confirmed that the alkyl sulfides were not transformed by incubation with polysulfides (e.g., by polymerization)

by analyzing the Cu-treated ether extracts of the incubated and control bottles by GC-MS, which yielded indistinguishable recoveries and indicated that labeled S^0 was fully removed by Cu treatment (Table 5). Forthcoming measurements of compound-specific $\delta^{34}S$ will test whether both compounds or only the disulfide is exchanging.

Table 5: Results of incubating polysulfides with organosulfur standard compounds

	dibenzo-diS	C_{12} sulfide	total OSC	bulk oxidation	
replicate	nmol S	nmol S	μmol S	μmol S	$\delta^{34}S$
O1	59.2	41.9	10.1	13.5	78.4
O2	34.0	58.9	9.3	16.6	98.4
average	46.6	50.4	9.7	15.0	88.4
control	44.6	60.0	10.5	12.3	-0.96

Humic Acids – We investigated a common standard material, Sigma Aldrich humic acid, which we recover primarily in the aqueous dissolved S pool (Table 4). The concentration of aqueous S after incubation is about 1.3 mM higher than in the humic acid control, as highlighted by the hashed area in Fig. 5b. At the same time, sulfide concentrations dropped by 0.73 mM, leaving 0.94 ± 0.3 mM sulfide with a $\delta^{34}S$ value within 3‰ of aqueous S. Sulfide may be incorporated into humic acids via OM sulfurization, and this abiogenic OS may be exchangeable with sulfide. Alternatively or in addition, humic acids can directly oxidize sulfide (Heitmann and Blodau, 2006; Yu et al., 2015), yielding salts like sulfate, sulfite, or thiosulfate that should also be recovered in the aqueous pool.

A net oxidation of the dissolved sulfur pool is consistent with the observed increase in polysulfide S^0 concentration relative to sulfide. Unlike experiments with cysteine, organic sulfide, and sediment, the $\delta^{34}S$ values of neutral and polysulfide S^0 change only slightly after incubation with humic acids.

Sedimentary organic matter – Incubations with sedimentary organic matter generated the largest changes in polysulfide S^0 and sulfide $\delta^{34}S$ and the smallest change in OS $\delta^{34}S$ after two days. We discuss this data in the context of additional results in Sections 3.3 and 3.4.

3.2 Chemical interactions between $\sum S^{\leq 0}$ and cysteine (experiment #2)

Approximately 1.5 mM cysteine was incubated with ~3 mM $\sum S^{\leq 0}$ (Zn-reactive sulfide + polysulfide S^0) for 14 days. One bottle was sampled at six time points, and a duplicate bottle was sampled at 1 and 14 days, and a $\sum S^{\leq 0}$-free control was sampled after 14 days. The total amount of dissolved S and its $\delta^{34}S$ value remained invariant (within uncertainties) throughout the experiment. Sulfur recovered in the aqueous fraction should be primarily cysteine, although this fraction may also contain products of unintentional $\sum S^{\leq 0}$ oxidation during sampling. The concentration of S in this fraction remains effectively constant throughout the experiment (given recoveries of 77–81% for an earlier method and 83–94% for a revised method). Cysteine was derivatized with a trifluoracetyl group and a methyl ester, which should not impact the thiol moiety. We recovered the

same two products of cysteine derivatization in indistinguishable amounts from cysteine incubations and the control (Table 6). The dominant derivatization product is cystine (Cys–Cys), and the minor product may contain an additional S atom (potentially Cys–S–Cys). Their sum is shown as 'total OSC' in Table 6. Cysteine and cystine are readily interconverted in proteins, with cystine representing the more oxidized form.

$$2\ HO_2CCH(NH_2)CH_2SH \rightarrow HO_2CCH(NH_2)CH_2S\text{–}SCH_2CH(NH_2)CO_2H + 2H^+ + 2e^-$$

Cystine formation is favored in air and likely would be formed by our derivatization scheme. Additionally, cysteine could have been converted to cystine by reactions with polysulfides, prior to sampling and analysis.

Table 6: Cysteine derivative recovered after polysulfide incubations

	total OSC	bulk oxidation	
replicate	μmol S	μmol S	$\delta^{34}S$
C1	0.30	1.23	57.4
C2	0.75	1.18	56.1
control	0.26	1.26	**5.1**

The aqueous (cysteine), polysulfide S^0, neutral S^0, and sulfide pools all undergo significant $\delta^{34}S$ changes during the experiment (Fig. 6). Over the first few hours, the $\delta^{34}S$ values of the polysulfide S^0 and aqueous pools move toward each other, and neutral S^0 follows with a time lag. At the same time, the drop in sulfide $\delta^{34}S$ is much smaller

(16‰). After about 72 hours, cysteine $\delta^{34}S$ is effectively constant while first polysulfide S^0 and then neutral S^0 return to S-isotope equilibrium with sulfide.

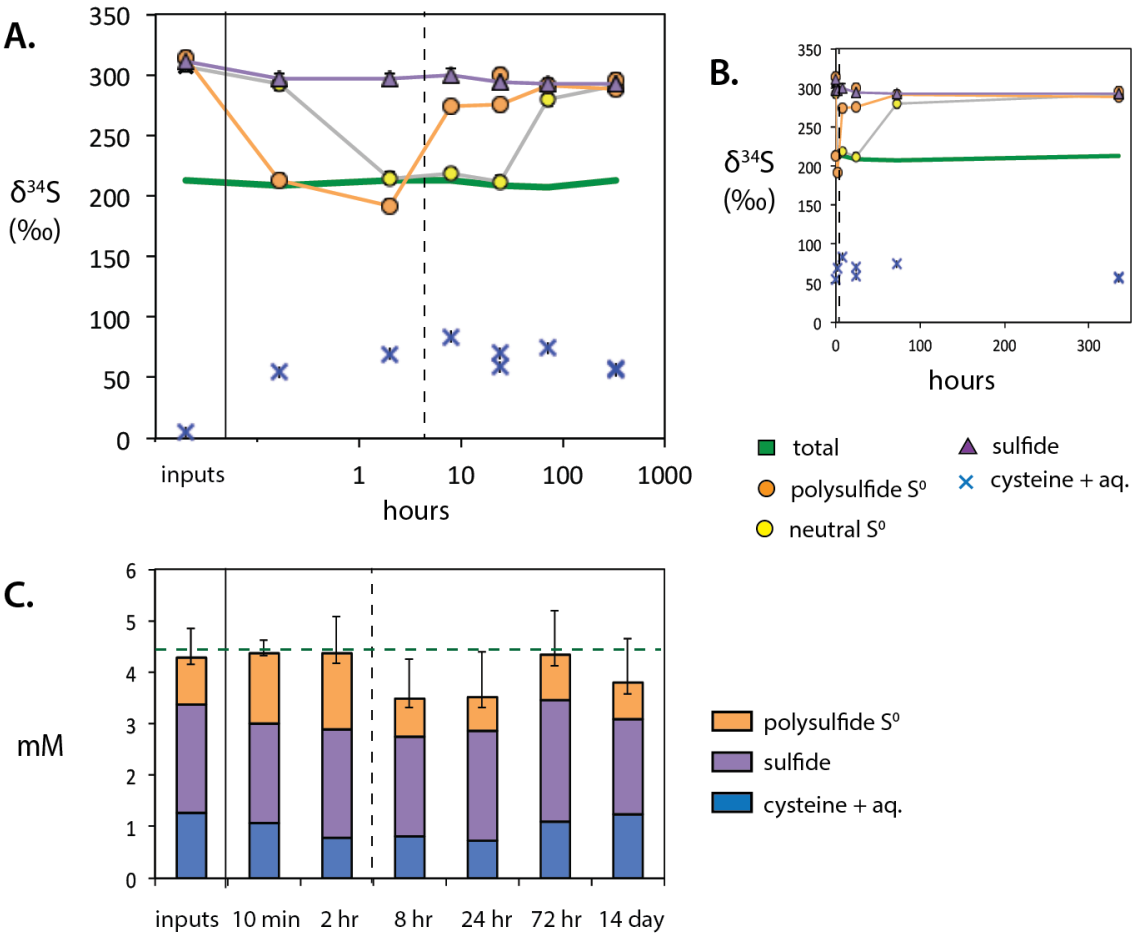

Fig 6: Results of experiment #3 with cysteine. *Chart (a) shows $\delta^{34}S$ values (in per mil relative to VCDT) for pools of dissolved sulfur on a logarithmic time axis; chart (b) shows the same data on a linear scale. Chart (c) presents concentrations of the three main dissolved S pools. Throughout, dashed vertical lines separate the early and late phases of the experiment, discussed in the text. The horizontal dashed line in (c) emphasizes the statistically invariant total dissolved S concentration.*

Potential role of organic polysulfides – During the first two hours of the experiment, the $\delta^{34}S$ values of sulfide and polysulfide S^0 differed by as much as 105‰. In contrast, free S_x^{-2} molecules should be in rapid equilibrium with sulfide, as we observed in polysulfide solutions (Fig. 4). Unless this large $\delta^{34}S$ difference between sulfide and polysulfide S^0 represents a yet-unidentified analytical artifact, sulfur in the polysulfide S^0 fraction must be largely in a form where equilibration with sulfide is inhibited. Reactions between cysteine and polysulfides are likely to generate organic polysulfides, which have been previously described as products of natural OM sulfurization (Vairavamurthy and Mopper, 1991). Organic polysulfides have also been synthesized experimentally under phase-transfer conditions (de Graaf et al., 1992; Schouten et al., 1994). We propose that organic polysulfides may exchange with the rest of the $\sum S^{\leq 0}$ pool less rapidly or thoroughly than free S_x^{-2} molecules, which would make them capable of maintaining a distinct $\delta^{34}S$ value from sulfide. We also assume that there is complete and rapid isotope mixing within the polysulfide chains in cysteine polysulfides, as is the case for S_x^{2-} (Amrani and Aizenshtat, 2004). Both ends of polysulfide chains could potentially react with cysteine thiol groups, generating cysteine dimers linked by various numbers of zero-valent sulfur atoms (Cys–S_n–Cys). At low pH, we assume that cysteine polysulfides will dissociate, with zero-valent sulfur atoms ending up in the polysulfide S^0 fraction and carbon-bound sulfur (the cysteine thiol group) ending up in the aqueous fraction. If true, the $\delta^{34}S$ patterns we observe in experiment #2 could be generated by cysteine polysulfide synthesis and maturation.

Potential mechanisms for the formation of cysteine–polysulfide (Cys–S_n^-) can be distinguished by their effects on S-isotope patterns. One is for the polysulfide sulfhydryl group, a strong nucleophile, to attack the thiol carbon and replace the S atom, forming a new C-S bond.

$$^-S–S_n–S^- + ^-\mathbf{S}\text{-}CH_2CHNH_3^+COO^- \rightarrow ^-S–S_n–S\text{-}CH_2CH_2COO^- + \mathbf{S}H^- \quad (1)$$

In this model, the relatively ^{34}S-depleted thiol S from cysteine would be released and mix with sulfide, quickly making sulfide more ^{34}S-depleted. The zero-valent S from Cys–S_n^- and Cys–S_n–Cys, as measured in the polysulfide S^0 pool, would have an S-isotope composition similar to the original polysulfide spike. Our results meet neither of these predictions; instead, the change in polysulfide $\delta^{34}S$ value is much larger than the change in sulfide $\delta^{34}S$. Alternatively, the thiol may react with α-S_8 or other types of S^0.

$$S_8 + ^-\mathbf{S}\text{-}CH_2CHNH_3^+COO^- \rightarrow ^-S–S_n–S\text{-}CH_2CH_2COO^- + \mathbf{S}H^- \quad (2)$$

The feasibility of this reaction depends on the kinetics of exchange among S_8, nanoparticulate S^0, and polysulfides, so it is challenging to assess. Still, rather than converge immediately with cysteine, the $\delta^{34}S$ value of neutral S^0 lags that of polysulfide S^0.

As a third option, organic polysulfides could bind to the cysteine thiol according to a polysulfide chain-elongation mechanism.

$$^-S–S_n–S^- + ^-\mathbf{S}\text{-}CH_2CHNH_3^+COO^- \rightarrow ^-S–S_n–S–\mathbf{S}\text{-}CH_2CHNH_3^+COO^- \quad (3)$$

Because reaction (3) lengthens the polysulfide chain, it should increase the number of S^0 atoms per molecule relative to the initial polysulfide solution. Accordingly, we observe a

~50% increase in polysulfide S^0 concentrations in the first two hours (Fig. 6c). Crucially, the concentration of cysteine in this experiment exceeded that of polysulfide molecules (assuming an average composition of S_5^{2-}), so the final $\delta^{34}S$ value of the aqueous fraction is likely to include both cysteine polysulfides and unreacted cysteine. The isotopic composition for Cys–S_n^- is therefore best estimated by the $\delta^{34}S$ value of polysulfide S^0 (corrected for neutral S^0), which is intermediate between the original polysulfide and the cysteine (192‰ after two hours). To first order, organic polysulfide formation via reaction (3) appears to offer a reasonable fit to our experimental results.

The initial product of reaction (3) should contain polysulfide-derived and cysteine-derived S atoms in an average ratio of ~5:1 and may react further to produce a cysteine–polysulfide dimer with an average ratio of ~5:2. The predicted $\delta^{34}S$ value for this molecule with two cysteines, ~225‰, is comparable to that of polysulfide S^0 after ten minutes (214‰). The change in the $\delta^{34}S$ value of the aqueous fraction and the amount of S recovered in the polysulfide S^0 fraction imply that between 25 and 44% of the cysteine is in the form of organic polysulfides during the first two hours of the experiment, with a $\delta^{34}S$ value similar to the polysulfide S^0 fraction.

Changes in cysteine reactivity over time – After about 72 hours of incubation, the S-isotope compositions of polysulfide S^0, neutral S^0, and sulfide fractions converged at $\delta^{34}S$ values that are an average of 21‰ more ^{34}S-depleted than the initial spike. Although polysulfide $\delta^{34}S$ changed dramatically between 2 and 8 hours, the $\delta^{34}S$ value of the

aqueous fraction did not change significantly after the 10 minute time point. Our best hypothesis to explain these observations at present is that ongoing chain-rearrangement reactions transformed the cysteine polysulfides (e.g., Cys–S_5–Cys) into a more stable and less exchangeable forms with shorter sulfur chains (e.g., cystine and/or Cys–S–Cys) on a timescale of hours. As polysulfide chains shorten, the amount of zero-valent S in these structures drops. Later in the experiment, S in the polysulfide S^0 fraction would derive predominantly from S_n^{2-} rather than cysteine polysulfide. We observe Cys–Cys and perhaps Cys–S–Cys by GC-MS from both the polysulfide-incubated and control experiments. In the control bottle, dimerization likely occurred during derivatization.

The results of experiment #2 suggest that cysteine and polysulfides may react to form organic polysulfides via a chain-elongation-type mechanism without requiring phase transfer conditions. These organic polysulfides have an S-isotope composition that reflects the mixture of the initial thiol group and the polysulfide. Polysulfide chain-rearrangement reactions may also facilitate the formation of relatively stable disulfide structures from polysulfides and cysteine. Cysteine is generally the single most abundant type of OS in fresh biomass and serves as a decent model for other organic thiols, so organic polysulfide formation and maturation could be a major contributor to the reactivity between natural OM and $\sum S^{\leq 0}$. In the following two sections, we ask whether the reactivity of natural OM toward $\sum S^{\leq 0}$ is similar to that of cysteine or other standards.

3.3 Chemical interactions between $\sum S^{\leq 0}$ and sedimentary OM (experiments #3 and #4)

In experiments #3 and #4, we conducted a set of experiments with polysulfide solutions and sediments from Santa Barbara Basin, sampling bottles at 1, 2, or 30 days. Experiment #3 was conducted on sediments from two depths (0–10 cm and ~30 cm); experiment #4 investigated only the shallower sediment.

Effects of incubation on sedimentary OM – The $\delta^{34}S$ values of proto-kerogen from both sediment depths increased following incubation with ^{34}S-enriched polysulfide solutions (Fig. 7). After one and two days, proto-kerogen in all of the experiments averaged 32 ± 6‰, an average increase of 49‰ over initial proto-kerogen values (–17‰). After 30 days, proto-kerogen $\delta^{34}S$ values averaged 68 ± 2‰. Polar extractable OM was consistently more ^{34}S-enriched than proto-kerogen, but shared a similar trend with time. The abundance of polar extractable OS did not significantly change during the experiment, and the amount of proto-kerogen S in the deeper sediment also remained effectively unchanged. In the shallow sediment, however, proto-kerogen S increased from an initial concentration of 55 ± 3 μmol/g to 70 ± 5 μmol/g after 1–2 days and 105 ± 5 μmol/g by 30 days. This change is equivalent to an increase in OS in our experiments of 7.6 μmol (in 20 mL, or "0.38 mM" for comparison with dissolved fractions) in the first ~2 days and 20 μmol (1.3 mM) within 30 days.

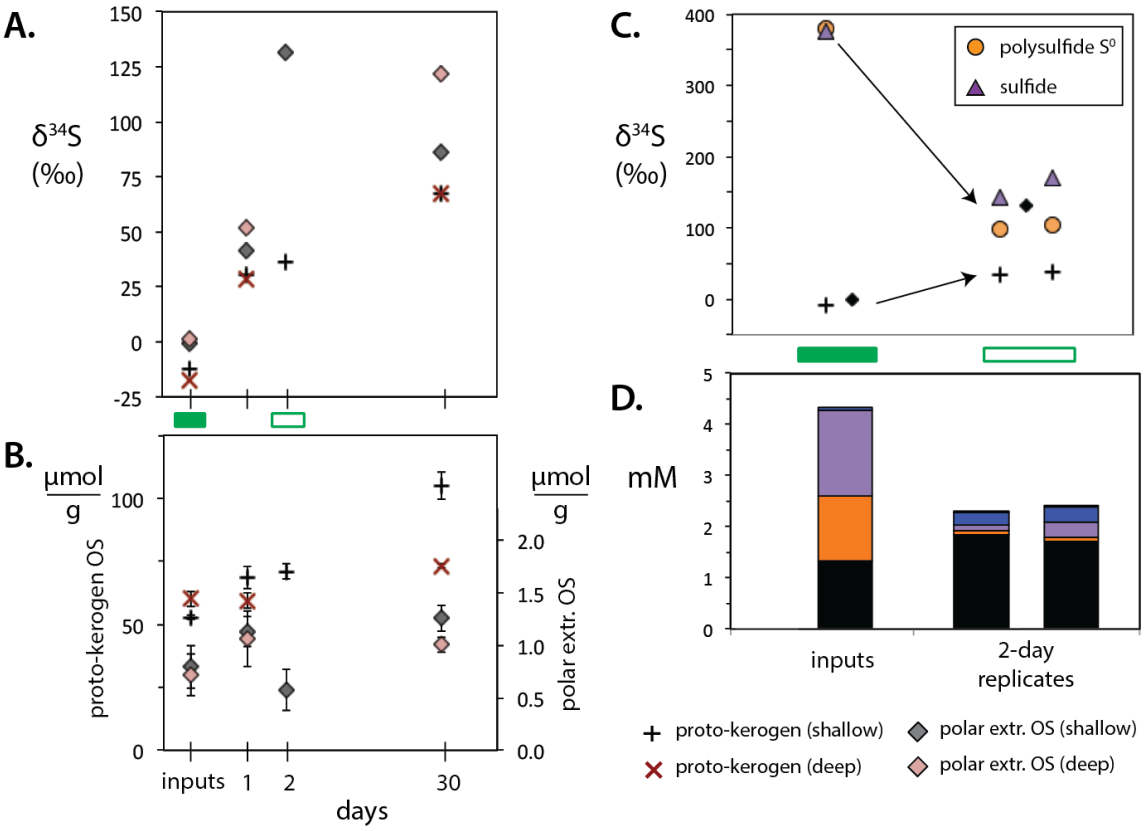

Fig 7: Sedimentary organic sulfur average $\delta^{34}S$ values and concentrations following incubation with ^{34}S-labeled polysulfides*. Charts (a) and (b) show the $\delta^{34}S$ values and concentrations of organic S (proto-kerogen and polar extractable OS) for two sediments after 1, 2, and 30 days of incubation. Symbols represent the average of duplicate samples in most cases, with error bars in (b) depicting their range. Charts (c) and (d) show only data from experiment #4, with duplicates shown separately. The second replicate of the dissolved pools after 2 days (right) was unfiltered (filter failed).*

Dissolved S pools –Sediments for the 1- and 30-day incubations (experiment #3) were not soaked in formaldehyde prior to incubation (see Methods). Control samples that were

incubated with ^{34}S-labeled sulfate rather than polysulfide contained significant ^{34}S-rich sulfide after 30 days, indicating that sulfur-cycling microorganisms were active in these bottles. Accordingly, the results for dissolved S fractions from experiment #3 are discussed only in terms of general trends. We have greater confidence in dissolved S data from experiment #4, which included a formaldehyde treatment.

After a 2-day incubation (experiment #4), the concentration of $\sum S^{\leq 0}$ (Zn-reactive sulfide + polysulfide S^0) dropped by 90% (from 3.0 ± 0.2 mM to 0.29 ± .09 mM). Some of this lost S can be accounted for by the addition of S to proto-kerogen, which amounted to the equivalent of 0.38 mM. The rest of this S must be present in a solid phase that dissolves or volatilizes in nitric acid, like iron–sulfide minerals and hydrolysable OM. We observed a change in color in the solutions from brown to black on polysulfide addition that is consistent with the nucleation of FeS. The $\delta^{34}S$ values of polysulfide S^0 and Zn-reactive sulfide after two days were 101‰ and 157‰, respectively, representing major declines of 278‰ and 219‰ from initial spike values. Final $\sum S^{\leq 0}$ $\delta^{34}S$ values are trending toward to those of proto-kerogen (36.2 ± 1.8‰), which suggests that these pools are equilibrating, but equilibrium is not complete after two days. After 30 days (experiment #3), proto-kerogen $\delta^{34}S$ values are higher (67.2 ± 1.5‰) and more similar to polysulfide S^0 (63‰ ± 2‰, with the caveats noted above), consistent with more complete exchange.

Effect of sediment age – In the shallow sediment incubations, $\sum S^{\leq 0}$ concentrations after two days of hydrolysable solid precipitation are low (~0.29 mM) relative to the

concentration of OS (~3.5 mM). We expect less FeS precipitation in the deep sediment than for the shallow sediment because interpolated dithionite–reducible iron (Fe_R) concentrations are about half as large in the deep sediment (~40 μmol/g, equivalent to 2 mM) than in the shallow sediment (79 μmol/g, or 4 mM, Chapter 4). Accordingly, less sulfide likely precipitated as iron sulfides in the incubations with the deeper sediment, leaving a higher residual sulfide concentration. For both proto-kerogen samples to achieve the same final $\delta^{34}S$ value (which they do, Fig. 6a), the deeper sediment would therefore need a smaller proportion of its proto-kerogen S to equilibrate with the relatively large $\sum S^{\leq 0}$ pool than the shallow sediment. Although dissolved S data from experiment #3 were potentially impacted by microbial S cycling, polysulfide S^0 is more abundant and more ^{34}S-enriched in incubations with the deeper sediment than with the shallow sediment after both 1 day (deep = 0.34 mM, 142‰; shallow = 0.19 mM, 69‰) and after 30 days (deep = 0.37 mM, 219‰; shallow = 0.06 mM, 63‰). In the shallow sediment incubations, this final isotopic composition of polysulfide S^0 compares well to that of proto-kerogen S (68 ± 2‰), which is consistent with $\sum S^{\leq 0}$ and OS being at or near equilibrium. On the other hand, proto-kerogen S and polysulfide S^0 $\delta^{34}S$ values in the deeper sediment incubation are quite different (68‰ and 219‰, respectively), consistent with only part of the OS in the deeper sediment having exchanged with $\sum S^{\leq 0}$ in the deeper sediment after 30 days. It thus appears that sediment from 30 cm depth in Santa Barbara Basin is less rapidly or thoroughly exchangeable than sediments from near the sediment-water interface. Understanding the mechanisms and timescales of the loss of OS exchangeability will be an important topic for future research.

3.4 Chemical reactivity of $\sum S^{\leq 0}$ and sedimentary OM (experiment #5)

Methods for experiment #5 were identical to experiment #4 except that both solids and dissolved S fractions were collected at six time points between 10 minutes and 14 days, and the incubations were conducted in an anaerobic chamber rather than on the benchtop. The shallow (0–10 cm) SBB sediment was investigated in duplicate alongside a polysulfide-free control, concurrently with experiment #2 (cysteine).

As seen in experiment #4, the total amount of S measured by our methods (Zn-reactive sulfide + polysulfide S^0 + aqueous + proto-kerogen) dropped over the first few days of the experiment (Fig. 8). These S atoms must accumulate in solids that volatilize or solubilize in nitric acid, such as iron mono- and di-sulfides and organic polysulfides. After three days, Zn-reactive sulfide concentrations were ≤ 0.35 mM and polysulfide S^0 concentrations were near oxidation blank limits (≤ 0.04 mM). The combined reduction in these pools can be coarsely fit to an exponential loss function of $[HS^- + S_x^{2-}] = 5.6*e^{-.4/t} +$ 0.4 mM, which implies a λ for the precipitation reaction of 0.4 hr^{-1} ($t_{1/2}$ = 1.7 hrs). The net change in total dissolved S (Zn-reactive sulfide + polysulfide S^0 + aqueous) is 6.6 mM, of which 4.1 mM occurs in the first ten minutes. Especially if some precipitates are disulfides, reaction with Fe^{3+}, which is present at an initial concentration of 79 μmol/g ("2.0 mM") could account for much of the $\sum S^{\leq 0}$ loss we observe over the first few hours of the experiment.

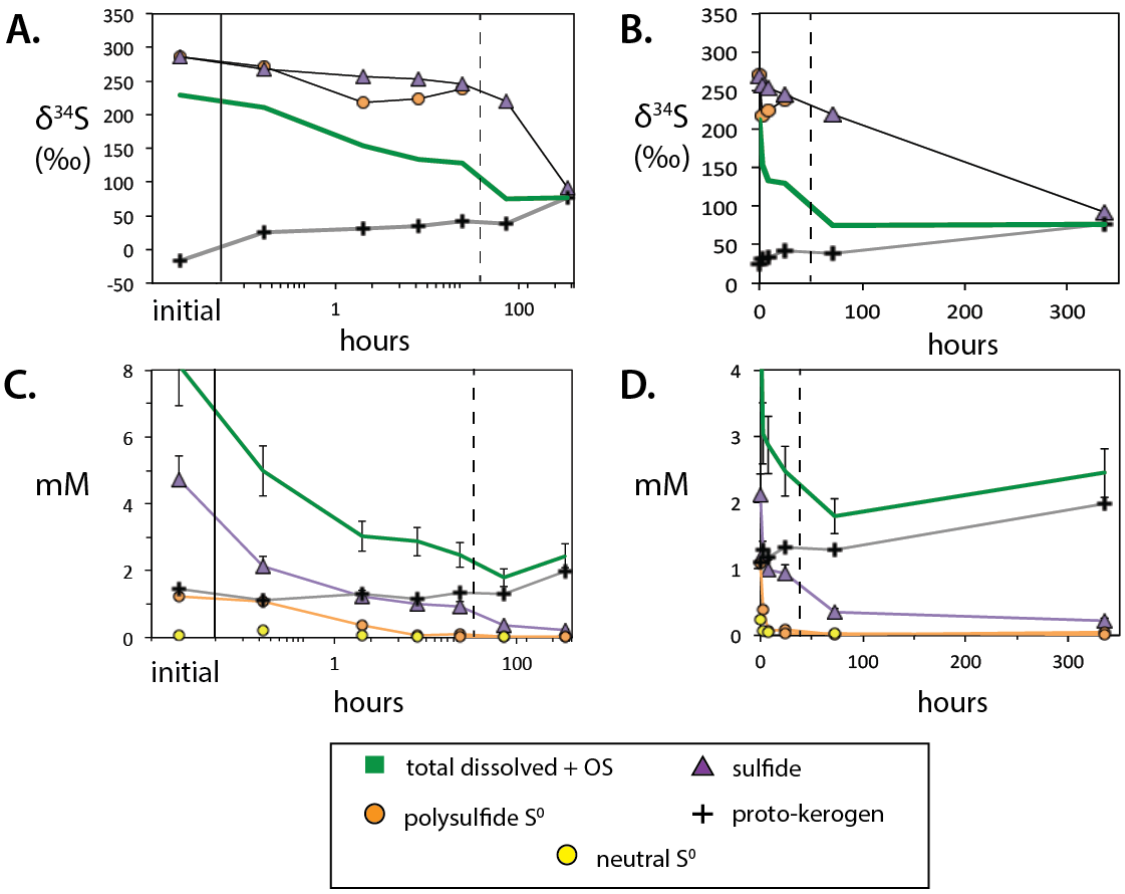

Fig 8: *S-isotope composition and concentration of dissolved S pools and proto-kerogen over a 14-day sediment + polysulfide incubation. Charts (a) and (c) show S-isotope compositions (in per mil relative to VCDT) and concentrations, respectively, on a logarithmic time axis. Charts B and D duplicate this data on a linear time axis. The solid vertical lines mark the beginning of the experiment, and the dashed vertical lines highlight the transition from a precipitation-dominated system to an equilibration-dominated system (see text).*

Proto-kerogen becomes more ^{34}S-enriched upon incubation with ^{34}S-labeled $\sum S^{\leq 0}$. After ten minutes, proto-kerogen $\delta^{34}S$ values increased from –17.4‰ to 24.7‰ while there was no significant change in proto-kerogen S concentration. This indicates rapid mixing between proto-kerogen and dissolved S but is not consistent with equilibrium reactions moving toward completion. Between 3 and 14 days, OS $\delta^{34}S$ values continue to increase, reaching 80.2 ± 4‰ after 14 days. Over the same period, proto-kerogen S concentrations also increase by the equivalent of 0.65 ± 0.05 mM S. The net drop in sulfide concentration between 3 and 14 days is only 0.13 ± 0.05 mM, so the immediate source of this added OS does not appear to be porewater sulfide. Instead, the additional S that appears in the proto-kerogen pool may represent organic polysulfide structures that precipitated during the early part of the experiment transforming into more stable, non-hydrolysable OS. Simple addition of 0.65 mM OS with a $\delta^{34}S$ value near that of polysulfide S^0 at 2 or 8 hrs (~220‰) to 1.3 mM proto-kerogen S at 38.3‰ could account for the entire change in proto-kerogen $\delta^{34}S$ value over this period. This feature is reminiscent of incubations with cysteine, where there was a very rapid shift in OS $\delta^{34}S$ value within 10 minutes followed by a more gradual process that changed the properties of the OS.

Between 3 and 14 days, the $\delta^{34}S$ difference between proto-kerogen and sulfide collapses from 181‰ to only 16.2‰, indicating the occurrence of sulfide–OS exchange. Sulfide–disulfide exchange is a common process within enzymes in which the nucleophilic thiolate (S^-) attacks and displaces an S atom in a disulfide bond (Gilbert, 1995). Under

our stirred experimental conditions, we can coarsely estimate rates of exchange between sulfide and OS by treating OS as if it is in excess and applying the equation:

$$(F_t - F_{eq})/(F_0 - F_{eq}) = e^{-kt};$$

to the period between 3 days (F_0) and 14 days (F_t), where F is the fractional abundance of ^{34}S in the dissolved sulfide fraction and F_{eq} is taken as the $\delta^{34}S$ of proto-kerogen. Equilibrium exchange rates for sulfide in this system are on the order of 0.1 to 0.2 d^{-1}. We might expect a small (few per mil) offset between sulfide and OS at equilibrium, but an additional time point is needed to assess whether the 16‰ difference between sulfide and OS after 14 days represents an equilibrium fractionation factor.

4. IMPLICATIONS FOR SEDIMENTARY $\delta^{34}S$ RECORDS

4.1 Interpreting $\delta^{34}S$ records from Santa Barbara Basin

In general, the results of experiments with sediments from Santa Barbara Basin confirm the hypothesis from Chapter 4 and Dale et al. (2009) that interactions between OM and $\sum S^{\leq 0}$ can strongly affect the $\delta^{34}S$ values of these pools. In the upper 50 cm of Santa Barbara Basin sediments, porewater sulfide is characterized by consistently low concentrations and complex $\delta^{34}S$ patterns with steep $\delta^{34}S$ gradients that should be difficult to maintain in the face of diffusion. These sulfide $\delta^{34}S$ gradients could be supported by sulfur exchange with organic disulfides in OM. In the natural SBB environment, the susceptibility of sulfide $\delta^{34}S$ values to control by excess OS depends on

the mixing ratio between OM and the integrated production of sulfide. Effective concentrations of OM are approximately ten times higher in the environment than in our experiments, but the size of the integrated sulfide pool is harder to estimate. Accumulated sulfide concentrations in porewater reach ~ 0.5 mM by 20 cm in profiles by Reimers et al. (1996), and sit near 0.7 mM in the top 20 cm of multi-core sediments (Chapter 4). These sulfide concentrations are much lower than would be expected from sulfate reduction rates of 0.01 to 8 mM (Reimers et al., Chapter 4), and much of the sulfide produced by microbial sulfate reduction may be reoxidized or precipitated locally, without passing through the porewater sulfide pool. For comparison, the OS pool in SBB sediments is present at the equivalent of ~15 mM. If proto-kerogen were to exchange only with accumulated porewater sulfide (i.e., all sinks for sulfide are local), there would be ~30 times more sulfur in OS than sulfide. If 1 mM/yr sulfide were to pass through the porewater pool (i.e., sulfide is oxidized or precipitated mainly from bulk porewater), ~15 mmol OS would be exposed to ~50 mmol sulfide by the time it was buried to 20 cm depth. The effect of sulfide-OS exchange on sedimentary $\delta^{34}S$ patterns thus depends on the relative availability of sulfide and exchangeable OS and on the importance of local sulfide sinks.

In deeper sediments, the exchangeability of OS gradually declines. In a comparison of sediments from two depths in Santa Barbara Basin (experiment #3), we find hints of decreasing OS exchangeability with sediment age. This is also consistent with what we see in the environmental profile, where proto-kerogen and sulfide $\delta^{34}S$ values diverge

below about 40 cm depth and exchange appears to be effectively complete by 15.6 m (Bruchert et al., 1995). The importance of later-diagenetic exchange on sedimentary $\delta^{34}S$ records will depend on how the exchangeability of OS changes with age and depth. If OS remains exchangeable over a long diagenetic window with changing sulfide $\delta^{34}S$ values, the bulk proto-kerogen $\delta^{34}S$ value may be partially overprinted by later exchange. In SBB, however, OS $\delta^{34}S$ values diverges from those of sulfide and have only a slight trend toward sulfide $\delta^{34}S$ below ~50 cm depth. The deeper OS $\delta^{34}S$ profile also shares features with the pyrite $\delta^{34}S$ records, indicating that it retains early-diagenetic information and is not fully 're-set' by later exchange. Additional work is clearly warranted to better understand the window of sediment diagenesis over which OM is exchangeable and the kinetics of exchange in natural environments.

4.2 Potential importance for global records

Exchange with sulfide is one way for OS to become more ^{34}S-enriched than pyrite over the course of sediment diagenesis. Another way is for relatively ^{34}S-enriched biogenic S to be incorporated into stable structures along with $\sum S^{\leq 0}$. The organic polysulfides that we infer to form in incubations with cysteine have a $\delta^{34}S$ value that suggests mixing between $\sum S^{\leq 0}$ and biomass. In typical marine sediments, proto-kerogen that incorporated cysteine S via organic polysulfide formation would initially have a more ^{34}S-enriched composition than its sulfide reactant, consistent with the global relationship between proto-kerogen and pyrite. After initial formation, the $\delta^{34}S$ value of OS could still be modified by exchange.

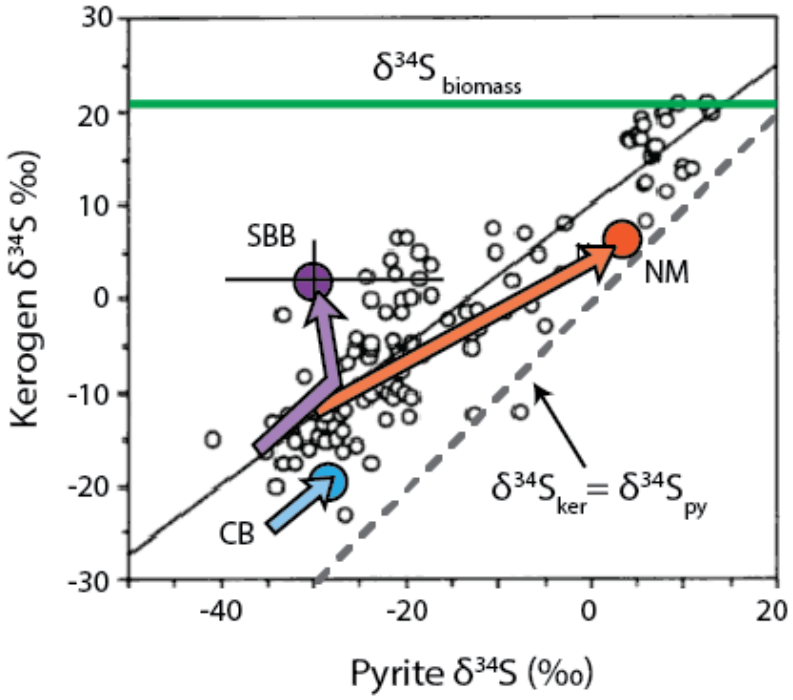

Fig. 9. *Global compilation of $\delta^{34}S$ values of combined kerogen and pyrite in rocks (Bottrell and Raiswell, 2000). The dashed line indicates the 1:1 line, and the solid line is the global regression (Anderson and Pratt, 1995). The bold horizontal line indicates the estimated $\delta^{34}S$ value of marine biomass, one potential component of S in kerogen. Colored arrows indicate trends in concurrent pyrite and OM $\delta^{34}S$ values with depth in three modern sites: Cariaco Basin (CB, Werne et al., 2003), Santa Barbara Basin (SBB, Bruchert et al., 1995), and the Namibian Shelf (NM, Dale et al., 2009). Filled circles with error bars represent 'final' S-isotope compositions and their range among individual samples.*

Patterns in $\delta^{34}S$ from modern sites suggest a potentially important role for S-isotope exchange reactions in creating the $\delta^{34}S$ patterns preserved in sedimentary rocks. Modern

environments generate pyrite and kerogen $\delta^{34}S$ values that span the entire range of variability in ancient environments, in terms of both absolute values and their difference. Fig. 9 compares this global compilation to the evolution of proto-kerogen and pyrite $\delta^{34}S$ values with sediment depth in three modern environments with different redox conditions. All three modern environments start with relatively low $\delta^{34}S$ values in both phases but evolve differently during early diagenesis.

Sediments from Santa Barbara Basin (Chapter 4) fall along the global trend at first, with parallel increases in pyrite and OM $\delta^{34}S$ values. In deeper Santa Barbara Basin sediments, OM becomes increasingly ^{34}S-enriched, suggesting that it continues to exchange with increasingly ^{34}S-enriched porewater sulfide. Pyrite in this environment does not appear to exchange with $\sum S^{\leq 0}$, so the net effect of exchange is to increase the $\delta^{34}S$ difference between pyrite and OM that would be preserved in rocks. In sediments from the Namibian shelf, Dale and colleagues (2009) proposed that both pyrite and proto-kerogen exchange with $\sum S^{\leq 0}$, producing similarly high $\delta^{34}S$ values in both pools. Reasons for the discrepancy in apparent pyrite exchangeability are unclear, but could reflect different selectivity of the different extraction procedures used or the effects of non-steady-state deposition in the Namibian Margin system. In contrast with both of these sites, the $\delta^{34}S$ values of pyrite and proto-kerogen in Cariaco Basin start low and change relatively little in the upper 6 m of sediment. Porewater sulfide and OM $\delta^{34}S$ values in Cariaco Basin stay within 15‰ of each other throughout the core (ODP Hole 1002B, Werne et al., 2003), so the impact of equilibration on OM $\delta^{34}S$ would be limited

regardless of its extent. Overall, differences in the $\delta^{34}S$ compositions of pyrite and OM preserved in each of these three modern sites are sensitive to differences in the exchangeability of these pools and their abundances relative to sulfide. Understanding the exchangeability of OS and pyrite may prove to be essential for explaining the $\delta^{34}S$ offsets between pyrite and OS in rocks globally.

5. CONCLUSIONS

Several types of OS were incubated with ^{34}S-labeled polysulfides ($\sum S^{\leq 0}$) to assess whether S-isotope exchange between $\sum S^{\leq 0}$ and OS might help explain the S-isotope distribution in environments like Santa Barbara Basin and the Namibian shelf. We find evidence for sulfide–disulfide exchange in both low-molecular-weight organic (di)sulfides and in natural proto-kerogen, where exchange rates between sulfide and OS are on the order of 0.1 to 0.2 day^{-1}.

Solutions containing abundant polysulfides in addition to sulfide also react rapidly with OS, including cysteine. We infer that the initial products of this reaction are organic polysulfides that may evolve toward shorter chain lengths on a timescale of hours. These organic polysulfides likely form by a chain-elongation mechanism that incorporates the original thiol S atom from cysteine. In natural environments, OM sulfurization via organic polysulfide formation and maturation could facilitate the preservation of biogenic S in proto-kerogen.

Proto-kerogen appears to become less exchangeable with sediment depth. Still, some sulfide–disulfide exchange appears to continue over thousands of years. In Santa Barbara, this process appears to drive the relatively large $\delta^{34}S$ difference between OS and pyrite recorded in deep sediments. Sulfide–OS exchange may be an important mechanism affecting the distribution of OS and pyrite $\delta^{34}S$ values globally.

REFERENCES

Amrani, A., & Aizenshtat, Z. (2004). Mechanisms of sulfur introduction chemically controlled: δ34S imprint. *Organic Geochemistry*, *35*(11-12), 1319–1336. http://doi.org/10.1016/j.orggeochem.2004.06.019

Amrani, A., Ma, Q., Ahmad, W. S., Aizenshtat, Z., & Tang, Y. (2008). Sulfur isotope fractionation during incorporation of sulfur nucleophiles into organic compounds. *Chemical Communications*, (11), 1356. http://doi.org/10.1039/b717113g

Anderson, T. F., & Pratt, L. M. (1995). Isotopic evidence for the origin of organic sulfur and elemental sulfur in marine sediments, *612*, 378–396.

Berner, R. (1984). Sedimentary pyrite formation: An update. *Geochimica Et Cosmochimica Acta*, *48*, 605–615.

Berner, R. A. (1987). Models for carbon and sulfur cycles and atmospheric oxygen; application to Paleozoic geologic history. *American Journal of Science* (Vol. 287, pp. 177–196). American Journal of Science. http://doi.org/10.2475/ajs.287.3.177

Bottrell, S. H., & Raiswell, R. (2000). Sulphur isotopes and microbial sulphur cycling in sediments. In R. E. Riding & A. S. M (Eds.), *Microbial Sediments* (Springer, pp. 96–104).

Boyd, E. S., & Druschel, G. K. (2013). Involvement of Intermediate Sulfur Species in Biological Reduction of Elemental Sulfur under Acidic, Hydrothermal Conditions. *Applied and Environmental Microbiology*, *79*(6), 2061–2068. http://doi.org/10.1128/AEM.03160-12

Brendel, P. J., & Luther, G. (1995). Development of a gold amalgam voltammetric microelectrode for the determination of dissolved Fe, Mn, O2, and S (-II) in porewaters of marine and freshwater …. *Environmental Science and Technology*, *29*(3), 751–761. http://doi.org/10.1021/es00003a024

Brüchert, V. (1998). Early diagenesis of sulfur in estuarine sediments: The role of sedimentary humic and fulvic acids. *Geochimica Et Cosmochimica Acta*, *62*(9), 1567–1586. http://doi.org/10.1016/S0016-7037(98)00089-1

Brüchert, V., & Pratt, L. M. (1996). Contemporaneous early diagenetic formation of organic and inorganic sulfur in estuarine sediments from St. Andrew Bay, Florida, USA. *Geochimica Et Cosmochimica Acta*, *60*(13), 2325–2332.

Brüchert, V., Pratt, L. M., Anderson, T. F., & Hoffmann, S. R. (1995). Abundance and isotopic composition of organic and inorganic sulfur species in laminated and bioturbated sediments from Hole 893A, Santa Barbara Basin. *Proceedings of the Ocean Drilling Program, Scientific Results*, *146*(2), 219–230.

Canfield, D. E. (2005). THE EARLY HISTORY OF ATMOSPHERIC OXYGEN: Homage to Robert M. Garrels. *Annu. Rev. Earth Planet Sci.*, *33*(1), 1–36.

http://doi.org/10.1146/annurev.earth.33.092203.122711

Canfield, D. E., & Thamdrup, B. (1994). The production of 34S-depleted sulfide during bacterial disproportionation of elemental sulfur. *Science*, *266*, 1973.

Dale, A. W., Bruchert, V., Alperin, M., & Regnier, P. (2009). An integrated sulfur isotope model for Namibian shelf sediments. *Geochimica Et Cosmochimica Acta*, *73*(7), 1924–1944. http://doi.org/10.1016/j.gca.2008.12.015

Ferdelman, T., Church, T. M., & Luther, G. I. (1991). Sulfur enrichment of humic substances in a Delaware salt marsh sediment core, *55*, 979–988.

Francois, R. (1987). A study of sulphur enrichment in the humic fraction of marine sediments during early diagenesis. *Geochimica Et Cosmochimica Acta*, *51*, 17–27.

Gilbert, H. F. (1995). Thiol/disulfide exchange equilibria and disulfide bond stability. *Biothiols Part A Monothiols and Dithiols, Protein Thiols, and Thiyl Radicals* (Vol. 251, pp. 8–28). Methods Enzymol. http://doi.org/10.1016/0076-6879(95)51107-5

Glazer, B. T., Luther, G. W., III, Konovalov, S. K., Friederich, G. E., Nuzzio, D. B., Trouwborst, R. E., et al. (2006). Documenting the suboxic zone of the Black Sea via high-resolution real-time redox profiling. *Deep Sea Research Part II: Topical Studies in Oceanography*, *53*(17-19), 1740–1755. http://doi.org/10.1016/j.dsr2.2006.03.011

Halevy, I., Peters, S. E., & Fischer, W. W. (2012). Sulfate Burial Constraints on the Phanerozoic Sulfur Cycle. *Science*, *337*(6092), 331–334.

Hartgers, W. A., Lopez, J. F., Damste, J. S., Reiss, C., Maxwell, J., & Grimalt, J. O. (1997). Sulfur-binding in recent environments: II. Speciation of sulfur and iron and implications for the occurrence of organo-sulfur compounds. *Geochimica Et Cosmochimica Acta*, *61*(22), 4769–4788.

Heitmann, T., & Blodau, C. (2006). Oxidation and incorporation of hydrogen sulfide by dissolved organic matter. *Chemical Geology*, *235*, 12–20.

Kamyshny, A. J., Goifman, A., Rizkov, D., & Lev, O. (2003). Kinetics of disproportionation of inorganic polysulfides in undersaturated aqueous solutions at environmentally relevant conditions. *Aquatic Geochemistry*, *9*, 291–303.

Kamyshny, A., Goifman, A., Gun, J., Rizkov, D., & Lev, O. (2004). Equilibrium Distribution of Polysulfide Ions in Aqueous Solutions at 25 °C: A New Approach for the Study of Polysulfides' Equilibria. *Environmental Science and Technology*, *38*(24), 6633–6644. http://doi.org/10.1021/es049514e

Kamyshny, A. (2009). Solubility of cyclooctasulfur in pure water and sea water at different temperatures. *Geochimica Et Cosmochimica Acta*, *73*(20), 6022–6028. http://doi.org/10.1016/j.gca.2009.07.003

Li, X., Taylor, G. T., Astor, Y., & Scranton, M. I. (2008). Relationship of sulfur speciation to hydrographic conditions and chemoautotrophic production in the Cariaco Basin. *Marine Chemistry*, *112*(1-2), 53–64.

Matrai, P. A., & Eppley, R. W. (1989). Particulate organic sulfur in the waters of the southern California bight. *Global Biogeochemical Cycles*, *3*(1), 89–103.

Mossman, J. R., Aplin, A. C., Curtis, C. D., & Coleman, M. L. (1991). Geochemistry of inorganic and organic sulphur in organic-rich sediments from the Peru Margin. *Geochimica Et Cosmochimica Acta*, *55*, 3581–3595.

Paris, G., Adkins, J. F., Sessions, A. L., & Subhas, A. (2013). MC-ICP-MS measurement of δ34S and Δ33S in small amounts of dissolved sulfate. *Chemical Geology*, *345*, 50–61.

Rickard, D., & Luther, G. I. (2007). Chemistry of Iron Sulfides. *Chemical Reviews*, *107*, 514–562.

Schimmelmann, A., & Kastner, M. (1993). Evolutionary changes over the last 1000 years of reduced sulfur phases and organic carbon in varved sediments of the Santa Barbara Basin, California. *Geochimica Et Cosmochimica Acta*, *57*(1), 67–78.

Steudel, R. (2003). Inorganic Polysulfides S n 2− and Radical Anions S n ·−. In *Topic in Current Chemistry* (Vol. 231, pp. 127–152). Berlin, Heidelberg: Springer Berlin Heidelberg. http://doi.org/10.1007/b13183

Teder, A. (1969). The spectra of aqueous polysulfide solutions. Part II: The effect of alkalinity and stoichiometric composition at equilibrium. *Arkiv. Fo ̈r. Kemi. 31*, 173-198.

Vairavamurthy, A., & Mopper, K. (1987). Geochemical formation of organosulphur compounds (thiols) by addition of H2S to sedimentary organic matter. *Nature*, *329*(6140), 623–625.

Van Mooy, B., Keil, R. G., & Devol, A. H. (2002). Impact of suboxia on sinking particulate organic carbon: Enhanced carbon flux and preferential degradation of amino acids via denitrification. *Geochimica Et Cosmochimica Acta*, *66*(3), 457–465.

Werne, J., Lyons, T., Hollander, D., Formolo, M., & Sinninghe Damsté, J. (2003). Reduced sulfur in euxinic sediments of the Cariaco Basin: sulfur isotope constrains on organic sulfur formation. *Chemical Geology*, *195*, 159–179.

Yu, Z.-G., Orsetti, S., Haderlein, S. B., & Knorr, K.-H. (2015). Electron Transfer Between Sulfide and Humic Acid: Electrochemical Evaluation of the Reactivity of Sigma-Aldrich Humic Acid Toward Sulfide. *Aquatic Geochemistry*, 1–14. http://doi.org/10.1007/s10498-015-9280-0